Examination of Measurement Techniques Used for Current and Emerging UV Treatment Technologies

by

Kyle David Rauch

Submitted in partial fulfilment of the requirements
for the degree of Master of Applied Science

at

Dalhousie University
Halifax, Nova Scotia
September 2018

For my mother, who taught me anything is possible

TABLE OF CONTENTS

LIST OF TABLES

LIST OF FIGURES

LIST OF ABBREVIATIONS AND SYMBOLS USED

A	Area in Square cm, or Absorbance
AlN	Aluminum Nitride
AlGaN	Aluminum Gallium Nitride
APHA	American Public Health Association
ATP	Adenosine Triphosphate
ATCC	American Type Culture Collection
AWWA	American Water Works Association
°C	Degrees Celsius
c	Speed of Light Defined as 2.9972458×10^8 m s^{-1}
cATP	Cellular Adenosine Triphosphate
CBA	Collimated Beam Apparatus
CFU	Colony Formation Unit
$CH_3COONa \cdot 3H20$	Sodium Acetate
d	Depth in cm
D	UV Dose in mJ cm^{-2}
D.F.	Divergence Factor
DI	Deionized
DNA	Deoxyribonucleic Acid
E. coli	*Escherichia coli* K12
$Fe_2(SO4)_3$	Ferric Sulfate
Fe^{2+}	Ferrous Iron
Fe^{3+}	Ferric Iron
FeOX	0.0060 M Potassium Ferrioxalate in 0.1 N H_2SO_4
FWHM	Full-Width Half Maximum
GaN	Gallium Nitride
GGR	Global Genomic Repair

h	Planck's Constant defined as $6.62606896 \times 10^{-34}$ J s
H_2S0_4	Sulfuric Acid
HPC	Heterotrophic Plate Count
hr	Hour
I	UV Intensity in mW cm^{-2}
I.F.	Integration Factor
k	Inactivation Rate Constant in cm^2 mJ^{-1}
$K_2C_2O_4 \cdot H2O$	Potassium Oxalate Monohydrate
λ	Wavelength in nm
L	Length in cm
LED	Light Emitting Diode
LPHO	Low Pressure High Output
LPUV	Low Pressure Ultraviolet
M	Molar Concentration
MAC	Maximum Allowable Concentration
MF	Membrane Filtration
mg	Milligram (10^{-3} gram)
min	Minute
MPN	Most Probable Number
MPUV	Medium Pressure Ultraviolet
MTF	Multiple Tube Fermentation
N	Normality Units
n	Number of Replicates
N_0	Initial Concentration of Microorganisms
N_a	Avogadro's Number as Defined as $6.02214179 \times 10^{23}$ mol^{-1}
NB	Nutrient Broth
NER	Nucleotide Excision Repair

N_d	Concentration of Microorganisms after Disinfection
$NH_2OH \cdot HCl$	Hydroxylamine Hydrochloride
NOM	Natural Organic Matter
NTU	Nephelometric Turbidity Unit
OD600	Optical Density at 600 nm
O&M	Operation and Maintenance
Φ Fe(II)	Quantum Yield of Ferrous Iron
P. aeruginosa	*Pseudomonas Aeruginosa* PA01
P-A	Presence-Absence
PBS	Phosphate Buffer Solution
PF	Petri Factor
QGA	Quench-Gone Aqueous
R	Reflective Coefficient
R^2	Pearson Correlation Coefficient
R2A	Reasoner's 2A Agar
RF	Reflection Factor
RLU	Relative Light Unit
RPM	Revolutions per Minute
s	Seconds
SD	Standard Deviation
S.F.	Sensitivity Factor
SPC	Standard Plate Count
t	Time in Seconds
TCR	Transcription Coupled Repair
TSA	Tryptic Soy Agar
TSB	Tryptic Soy Broth
TSS	Total Suspended Solids

UV	Ultraviolet
UV-LED	Ultraviolet Light Emitting Diode
UV-T	Ultraviolet Transmittance
U_λ	Energy per Einstein
v/v	Volume per Volume Ratio
VBNC	Viable but Nonculturable
VE	Variance Explained
W	Watt as Defined as N m s^{-1}
WEF	Water Environment Foundation
W.F.	Water Factor
WWTF	Wastewater Treatment Facility

ABSTRACT

A rapid monitoring technique for UV disinfection and the impact that characterizing UV-LED based collimated beam apparatuses has on computed inactivation rates were studied. A biomass recovery method was developed to monitor UV disinfection efficacy using adenosine triphosphate (ATP). ATP quantification immediately before and after UV treatment, which takes only minutes, shows little reduction in the microbial population. The biomass recovery method incorporates an incubation step to encourage life cycling of microbes and allows for quantification of UV disinfection using an ATP assay in 4 hr. UV-LEDs are inherently different then traditional mercury-based technologies. This study found that inactivation rates of *E. coli* were underestimated when a radiometer was used to determine average intensities. A protocol which accounts for the inherent differences of UV-LEDs was developed to more accurately determine UV inactivation rates. Overall, two new methods are presented to further the ability to monitor and research UV based technologies.

ACKNOWLEDGMENTS

Firstly, I would like to thank my supervisor, Dr. Graham Gagnon, for his support, encouragement and guidance over the last two years. I would also like to thank him for always presenting me with new opportunities and pushing me to better myself as a researcher. I would not be where I am today if it were not for his support.

I would also like to thank Dr. Allison Mackie for all her time and effort in helping me prepare Chapter 4 for publication, Lindsay Anderson for her help with shaping the structure of this thesis, Dr. Benjamin Trueman for all his coding help, Nicole Allward for teaching me the ins-and-outs of microbiology, and Heather Daurie for all her technical help.

Finally, I would like to thank my wife Sheliza for her unwavering support of my academic goals, and her incredible patience with me as I put together this document; my father Kelly for his never-ending encouragement, and his ability to always get me to see the bigger picture; and my sister Katie, for always being around when I need her the most, and always making sure I had a full stomach

CHAPTER 1: INTRODUCTION

Disinfection is a key component of water treatment processes to ensure the well-being of humans. Improper disinfection of drinking water can cause severe illness and even death (Meays, Broersma, Nordin, & Mazumder, 2004; WHO, 2014); furthermore, improper disinfection of effluents from wastewater treatment plants can result in illness if the receiving bodies are used as recreational waters (Calderon, Mood, & Dufour, 1991; Craun, Calderon, & Craun, 2005; Zmirou, Pena, Ledrans, & Letertre, 2003). Ultraviolet (UV) light has been increasingly used as a method of disinfection over the last few decades in the water and wastewater industries as it effectively inactivates chlorine resistant protozoans, produces no disinfection by products, and requires contact times in the range of seconds (Bolton & Cotton, 2008).

While UV disinfection offers many benefits, cultivation based enumeration techniques used to determine inactivation efficiencies take at least a day to complete and underestimate the total viable microbial community (Berney et al., 2008). Adenosine triphosphate (ATP) assays are able to determine the total viable microbial populations in minutes and have been used to determine disinfection efficiencies for chemical disinfectants. Unfortunately, ATP assays have been unsuccessful in determining disinfection efficiencies for UV treated waters as the main mechanism of disinfection renders the microorganisms harmless but still producing ATP.

Furthermore, while mercury-based UV treatment systems are widely implemented and an effective form of disinfection, they suffer from relatively high operation and maintenance costs and pose an environmental risk. The lamps used in these systems have a short lifespan as a result of needing to continuously run the systems and the lamps having around 4,500-

10,000 hr lifespan depending on the type of lamp being used (Bolton & Cotton, 2008). This leads to frequent replacement. Furthermore, typical systems have low power efficiencies of around 30-35% (Ibrahim, MacAdam, Autin, & Jefferson, 2014), and it has been estimated that 14-23% of a wastewater treatment plants energy costs comes from the UV treatment (Dabkowski, Lunn, De Kock, & Ingelright, 2011). Moreover, the mercury used in the lamps are contained by fragile materials and require careful disposal to ensure that there is no contamination of the environment.

Emerging UV Light Emitting Diodes (UV-LEDs) offer solutions to the short comings of traditional lamps. UV-LEDs have the potential to reach energy efficiencies of 75% with lifespans between 50,000 and 100,000 hr (Ibrahim et al., 2014). Additionally, they contain no mercury. These improvements would reduce the O&M costs and completely remove the risk of environmental contamination. However, UV-LEDs are fundamentally different than the traditional mercury-based systems and this produces some unique challenges.

UV-LEDs, unlike their traditional mercury-based counterpart, can be manufactured to emit light at specific wavelengths throughout the UV region. The additional flexibility in wavelength selection is an exciting prospect because the impacts from different wavelengths can now be easily studied; however, the majority of system characterization techniques have been developed for mercury-based UV systems that emit light monochromatically at 254 nm and may not be ideal for this emerging technology. While UV-LED based systems offer some exciting new benefits for UV disinfection, a better understanding on how to accurately determine UV dose requires additional research.

1.1 RESEARCH OBJECTIVES

Whether it is measuring inactivation efficiencies or accurately determine the UV energy being delivered by a system, proper measurement techniques are required. There were two main objectives in this study:

1. To understand how ATP assays can be used to rapidly monitor UV inactivation efficiencies.

2. To understand how characterization of UV-LED collimated beam systems impact computed inactivation efficiencies, and to determine an optimal protocol for determining UV dose.

1.2 ORGANIZATION OF THESIS

This thesis is organised into five chapters:

Chapter 1 provides introductory information regarding the research project, highlights the need for the work completed, and outlines the objectives for the study

Chapter 2 provides the necessary background information. This includes a description of the microorganisms used, a descriptions of ATP assay mechanisms, description of UV technology and inactivation and reactivation mechanisms, and descriptions of emerging UV-LED technology.

Chapter 3 reports the results of the first objective of the study. Explicitly, this chapter explores the potential of using ATP assays for rapid monitoring of UV inactivation and examines the impact that UV dose has on ATP production. This chapter has been prepared

as a journal article and accepted for publication, a list of coauthors and this author's contribution to the manuscript a is on file at the Dalhousie Faculty of Graduate Studies.

Chapter 4 reports the results from the second objective of this study. Explicitly, this chapter examines the importance of proper characterization of UV-LED based collimated systems, highlights the impact characterization has on reported inactivation rates and presents a comparison of inactivation rates from this study to literature for multiple wavelengths.

Chapter 5 provides a summary of the results of the work completed and provides some recommendations for future work.

CHAPTER 2: BACKGROUND INFORMATION

2.1 ESCHERICHIA COLI

Escherichia coli (*E. coli*) are a rod shaped facultative anaerobic coliform bacteria. *E. coli* cultures grow optimally at a temperature of 37 °C and can be easily enumerated on many types of substrates. Non-pathogenetic strains of *E. coli* are commonly found within the digestive tract of humans. However, some strains, such as O157:H7, are pathogenic and can cause serious illness or even death in the young, old and immunocompromised subpopulations (Griffin & Tauxe, 1991). Furthermore, it has been shown that *E. coli* are able to survive in the environment for days (Ishii & Sadowsky, 2008), indicating the importance of proper treatment of effluent at wastewater treatment facilities. As *E. coli* are easy to enumerate (Meays et al., 2004) and the most common faecal coliform bacteria (Rompré, Servais, Baudart, De-Roubin, & Laurent, 2002), they are often used as an indicator organism for fecal contamination in drinking or recreational waters. As such, many regulations set out by governments have placed limits on the total number of *E. coli* allowed to be present.

2.1.1 *E. coli* Regulations

In Canada, the regulations set for total *E. coli* depends on the type of water. For drinking water, a maximum allowable concentration (MAC) of 0 *E. coli* 100-mL^{-1} is in place for both *E. coli* and Total Coliforms (Health Canada, 2012a). For wastewater, no MAC has been set by the federal government (Government of Canada, 2013), but some provincial governments have provided guidelines (Canadian Council of Ministers of the Environment, 2014). In Atlantic Canada, the guideline is set to < 200 *E. coli* 100-ml^{-1}. For freshwater recreational sources the Canadian guideline is set at < 200 *E. coli* 100-ml^{-1} based on a 5

sample minimum geometric mean, and < 400 *E. coli* 100-ml^{-1} for a single sampling event (Health Canada, 2012b). For marine waters, *Enterococci* are used as the faecal coliform indicator and the regulations are set at 35 *Enterococci* 100-ml^{-1} based on a minimum 5 sample geometric mean, and 70 *Enterococci* 100-ml^{-1} for a single sampling event. Currently three methods are accepted by the government of Canada for Coliform enumeration: Presence-Absence (P-A), Membrane Filter (MF), and Multiple Tube Fermentation (MTF) tests (Health Canada, 2012a). Full detailed descriptions of each of these methods can be found in S*tandard Methods for the Examination of Water and Wastewater* (APHA, AWWA, & WEF, 2012).

2.2 ADENOSINE TRIPHOSPHATE

Adenosine triphosphate is a chemical compound that is used as the main energy source for metabolism of every cellular structure (Knowles, 1980). The compound consists of a ribose and adenine base (Adenosine) attached to a triphosphate molecule (Figure 2.1). This molecule is an energy storage mechanism for cells and when energy is required the triphosphate molecule is cleaved to remove one or two phosphate groups to become adenosine diphosphate (ADP) or adenosine monophosphate (AMP), respectively. ADP and AMP then undergo phosphorylation and are converted back to ATP when energy is required to be stored again. In the process of ATP cycling, the adenosine backbone rarely undergoes any structural change.

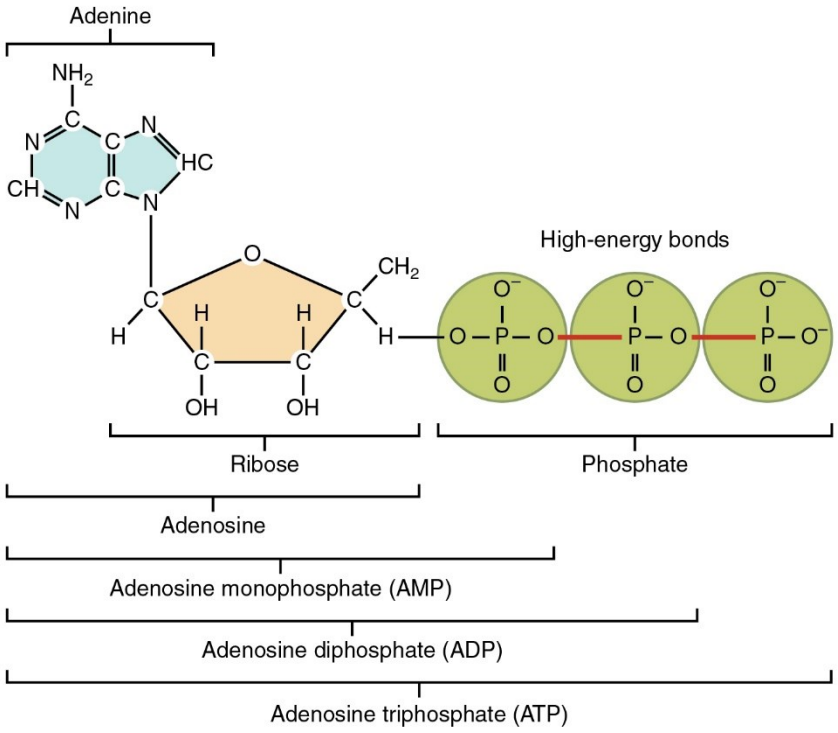

Figure 2.1: Structure of adenosine triphosphate molecule (Openstax College, 2013)

ATP is found intra- and extra-cellularly in all living microorganisms. The intracellular concentration for *E. coli* has been shown to be in the range of 1-5 µM (Lasko & Wang, 1996; Soini et al., 2005) and to be impacted by temperature (Soini et al., 2005), oxygen concentrations (Mathis & Brown, 1976), and growth phase (Schneider & Gourse, 2004). Extracellular ATP concentrations for *E. coli* have been shown to be in the range of 2-14 nM, and are largely impacted by the growth rate of the microorganism (Mempin et al., 2013).

2.2.1 ATP Assay

Unlike culture based methods, which only capture around 1% of viable bacteria (Amann, Ludwig, & Schleifer, 1995; Hugenholtz, Goebel, & Pace, 1998; Sharma, Ranjan, Kapardar, & Grover, 2005; Staley & Konopka, 1985; Vartoukian, Palmer, & Wade, 2010), ATP

assays are a nonselective method that capture the entire microbial population present in a sample in under 5 min. ATP assays use a combination of Luciferase, the compound responsible for bioluminescence (Ohmiya & Hirano, 1996), and Luciferin to react with ATP to produce a photon of light. The quantity of photons produced is proportional to the concentration of ATP as per Equation 2-1 (LuminUltra, 2018) and can be measured by a luminometer.

$$\boldsymbol{ATP + Luciferin \xrightarrow[Luciferase]{MG++} AMP + PP_i + Oxyluciferin + Photon} \quad \textbf{(2.1)}$$

ATP within a sample needs to be isolated prior to quantification. This is done by means of a lysing agent that can use either enzymatic reactions or osmotic pressure to destroy the cell membrane. Further isolation of only the intracellular ATP can be accomplished by filtering the sample through a 0.2 µm filter to capture the cells prior to lysing.

ATP assays have been used in many applications. The first generation of ATP assays were commonly used for hygienic studies of surfaces (Davidson, Griffith, Peters, & Fielding, 1999; Lappalainen et al., 2000; Turner, Daugherity, Altier, & Maurer, 2010). These assays were not used for water or wastewater samples because they were unable to accommodate many of the interferences present in the source waters (LuminUltra, 2016). The second generation of ATP assays were designed to address these interferences and have since been used in many applications in the water and wastewater industries. For example, these assays have been used in sludge monitoring (Chu, Lee, Chang, & Liao, 2001), contamination of recreational and drinking waters (Deininger & Lee, 2001; Delahaye, Welté, Levi, Leblon, & Montiel, 2003; Lee & Deininger, 2004), and disinfection efficiency

studies (First & Drake, 2014; Linklater & Örmeci, 2014). Second generation ATP assays have shown to be effective tools for advanced monitoring of water and wastewater treatment.

2.3 ULTRAVIOLET DISINFECTION

Mercury-based UV technologies were first implemented in 1955 (Bolton & Cotton, 2008), and today are widely used for disinfection in many industries. UV is most effective against bacteria and protozoa and then increasingly less so for viruses, bacterial spores, adenovirus, and then least effective against algae (Bolton & Cotton, 2008). UV is also effective against chlorine resistant microorganisms, even at low doses (Bolton, Dussert, Bukhari, Hargy, & Clancy, 1998). In addition to being effective at inactivating microorganisms, UV disinfection systems also have the added benefits of requiring no additional chemicals, producing no harmful disinfection-by-products, and requiring only a short contact time in the range of seconds.

2.3.1 Disinfection Mechanisms

Ultraviolet (UV) disinfection uses light radiation between 200 and 400 nm to inactivate microorganisms. More specifically, it is the 200-300 nm range that is responsible for this inactivation, as the photons in this range are absorbed by the DNA and RNA of the microorganism. The term inactivation is most often used to describe the effects of UV disinfection as the microorganism are left in a state where they are still technically viable, but rendered harmless.

The main mechanism of disinfection occurs from the formation of UV photoproducts in the DNA structure of the microorganism. Two type of pyrimidine dimers can be formed:

cyclobutene pyrimidine dimer (CPD) and 6,4-photoproducts (Figure 2.2). These dimers occur when two neighboring thiamine bases absorb UV energy, which creates a cross link between them. The creation of these dimers disrupts the ability of the DNA to properly replicate, ultimately leaving the microorganism unable to replicate. Oguma, Katayama, & Ohgaki (2002) showed that around 100 of these photoproducts are required to form in order to properly disrupt the DNA and inactivate the microorganism. UV light also has the ability to disrupt the cell membrane, but this only occurs at very high doses (Bolton & Cotton, 2008)

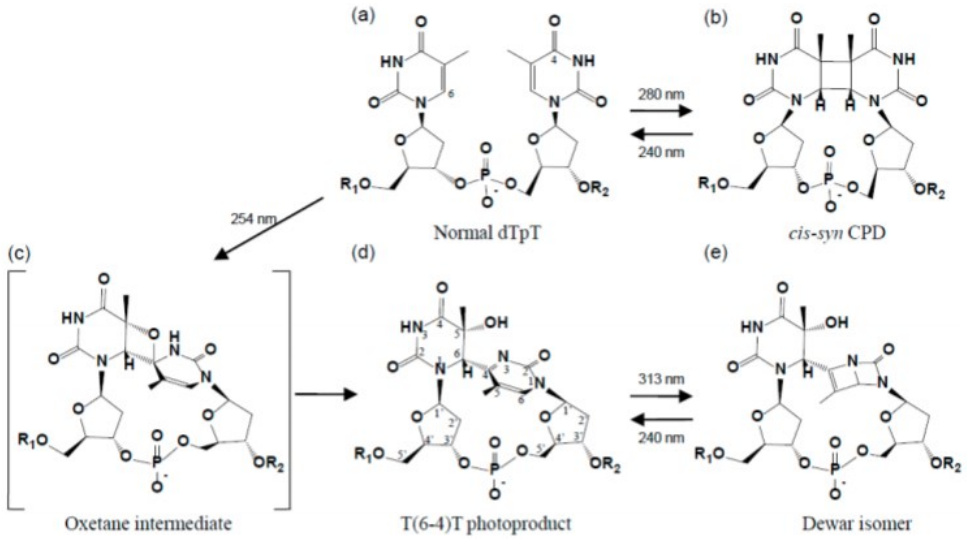

Figure 2.2: UV induced photoproducts and pathways (Yokoyama & Mizutani, 2014)

The action spectra of microorganisms describe the relative response of inactivation to various wavelengths of UV light. The action spectra exist for bacteria, protozoa, and viruses, and usually a peak in the relative response occurs near 260 nm, which corresponds to the peak in the absorption spectrum of DNA. The peaks for specific microorganisms have been shown to shift slightly around the peak of 260 nm. For example, MS2 Coliphage

has a peak near 265 nm (Mamane-Gravetz, Linden, Cabaj, & Sommer, 2005), *Cryptosporidium parvum* has a peak near 270 nm (Linden, Shin, & Sobsey, 2001), and *Escherichia Coli* has a peak near 270 nm (Wang, MacGregor, Anderson, & Woolsey, 2005). It is hypothesised that this shifting phenomenon is a result of the different compositions of the nucleotides in the DNA of a given microorganism (Bolton & Cotton, 2008).

2.3.2 Repair Mechanisms

Photoreactivation mechanisms are one pathway for UV photoproduct repair. Photoreactivation is a direct reversal of DNA photoproducts (Morita et al., 2010) and occurs when either CPD or 6-4-photoproducts are introduced to wavelengths between 300-500 nm. Photons in this range activate the photolyase enzyme in the cell (Morita et al., 2010; Whitmore, Potten, Chadwick, Strickland, & Morison, 2001), which breaks the cross link between the thiamine bases and allows for regular replication of the DNA to begin again. The enzyme used depends on the photoproduct formed (Yokoyama & Mizutani, 2014). It should be noted that not all microorganisms have the enzyme necessary for photo repair (Bolton & Cotton, 2008). Furthermore, photoreactivation is typically not a concern when UV treatment is used in drinking water facilities because the treated water is enclosed in pipes; however, as effluents from wastewater plants are discharged into open environments following treatment, photoreactivation mechanisms may impact regrowth.

Dark repair mechanisms are another pathway for UV photoproduct repair, and have shown to be used by almost all bacteria, spores when germinating, and some virus after infection (Hijnen, Beerendonk, & Medema, 2006). Nucleotide Excision Repair (NER) is one of the most common dark repair mechanisms and has two pathways to repair the UV

photoproducts: Transcription coupled repair (TCR), and Global Genomic Repair (GGR). Both of these pathways isolate, remove, and replace the photoproduct in the DNA; however, TCR does so with a higher efficiency (Morita et al., 2010). In *E. coli*, the NER is controlled by a multi enzyme complex know as UvrABC Endonuclease. Wherein, UvrA recognizes the damage in the DNA strand, UvrB, and UvrC form a dimer that cleaves a segment 12 nucleotides long around the photoproduct, UvrD removes the damaged section and then a new strand of DNA synthesised by DNA Polymerase I is ligated by means of the DNA Ligase enzyme (Morita et al., 2010). Dark repair is often less of a concern when compared to photoreactivation for coliform bacteria (Salcedo, Andrade, Quiroga, & Nebot, 2007)

2.3.3 Mercury Amalgam Systems

In treatment facilities, UV system configurations typically use mercury amalgam lamps and are found in many different arrangements. Systems can be designed as a closed pipe or as an open channel. (Figure 2.3) and are generally placed at the end of the treatment train. Typically, open-channel systems are used in wastewater treatment and closed-pipe systems are used in drinking water treatment. Flow in these systems can be cross flow or concurrent flow with one or more lamp (Bolton & Cotton, 2008) depending on the application.

Figure 2.3: Closed (left) and Open (right) UV disinfection systems (Trojan UV, 2018)

In each of the systems, the light source consists of one or more mercury amalgam lamps. These lamps are either a low-pressure (LP), low-pressure high output (LPHO), or medium-pressure (MP) type. The spectrum emitted is determined by the pressure of the lamps, with an increase in pressure increasing the width of the emission spectrum (Bolton & Cotton, 2008). LP and LPHO both emit monochromatically at 253.7 nm; whereas, MP emits spectrally with peaks occurring throughout the UV spectrum (Figure 2.4). Additionally, the LPHO and MP have higher intensity output compared to the LP lamp; however, the MP has a lower germicidal efficiency.

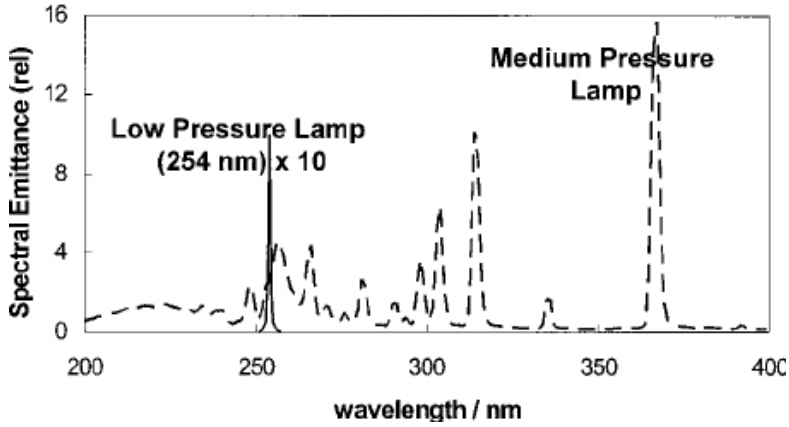

Figure 2.4: Emission spectra for LPUV and MPUV lamps (Bolton & Linden, 2003)

2.3.4 Ultraviolet Light Emitting Diodes

Ultraviolet Light emitting diodes (UV-LEDs) are semi-conductor p-n junction type diodes that emit radiation with a near monochromatic spectrum when a forward voltage is applied. The diodes are constructed of thin epitaxial layers of aluminum nitride (AlN), gallium nitride (GaN) and aluminum gallium nitride (AlGaN) grown on a sapphire crystal substrate (Figure 2.5). Narrow quantum wells are created in the active region of the LED and capture electrons. These captured electrons are brought to a lower energy state and a photon related to the bandgap, or the region of energy where no electron state can exist, is released (Shur & Gaska, 2010).

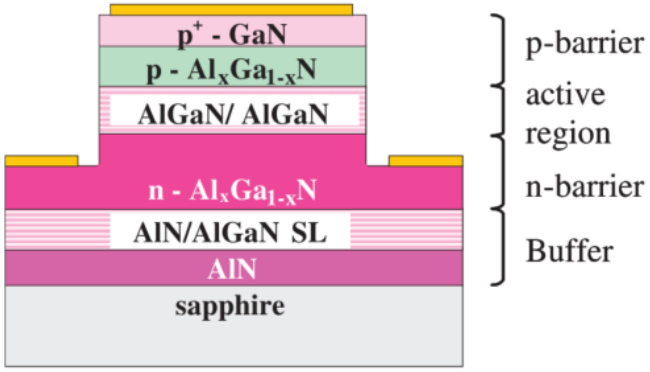

Figure 2.5: UV-LED schematic (Khan, 2006)

The bandgap of the UV-LED is based on the composition of the p- and n- type layers in the diode. By increasing the molar component of aluminum in the epitaxial layers, lower wavelengths are achieved (Figure 2.6). The lowest possible wavelength achieved based on this structure is 210 nm (Taniyasu, Kasu, & Makimoto, 2006), and the highest is near 350 nm. Wavelengths above 350 nm are achieved by introducing indium into the composition of the epitaxial layers (Muramoto, Kimura, & Nouda, 2014).

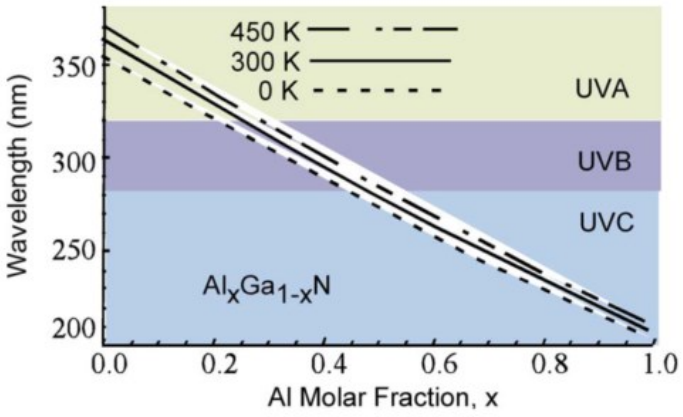

Figure 2.6: UV-LED wavelength output based on aluminum molar fraction (Shur & Gaska, 2010)

One of the largest factors hindering realization of UV-LED technology is the overall low power outputs. (Ibrahim et al., 2014). Theses low power outputs are largely due to low external quantum effciencies of the UV-LEDs, which stem from low conductivity of the substrate and absorption of the emitted UV energy by the GaN buffer layers of the LED (Allerman et al., 2004; Muramoto et al., 2014). Moreover, efficiencies decrease as wavlengths decrease due to the increaseing Al content in the epitaxial layers. By increasing the molar composition of Al, the layers become more brittle and cause increased dislocation densities within the active layer (Allerman et al., 2004; Khan, 2006; Shur & Gaska, 2010). Furthermore, increasing the Al component increases the ability of the buffer layers to absorb the light emitted from the active layer and casues the wavelengths to undergo a red-shift (Allerman et al., 2004).

However, each year the understanding of the material properties of these semiconducters are becoming better understood, leading to better manufacturing techniques and ultimately to better power output. For instance, in 2004 a 278 nm UV-LED only had a 0.47 mW output

(Allerman et al., 2004), then in 2010 a 280 nm UV-LED was produced with a 2.5 mW output (Shur & Gaska, 2010), and in 2017 DOWA realeased a 280 nm UV-LED with an output of 75 mW (DOWA Holdings CO., 2017). It is projected that by 2020 the overall efficiencies of UV-LEDs should increase to 75%, and power outputs should increase to 675 mW; furthermore, it is expected that each UV-LED should decrease to approximately $0.12 CAD (Ibrahim et al., 2014).

2.3.4.1 Recent Applications of UV-LEDs in Water Treatment

To date, many bench-scale studies have been conducted examining the inactivation efficiencies of microorganisms such as *Bacillus subtillis* (B.*subtillis)*, *Escherichia coli* (*E. coli*), Human adenovirus, MS2 coliphage, bacteriophage Qβ, and bacteriophage T7 in water using UV-LEDs at various wavelengths. The three tables in Appendix A were adapted from Malayeri et al. (2016), and summarize the required fluence for a given log reduction of various microorganisms found in the current literature. The following highlights some recent studies using UV-LEDs but is in no means exhaustive.

Bowker, Sain, Shatalov, & Ducoste (2011) compared the effects that LPUV and 255 nm and 275 nm UV-LEDs had on *E. coli*, MS2, and T7. The authors found for *E. coli* that the 255 nm UV-LED had a smaller log reduction versus a LPUV lamp, which could be as a result of the UV-LED much lower intensity. They also found that the 275 nm UV-LEDs had a greater effect on the microorganism. The authors attribute this to the absorbance spectrum of proteins, which peaks near 280 nm. For MS2, the authors found that both UV-LED wavelengths performed the same and were observed to perform worse compared to a LPUV lamp. For T7, the 275 nm UV-LED was found to have a greater impact. The authors attribute this to the action spectrum of T7 peaking near 270 nm.

The disinfection efficiencies of a novel ring style 285 nm UV-LED reactor on bacteria and viruses were studied by Oguma, Rattanakul, & Bolton (2015). The authors observed disinfection rates of 0.157, 0.029, 0.037, and 0.023 $cm^2\ mJ^{-1}$ for *E. coli*, MS2, Qβ, and human adenovirus type2 (HadvT2), respectively. The authors also examined the germicidal factor (the ratio of disinfection rate at a given wavelength to 254 nm), and found that *E. coli*, MS2, and Qβ had factor between 0.31 and 0.70; whereas, HadvT2 had a factor of 1.15 (Oguma et al., 2015). The author suggests that because 285 nm UV-LEDs perform well with HadvT2, but not the other organism, that a polychromatic UV-LED system may prove optimal when targeting organisms with different action spectra. This study highlights that unique reactor designs that are possible as a result of the specificity and compact nature of UV-LEDs.

Beck et al. (2017) examined the energy efficiencies for 1 log reduction of the 5 lamp types with the four microorganisms. The authors found that across all the combinations of UV treatments and microorganisms the LP lamp had the highest energy efficiency. They attribute the poor energy performance of the UV-LEDs to having low wall plug efficiencies and state that UV-LEDs need to increase efficiency by 50-90 times (25% for 260 nm; 39% for 280 nm) to achieve the same results of the LP lamps (2016).

2.3.5 Collimated Beam Studies

Collimated beam studies are used to determine UV sensitivities of different microorganisms. A collimated beam apparatus (CBA) is used to conduct these studies and consists of a light source attached to a collimator. The purpose of the collimator is to attempt to develop an evenly distributed light intensity that will arrive perpendicular to the surface of the water being treated. This reduces the amount of light reflected from the

surface and increases the efficiency of the treatment. Using these CBAs, dose response curves can be developed to determine the inactivation rate for a given species in pure culture, a synthetic water matrix, or for environmental samples. These inactivation rates can then be used to compare UV treatment studies and determine the optimal conditions for treatment of a given species or water matrix. A standard protocol has been developed to accurately determine the UV dose for mercury-based collimators (Bolton & Linden, 2003), but not for UV-LED based ones.

CHAPTER 3: BIOMASS RECOVERY METHOD FOR ADENOSINE TRIPHOSPHATE (ATP) QUANTIFICATION FOLLOWING UV DISINFECTION

3.1 ABSTRACT

A biomass recovery method was developed to monitor UV disinfection efficacy using adenosine triphosphate (ATP). Typically, disinfection monitoring at wastewater treatment facilities (WWTFs) involves quantifying fecal and total coliforms or colony forming units (CFU), the results of which take a minimum of 24 hr to produce. ATP quantification immediately before and after UV treatment, which takes only minutes, shows little reduction and often an increase in the microbial population since UV irradiation results in cells that are viable (i.e., still producing ATP) but not culturable. To overcome this, our biomass recovery method incorporates an incubation step to encourage life cycling of microbes. Average log reductions in cellular ATP (cATP) were found to be -0.28 ± 0.19, -0.011 ± 0.153, -0.17 ± 0.32, and 0.065 ± 0.074 using direct ATP measurements on UV-treated samples from WWTFs A, B, C, and D, respectively, while those using the recovery method were correspondingly 0.17 ± 0.34, 1.8 ± 0.8, 0.20 ± 0.35, and 0.72 ± 0.26. The response of the biomass recovery-ATP method indicated a significant direct correlation to the microbial population reduction observed in heterotrophic plate count (HPC) and Colilert® methods using both pure *E. coli* culture and secondary municipal wastewater effluent.

KEYWORDS: Adenosine triphosphate (ATP), coliforms, disinfection efficacy, luminase, microbial enumeration, UV disinfection, viable but nonculturable

3.2 INTRODUCTION

Ultraviolet (UV) irradiation is often used as a final disinfection step in municipal wastewater treatment facilities (WWTFs) due to its lack of harmful effects on receiving water bodies compared to chlorination, the most widely used water disinfection method. Typical tests to determine efficacy of UV disinfection on *E. coli* and other fecal coliforms rely on 24-hr to 7-day culturability studies (APHA et al., 2012; Chang et al., 1985; Lazarova et al., 1998). UV irradiation alters microbial DNA in such a way that they can no longer replicate or produce toxins, termed inactivation. However, organisms continue to be present in the water that has been treated and will continue to carry out their metabolic activities until their lifecycle is complete (Baron & Bourbigot, 1996; Ben Said, Masahiro, & Hassen, 2010; Zhang, Ye, Lin, Lv, & Yu, 2015). This state is referred to as viable but non culturable (VBNC), meaning microbes are still alive and consuming energy, but would not show growth in typical tests of culturability. This is significant for WWTFs in that if a rapid test were to be carried out for quantifying microbiological contamination (or disinfection performance) the results may falsely indicate poor disinfection performance since the organisms that have been inactivated are VBNC.

Adenosine triphosphate (ATP) analysis is gaining popularity as a robust method to quantify microbial content in water supplies and wastewater treatment processes. ATP testing provides cost effective and non-specific microbial analysis of water samples in a matter of minutes in the laboratory or field (Deininger & Lee, 2001; Delahaye et al., 2003; Lee & Deininger, 2004). To date, few studies have been conducted to investigate the application of ATP assays in assessing the effectiveness of UV disinfection of water (First & Drake, 2014; Linklater & Örmeci, 2014; van Slooten, Wijers, Buma, & Peperzak, 2015). The main

challenge with applying current ATP assays to UV disinfection efficacy testing is that, as described above, UV treatment merely inactivates microorganisms but they continue to contain ATP. UV irradiation thus results in little to no reduction in ATP and can even increase ATP concentrations as cells attempt to repair UV damage (First & Drake, 2014; Linklater & Örmeci, 2014; van Slooten et al., 2015; Villaverde, Guerrero, & Barbe, 1986).

The objective of this study was to develop a pre-treatment technique to employ prior to ATP testing that would result in detectable differences in cellular ATP (cATP) concentrations between pre- and post-UV treated wastewater within a single work shift (i.e., <8 hr) to improve compliance monitoring and disinfection performance at WWTFs.

3.3 MATERIALS AND METHODS

Development of the biomass recovery method involved incubating samples in a suitable growth environment to accelerate biological growth prior to ATP analysis. The method was optimized for incubation time and temperature using a pure *E. coli* suspension and was followed by two rounds of validation testing on samples collected from various WWTFs in Atlantic Canada. This new technique was tested against both HPC and Colilert® for environmental samples to compare the new ATP-based method to traditional enumeration techniques used in the water treatment industry.

3.3.1 Chemicals and Reagents

A Milli-Q system (Reference A+, Millipore Corporation, MA, USA) was used to provide deionized (DI) water. All growth media and agars were prepared according to instructions provided by the manufacturers and autoclaved at 121 °C for 15 min to ensure sterility (AMSCO Lab 250, Steris Co, United Kingdom). All glassware was triple rinsed with DI

water and autoclaved for sterility. Phosphate buffered saline (PBS) solution was prepared in accordance with *Standard Methods for the Examination of Water and Wastewate*r (APHA, AWWA, and WEF 2012) and autoclaved before use. PBS solution was used for cell cleaning and suspension dilution. Preparation of the growth medias tested for the ATP pre-treatment method will be discussed in the Biomass Recovery Development section 3.3.3.2.

3.3.2 Wastewater Samples

Municipal wastewater samples were taken from four WWTFs in Eastern Canada. Facilities A, B, and C all use enhanced primary treatment followed by UV disinfection, and share a similar design scaled for the appropriate average daily flows of 28 500, 83 800, and 139 900 m^3 d^{-1}, respectively. Facility D uses secondary treatment with a pure oxygen activated sludge system followed by UV disinfection with a design average daily flow of 28 400 m^3 d^{-1}. The number of sampling events for WWTF A, B, C and D were 16, 33, 15 and 24, respectively.

Samples were collected in sterile 1 L wide mouth bottles before (pre-UV) and after (post-UV) UV treatment. Samples were collected as close to UV banks as possible and were transported to the lab on ice in a cooler. Samples were processed as soon as possible upon returning to the lab. Samples were measured for total suspended solids (TSS) and UV transmittance (UVT). Samples from facilities A, B, C, and D had average UVT of 75.8 ± 8.0, 50.1 ± 10.7, 63.1 ± 5.1, and 52 ± 6.4 % and average TSS of 6.0 ± 6.2, 19.3 ± 28.2, 10.6 ± 12.7, and 12.6 ± 6.1 mg L^{-1} during the study period, respectively. Biological testing and UV treatment were performed on the same day as sampling.

3.3.3 Experimental Methods

3.3.3.1 E. coli Incubation and Preparation

On the day prior to running an experiment, 0.5 mL of an *E. coli* glycerol stock was used to inoculate 9 mL of TSB, which was then incubated at 37 °C overnight. The following morning, 1 mL of the overnight culture was suspended in 9 mL of TSB and incubated at 37 °C for approximately 4 hr to ensure the culture was in the late exponential growth phase. The growth phase was verified by a previously developed OD600 - CFU growth curves. After incubation, cells were pelleted in sterile 15 mL polypropylene tubes at 3500 RPM for 10 min. The supernatant was removed, and the cells were washed three times by vortexing in approximately 10 mL of PBS at 3000 RPM for 2 min. After the final wash, the cells were resuspended in sterile PBS to achieve a working solution concentration of approximately 10^6 CFU $mL^{-1.}$

3.3.3.2 ATP Pretreatment Method Development

In the growth media optimization experiment, nutrient broth (NB), TSB, and modified formulations of each were tested as a simulation of a wastewater environment to select the most suitable medium for bacterial cultivation. Media were tested at full strength and quarter strength, with and without the addition of glycerol at a concentration of 0.1% v/v. Media formulations were autoclaved for 15 min at 121 °C to ensure sterility. To determine the best growth formulation, 5 mL of pre-UV treated secondary wastewater effluent from Facility D was diluted 10 times into the media and incubated for 4 hr at 37 °C. Following incubation, a standard ATP assay was performed using QGA test kits. This testing was conducted by Xie (2014).

The incubation step was optimized by examining the effect temperature and time had on cATP concentrations. A pure suspension of *E. coli* was subjected to a UV dose of 10 mJ cm^{-2}. Following treatment, both the untreated and UV-treated samples were diluted 10-fold in the quarter strength tryptic soy broth with 0.1% v/v glycerol and incubated at either 20 or 37 °C. Samples were prepared in triplicate and cATP was evaluated at 0, 2, 4, 6, and 8 hr for each temperature using the QGA test kit.

The criteria established for selection of the optimal incubation conditions were: 1) time, temperature, and growth media sufficient to show a difference in ATP concentrations from before and after UV treatment to enable determination of a log reduction in ATP and 2) shortest possible incubation time to get the most rapid results possible. The incubation conditions that best met these criteria were considered the optimum for biomass recovery prior to ATP quantification.

3.3.3.3 Bench-Scale UV Disinfection Treatment

UV disinfection was performed using a low-pressure UV (LPUV) collimated beam system (Calgon Carbon Corporation, USA). UV dose-response curves were collected by portioning pure *E. coli* suspensions into 250 mL beakers to a depth of 1.5 cm, or an approximate volume of 50 mL. The suspensions were then exposed to UV doses of 2, 5, 7, 10, and 20 mJ cm^{-2} with a sixth beaker left untreated as a control. All treatments were performed in triplicate and treated in a dark room to reduce the effects of photo reactivation. UV dose-response curves for environmental samples were collected in a similar manner but used doses between 0 and 60 mJ cm^{-2} and were collected as singlets per sampling event. Exposure times to determine UV dose were calculated using the method supplied by Calgon Carbon. When the full power was attained, UV irradiance was measured at the

center of the beam and at the plane coincident with the surface of the water using an ILT-1400 radiometer photometer (International Light Technologies, MA, USA). Average irradiance was calculated using Equations 3.1.

$$\mathbf{I}_{avg} = \mathbf{I}_0 \times \mathbf{I.F.} \times \mathbf{P.F.} \times \boldsymbol{W.F.} \quad \textbf{(3.1)}$$

where I_0 is defined as the measured irradiance in mW cm^{-2}, *I.F.* is the integration factor provided by Calgon (1.403), and *P.F.* is the Petri factor provided by Calgon (0.97). The *W.F.* accounts for the attenuation of the UV light as it passes through the sample and was calculated using Equation 3.2.

$$\boldsymbol{W.F.} = \left(\mathbf{1} - \mathbf{10}^{-\boldsymbol{A_{1cm}} \times \boldsymbol{l}}\right) / \left(\mathbf{2.303} \times \boldsymbol{A_{1cm}} \times \boldsymbol{l}\right) \quad \textbf{(3.2)}$$

where A_{1cm} is the measured absorbance though a 1 cm pathlength at 254 nm, and l is the total pathlength of the water being treated. Exposure time for required UV dose was determined by dividing the required dose by the actual intensity.

3.3.3.4 Validation of the Biomass Recovery Method

Two rounds of testing were completed on the WWTF samples. In the first round, samples were collected from facilities A, B, and C, and pre- and post-UV samples from each plant were enumerated for HPC and ATP and subjected to the biomass recovery-ATP method. Round one sampling was completed by Middleton (2017). In the second round, samples were collected from facilities B and D, and pre-UV and post-UV samples were enumerated for *E. coli*, total coliforms, ATP, and biomass recovery-ATP. Additionally, pre-UV samples were subjected to UV doses between 10-60 mJ cm^{-2} using a collimated beam

apparatus, and then enumerated for the same parameters as the plant collected samples (only the 40 mJ cm^{-2} sample had ATP quantified).

3.3.4 Analytical Methods

3.3.4.1 Water Quality

Standard Methods was followed for measuring TSS (APHA, AWWA, and WEF 2012). UVT data were measured using a spectrophotometer (HACH DR 5000, ON, CA) and were recorded in triplicate for each sample to ensure accuracy.

3.3.4.2 Enumeration Techniques

A spread plate method was implemented according to *Standard Methods* (APHA, AWWA, and WEF 2012) to enumerate the culturable heterotrophic bacteria of environmental samples (heterotrophic plate count or HPC), and a standard plate count (SPC) was used to enumerate pure suspensions of *E. coli*. 10-fold serial dilutions in PBS were used to achieve proper dilution levels prior to plating on either sterile R2A or TSA plates for HPC and SPC, respectively. Samples were plated using an ethanol flame sterilized glass rod to spread 0.1 mL of sample evenly across the surface of the agar. The plates were incubated at 28 °C for 7 days or 37 °C for 18 to 24 hr for HPC or SPC, respectively. After the desired incubation time was achieved, plates with colony counts between 0-300 colony forming units (CFU) were counted with the aid of a Quebec colony counter (American Optical Company, NY, USA).

E. coli and total coliforms of environmental samples were enumerated using the Colilert® test kits (IDEXX, MA, USA). Volumes between 0.1-100 mL of treated and untreated samples were added to sterile 100 mL square cell culture bottles and then filled to 100 mL with sterile PBS if needed. One package of Colilert's nutrient-indicator was added to each

flask and mixed until dissolved. Samples were then transferred to a Quanti-Tray*/2000 (IDEXX, MA, USA), and sealed using a Quanti-Tray* Sealer (IDEXX, MA, USA). Samples were incubated at 36 ± 2 °C for 24 to 28 hr. Following incubation, samples were counted according to the manufacture's instructions to determine the most probable number (MPN) of *E. coli* and total coliforms per 100 mL.

ATP concentrations were quantified using Quench-Gone-Aqueous (QGA) test kits (LuminUltra Technologies Ltd., Fredericton, NB, Canada) and the Kikkoman Lumitester C-110 (HACH, CO, USA). Samples were quantified for cATP by passing a known volume of sample through a 0.2 µm filter syringe system. This step captures cells on the filter bed while expelling any extra-cellular ATP. Captured cells were then lysed with 1 mL of UltraLyse7 solution into 9 mL dilution buffer. Assays were prepared by combining 100 µL of the dilution and 100 µL of a Luminase enzyme and measured using the luminometer. The strength of the Luminase enzyme was determined by performing the same assay with the UltraCheck standard (1 ng ATP mL^{-1}). Results from the luminometer were collected in relative light units (RLUs) and were converted to cATP concentrations using Equation 3.3.

$$\boldsymbol{cATP = RLU_{cATP}/RLU_{UC1} \times 10,000(pgATP)/V} \quad \textbf{(3.3)}$$

where $cATP$ is the concentration of cATP in pg mL-1, RLU_{cATP} is the measured RLU of the sample, RLU_{UCI} is the measured RLU of the UltraCheck standard, and V is the known sample volume passed through the filter in mL.

3.3.5 Statistical Methods

All linear and orthogonal regressions were performed using R software (R Core Team, 2018). Linear regressions were computed using the built-in linear regression function.

Orthogonal regressions were computed by first performing a spectral decomposition on the variance matrix of the data to obtain the eigenvalues. Following that, the variance explained (VE) was computed using the ratio of the first eigenvalue to the sum of the total eigenvalues. The slope of the regression was computed using the ratio of the first eigenvalue to the second eigenvalue. The intercept was calculated using the means of the observations and the previously calculated slope.

3.4 RESULTS AND DISCUSSION

3.4.1 Development of Biomass Recovery ATP Pre-Treatment Method

3.4.1.1 Effect of Growth Medium

The effect of growth medium on cATP concentrations was tested using nutrient broth and tryptic soy broth at full strength and one quarter strength with and without the addition of 0.1 % v/v glycerol. Incubation of wastewater samples for 4 hr in quarter strength TSB with glycerol resulted in higher cATP concentrations (5.1 log cATP) compared to other media tested (3.4 ± 0.2 log cATP) and was therefore selected for use in all further experiments.

3.4.1.2 Effects of Temperature and Time

The effects of temperature and time are shown in Figure 3.1. Incubation at 20 °C did not increase cATP concentrations as highly or as rapidly as at 37 °C, and therefore 37 °C was selected for further testing. Incubation of untreated *E. coli* samples at 37 °C showed the largest increase in cATP concentration from 2 to 4 hr, while incubation of UV-treated *E. coli* samples at 37 °C began to show an increase in cATP between 6 and 8 hr (Figure 3.1 A). ATP concentrations in untreated samples incubated at 37 °C appeared to plateau after 6 hr. As shown in Figure 3.1 B, this led to the apparent log-reduction in cATP with UV treatment being lower at 8 hr than at 4 or 6 hr. One of the stated criteria for our incubation

method was speed, to determine UV disinfection efficacy as quickly as possible, and since the improvement in log-reduction of cATP seen from 4 to 6 hr incubation time was not as great (1.74 ± 0.10 to 2.35 ± 0.15, Figure 3.1 B) as from 2 to 4 hr (0.49 ± 0.09 to 1.74 ± 0.10, Figure 3.1 B), 4 hr incubation time was chosen for further testing.

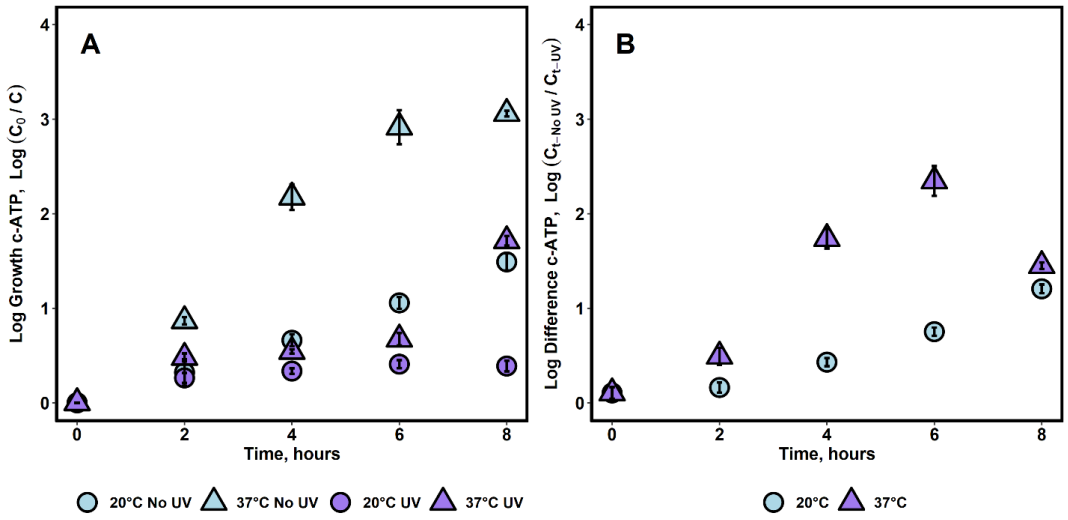

Figure 3.1: A) Effect of incubation time and temperature on cATP concentrations. Figure shows the log increase of cATP from 0 to 8 hr. Sample was a pure suspension of *E. coli*, and UV treatment was a 10 mJ cm^{-2} dose using an LP collimated beam. B) Log difference in ATP concentrations before and after UV treatment for *E. coli* suspension treated with a 10 mJ cm^{-2} dose

3.4.1.3 Effectiveness of Biomass Recovery Method for Pure Suspensions of E. coli

Cellular ATP quantification immediately prior to and after UV disinfection without pre-incubation of samples does not show any impact of UV treatment (Figure 3.2), as has been found by other researchers (First & Drake, 2014; Linklater & Örmeci, 2014; van Slooten et al., 2015). With the developed recovery method, it was observed that all points fall below

the y=x line on a graph of untreated versus UV-treated samples (Figure 3.2), indicating that UV-treated samples had significantly lower cATP concentrations than untreated samples after application of the biomass recovery method.

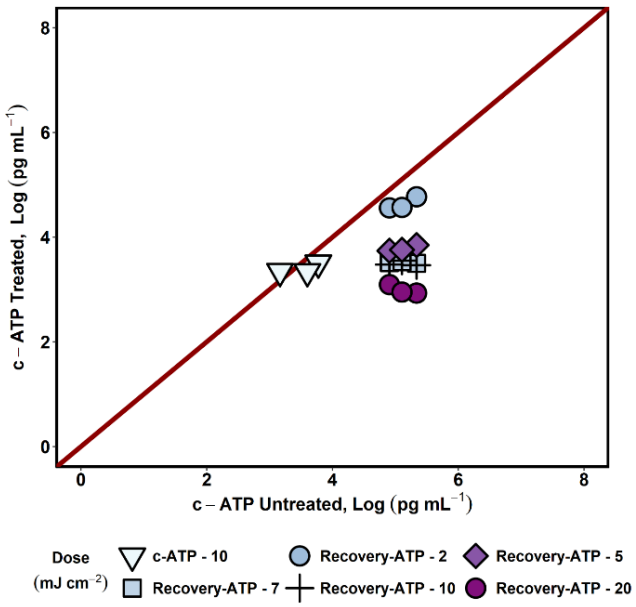

Figure 3.2: A comparison of untreated versus treated ATP using a standard ATP assay with and without the biomass recovery method for various UV doses. Disinfection was performed on pure suspensions of *E. coli*. UV dose for the c-ATP method was 10 mJ cm^{-2}

cATP concentrations following biomass recovery were also highly correlated to *E. coli* plate counts (Figure 3.3) that had a non-zero slope ($\alpha = 0.05$). An orthogonal regression found the equation of the first principal component to be $y = 2.57x - 4.09$ with the variance explained (VE) to be 0.958. The increased variance explained by the orthogonal regression is likely due to linear regressions only accounting for error in the y observations; whereas, the orthogonal regression accounts for error in both the x and y observations. Additionally,

UV dose and biomass recovery-ATP were found to be highly correlated ($R^2 = 0.889$) in the log linear phase (2-7 mJ cm^{-2}), and not as highly correlated ($R^2 = 0.574$) in the saturation phase (10-20 mJ cm^{-2}). The reduction in correlation in the saturation phase may indicate that the biomass recovery-ATP method has strong sensitivity for log-linear disinfection phase that are typical of a low UV dose.

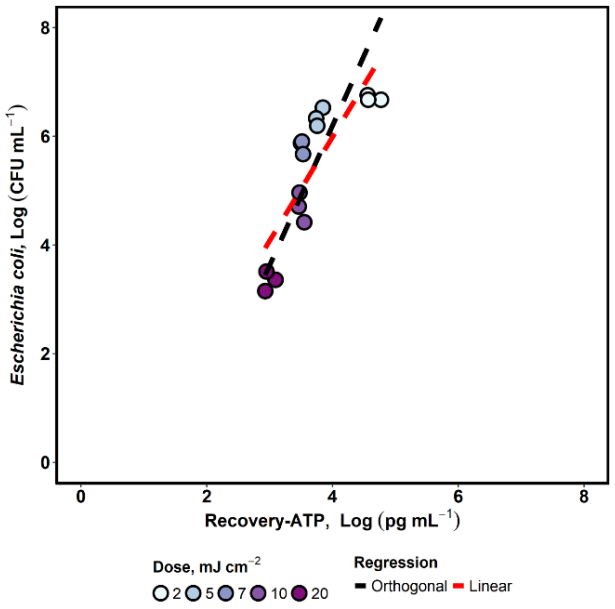

Figure 3.3: Regression of cATP concentrations on CFU across varying UV doses. Regressions performed on full data set

3.4.1.4 Effectiveness of Biomass Recovery-ATP Method for Real Water Samples

The developed biomass recovery ATP pre-treatment method was applied to samples taken from four municipal wastewater facilities employing UV disinfection as part of their treatment train. Figure 3.4 compares the UV-treated and untreated cATP concentrations found using direct ATP measurement and the biomass recovery-ATP method for these

facilities. These results confirm that direct ATP measurements are ineffectual at determining UV disinfection efficacy. Average log reductions in cATP were found to be -0.28 ± 0.19, -0.011 ± 0.153, -0.17 ± 0.32, and 0.065 ± 0.074 for direct ATP measurements for plants A, B, C, and D, respectively. No significant difference was found between direct ATP and biomass recovery-ATP measurements for facilities A and C (Figure 3.4), while facilities B and D showed clear differences between the two ATP testing methods. Average log reductions in cATP concentrations found using the biomass recovery method were 0.17 ± 0.34, 1.8 ± 0.76, 0.20 ± 0.35, and 0.72 ± 0.26 for facilities A, B, C, and D, correspondingly. This difference between facilities is likely related to differences in the microbial ecologies from plant to plant as well as lower disinfection efficacy at plants A and C. Log reductions in HPC were 0.54 ± 0.67, 0.76 ± 0.45, and 0.46 ± 0.47 for plants A, B and C, respectively, and log reduction in *E. coli* for facilities B and D was 3.2 ± 1.5 and 1.9 ± 0.70, respectively. Since the biomass recovery-ATP method depends on rapid growth of microorganisms during the incubation step, if the microbial community is largely made of slowly growing microorganisms, then it may be difficult to detect any differences using this method. Furthermore, if the disinfection at the plant is minimal, then both the untreated and UV-treated samples will grow at similar rates and ultimately show no log reduction in ATP even after biomass recovery. Facilities with lower disinfection efficiencies may benefit from extended incubation time from 4 to 6 hr, but this was not examined in the current study.

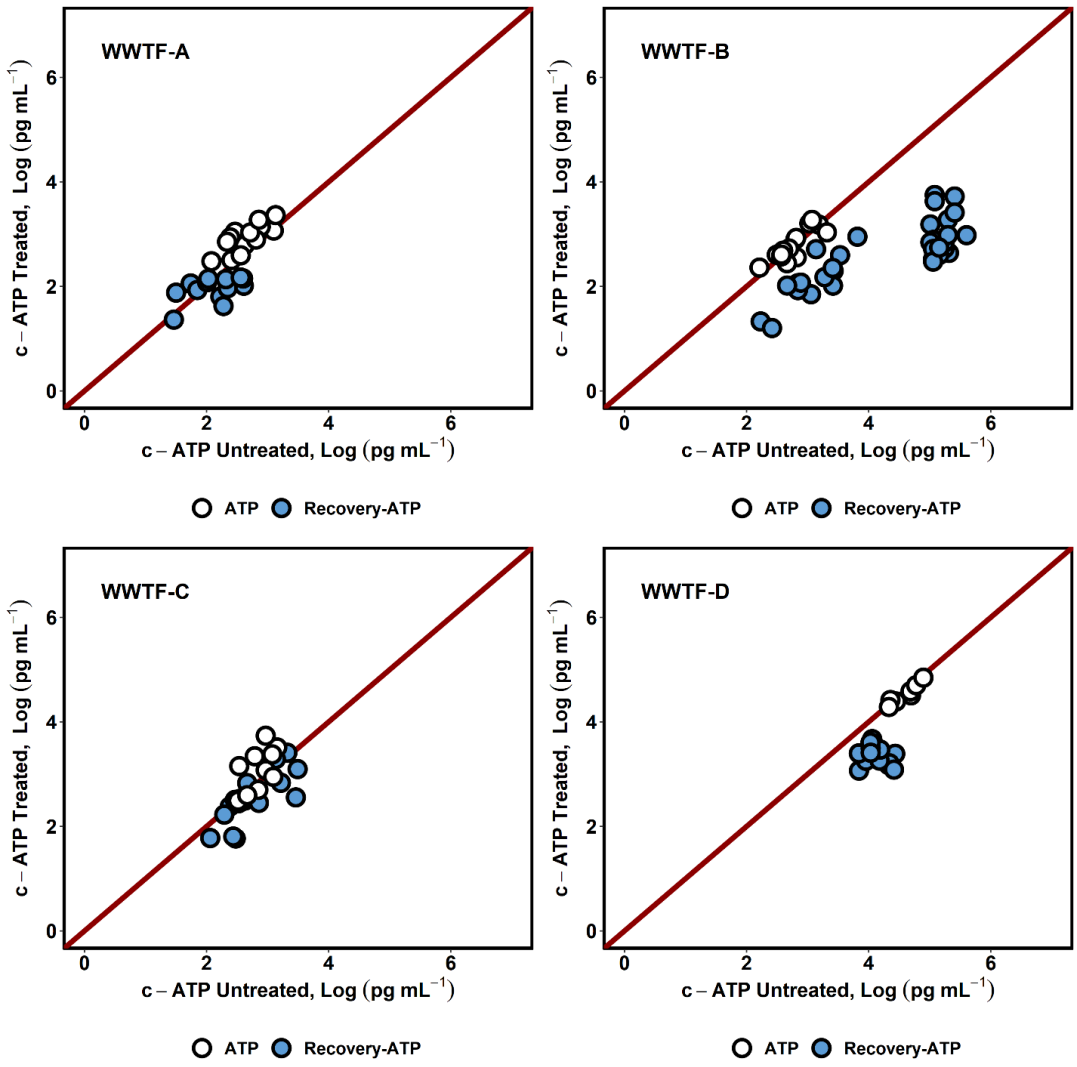

Figure 3.4: Effectiveness of biomass recovery method for four wastewater treatment facilities. Here untreated refers to water collected immediately before UV treatment at the plant and treated refers to samples collected immediately after the UV banks

Municipal wastewater samples from facilities B and D were also lab-treated using a UV collimated beam (Figure 3.5). A difference between untreated and UV-treated samples could be determined using the biomass recovery-ATP method for both plants across the range of doses. The response of each plant was unique, which may again be due to the difference in microbial populations between the plants. Moreover, the spread of the data

for each facility is likely due to the range disinfection efficiencies. For facility B at UV doses of 10 and 60 mJ cm^{-2} the log reductions in *E. coli* were 1.8 ± 0.64 and 3.0 ± 0.73, and the log reductions in biomass recovery-ATP were 1.7 ± 0.34 and 2.0 ± 0.45, respectively. Additionally, UV dose and recovery-ATP were found to be moderately correlated between the doses of 10 and 30 mJ cm^{-2} (R^2 = 0.132), and uncorrelated from doses 40 to 60 mJ cm^{-2} (R^2 = 0.02). For facility D for the same two doses the log reductions in *E. coli* and biomass recovery-ATP were found to be 0.96 ± 0.31 and 2.7 ± 0.82, and 0.47 ± 0.27 and 0.70 ± 0.29, respectively. Furthermore, UV dose and recovery-ATP had low correlation from 10 to 20 mJ cm^{-2} and again from 40 to 60 mJ cm^{-2}.

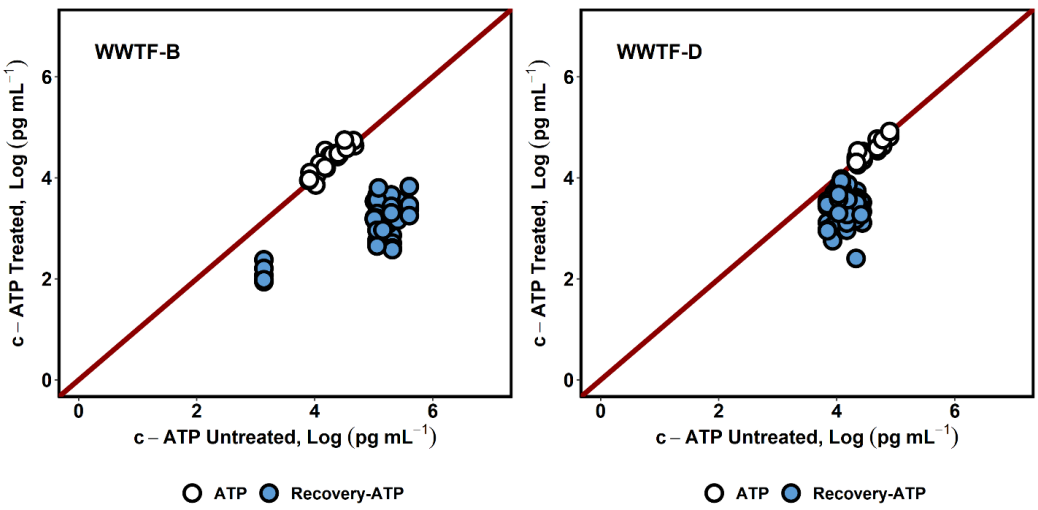

Figure 3.5: Effectiveness of biomass recovery method for two wastewater matrices and LP collimated beam for bench scale UV treatments. Treated samples range in UV doses from 10 to 60 mJ cm^{-2}

Figure 3.6 shows the disinfection curves with UV dose for total coliforms, *E. coli*, and biomass recovery-ATP, indicating a plateau for all three measurements. These plateaus, also know as the saturation phase, are typically seen in disinfection curves for wastewater

samples, and it is assumed that this phase in the curve results from particles in the water matrix producing a shielding effect for the microorganisms which limits the effectiveness of increased UV dose (Bolton and Cotton, 2011). The saturation phase seen in the recovery-ATP curves follow a similar trend to those of *E. coli* and total coliforms; however, the saturation phase for facility B occurs at a higher level versus facility D. This is likely resultant from the higher level of disinfection seen at facility B across the range of doses. Additionally, it is likely that the saturation phase seen for the biomass recovery-ATP results is not entirely due to particle shielding.

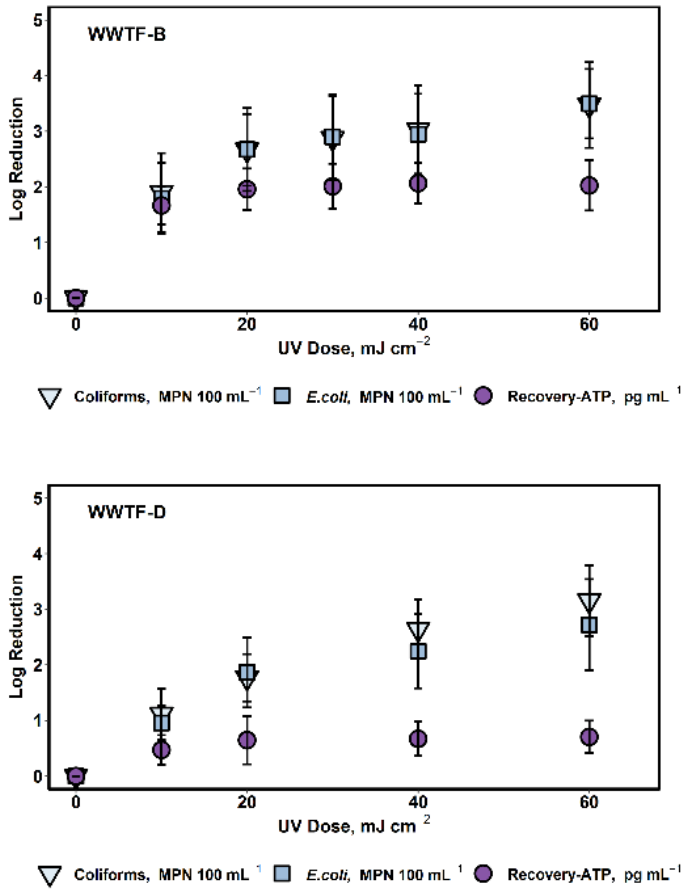

Figure 3.6: Disinfection curves for lab treated wastewater from facilities B and D

In the case of disinfection of pure *E. coli* suspensions, no saturation phase was observed in the CFU disinfection curve; however, a saturation phase was seen for the recovery-ATP curve (Figure 3.7).

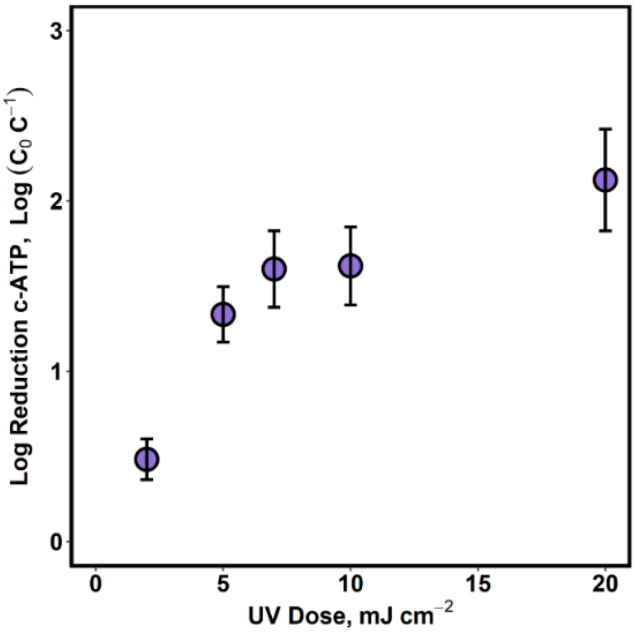

Figure 3.7: Log reductions in c-ATP concentrations for pure *E. coli* culture over a range of UV doses. A log linear phase is observed from a dose of 2 to 7 mJ cm^{-2}, with a shouldering phase observed from a dose of 7 to 20 mJ cm^{-2}

This saturation phase was conceivably due to using microbial growth as the main mechanism of the biomass recovery method. In this method, the untreated sample grows rapidly, often towards a plateau determined by the carrying capacity of the growth media. At the same time, the UV-treated samples will grow at a reduced rate relative to the UV dose. The difference in these two growth rates is what determines the final log reduction reported in the biomass recovery-ATP method. Thus, the saturation phase observed for the biomass recovery-ATP method may also be a result of when UV dose hinders any

significant growth in the treated sample, and thus the difference in ATP after grow-out between untreated and UV-treated samples remains the same with further increases in dose. This observation may show a limited ability for the biomass recovery-ATP method to distinguish between UV dose at higher doses but shows that it is capable of determining a threshold for required UV dose to hinder growth. This threshold may not hold importance for utilities using the method as a management tool but could provide researchers with insight on how UV radiation hinders growth of different microorganisms. However, further research would be required to better quantify this threshold to better understand its significance.

3.4.2 Biomass Recovery-ATP versus Standard Measurements in Wastewater Samples

Cellular ATP measurements have previously been shown to correlate to HPC in water samples (Deininger & Lee, 2001; Delahaye et al., 2003); however, correlation between HPC and cATP for UV-treated wastewaters has not been investigated due to lack of change in ATP concentration with treatment (First & Drake, 2014; Linklater & Örmeci, 2014; van Slooten et al., 2015). In this study it was observed that biomass recovery-ATP and HPC values were significantly correlated for treatment facilities A, B, and C (Figure 3.8). The equations of the lines using linear regression for facilities A, B, and C were found to be $0.918x + 2.54$ ($R^2 = 0.323$; p-value < 0.01), $0.859x + 2.22$ ($R^2 = 0.824$; p-value < 0.001) and $0.452x + 3.37$ ($R^2 = 0.228$; p-value < 0.05), respectively. The equations of the lines using orthogonal regression for facilities A, B, and C were found to be $2.21x - 0.12$ (VE = 0.838), $0.942x + 2.01$ (VE = 0.954) and $0.891x + 2.14$ (VE = 0.740), respectively. These

results indicate that incoming water matrix has a determining effect on the outcome of the biomass recovery-ATP test.

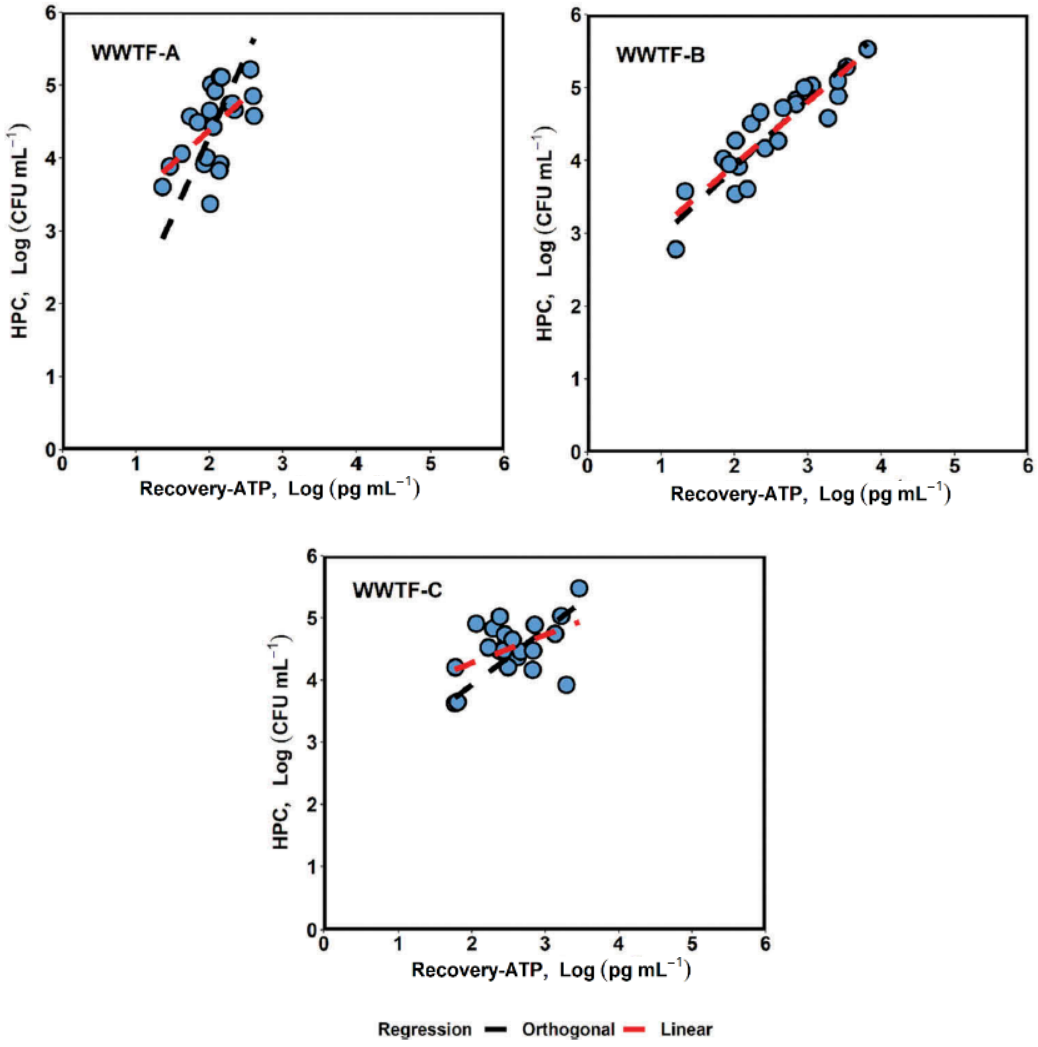

Figure 3.8: Linear and orthogonal regression fits between biomass recovery-ATP and HPC for untreated and UV-treated samples from wastewater treatment facilities A, B, and C

Similar findings were observed when comparing *E. coli* MPN and ATP for both plant and lab treated samples (Figure 3.9). The fits of the regressions were observed to be different between the plants. The lab treated samples follow the same trend as the plant but added

expanded the effect of different UV doses (Figure 3.9). The equations of the lines using linear regression for facility B plant and lab treated samples were found to be 0.871x + 0.869 (R^2 = 0.680; p-value > 0.05) and 0.867x + 0.342 (R^2 = 0.570; p-value <0.01), and using orthogonal regressions were found to be 1.07x + 0.09 (VE = 0.912) and 1.20x – 0.75 (VE = 0.880), respectively. For facility D, plant and lab treated samples linear correlations were found to be 2.34x – 5.41 (R^2 = 0.755; p-value > 0.05) and 1.92x – 5.93 (R^2 = 0.547; p-value <0.001), and orthogonal regressions were found to be 3.00x – 7.90 (VE = 0.973) and 3.28x – 12.2 (VE = 0.946), respectively.

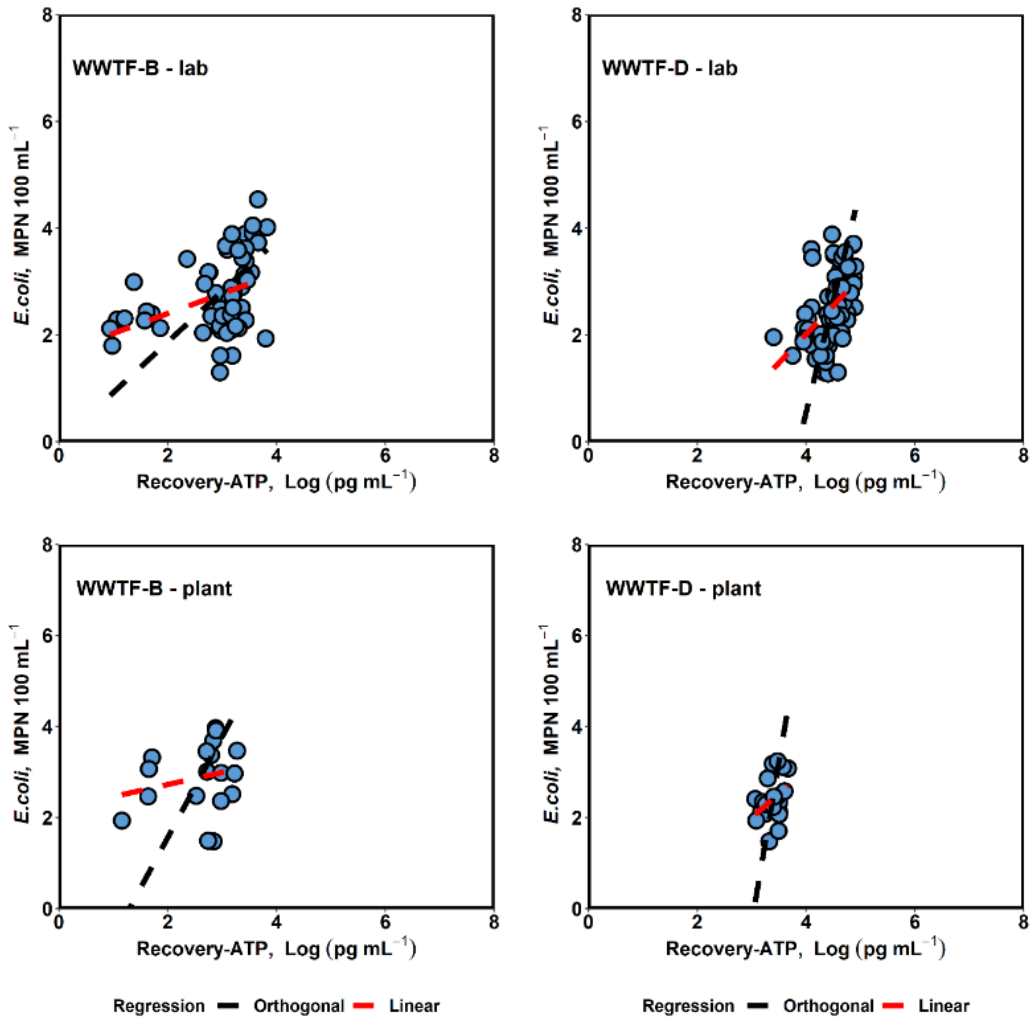

Figure 3.9: Linear and orthogonal regression fits between biomass recovery-ATP and *E. coli* MPN for two treatment facilities. The first and second column present treatment facilities B and D, respectively

These findings further indicate the importance the incoming water matrix has in the outcome of the biomass recovery-ATP test and that site-specific calibrations should be performed. This could be done by developing a historical record of standard methods (HPC, Colilert, etc.) paired with the biomass recovery-ATP method to determine what results indicate poor or good UV disinfection performance.

3.5 CONCLUSION

ATP testing coupled with the biomass recovery method was able to determine efficacy of UV treatment with regards to inactivation of microbes within one 8 hr shift. This is compared to traditional technologies which require 24 hr incubation at minimum, while the test developed in this work was effective with 4 hr of incubation time. Optimal incubation media, time, and temperature were determined, and the method was shown to be effective at determining differences before and after UV disinfection for pure *E. coli* cultures and real municipal wastewater samples.

The biomass recovery method was found to correlate strongly to both Colilert® and HPC methods, and it was concluded that the incoming water matrix has a large impact on results of the method. Thus, it is recommended that operators determine site-specific context for the biomass recovery-ATP results by building a historical record comparing the results to standard enumeration techniques.

3.6 AKNOWLEDGEMENTS

The authors would like to acknowledge and extend thanks for the financial support provided through the NSERC/Halifax Water Industrial Research Chair in Water Quality & Treatment at Dalhousie University. Funding partners for this Industrial Research Chair program include the Natural Science and Engineering Council of Canada (NSERC), Halifax Water, LuminUltra Technologies Ltd., Cape Breton Regional Municipality Water Utility, CBCL Ltd., Agat Laboratories Ltd., and Mantech Inc. Additional funding for this work was received from the NSERC Discovery Grant program. Dr. Mackie would also like to acknowledge funding received from NSERC's Postdoctoral Fellowship program. The

authors also thank Heather Daurie, Nicole Allward, and Dr. Ben Trueman for their technical support,

3.7 REFERENCES

APHA, AWWA, & WEF. (2012). *Standard Methods for the Examination of Water and Wastewater*. District of Columbia: American Public Health Association.

Baron, J., & Bourbigot, M. M. (1996). Repair of Escherichia coli and enterococci in sea water after ultraviolet disinfection quantification using diffusion chambers. *Water Research*, *30*(11), 2817–2821. https://doi.org/10.1016/S0043-1354(96)00159-5

Ben Said, M., Masahiro, O., & Hassen, A. (2010). Detection of viable but non cultivable Escherichia coli after UV irradiation using a lytic Qβ phage. *Annals of Microbiology*, *60*(1), 121–127. https://doi.org/10.1007/s13213-010-0017-4

Bolton, J. R., & Linden, K. G. (2003). Standardization of Methods for Fluence (UV Dose) Determination in Bench-Scale UV Experiments. *Journal of Environmental Engineering*, *129*(March), 209–215. https://doi.org/10.1061/(ASCE)0733-9372(2003)129:3(209)

Chang, J. C., Ossoff, S. F., Lobe, D. C., Dorfman, M. H., Dumais, C. M., Qualls, R. G., & Johnson, J. D. (1985). UV inactivation of pathogenic and indicator microorganisms. *Applied and Environmental Microbiology*, *49*(6), 1361–1365. Retrieved from http://www.ncbi.nlm.nih.gov/pubmed/2990336

Deininger, R. A., & Lee, J. Y. (2001). Rapid Determination of Bacteria in Drinking Water Using an ATP Assay. *Field Analytical Chemistry and Technology*, *5*(4), 185–189. https://doi.org/10.1002/fact.1020

Delahaye, E., Welté, B., Levi, Y., Leblon, G., & Montiel, A. (2003). An ATP-based method for monitoring the microbiological drinking water quality in a distribution network. *Water Research*, *37*(15), 3689–3696. https://doi.org/10.1016/S0043-1354(03)00288-4

First, M. R., & Drake, L. A. (2014). Life after treatment: Detecting living microorganisms following exposure to UV light and chlorine dioxide. *Journal of Applied Phycology*, *26*(1), 227–235. https://doi.org/10.1007/s10811-013-0049-9

Lazarova, V., Janex, M. L., Fiksdal, L., Oberg, C., Barcina, I., & Pommepuy, M. (1998). Advanced wastewater disinfection technologies: short and long term efficiency. *Water Science and Technology*, *38*(12), 109 LP-117. Retrieved from http://wst.iwaponline.com/content/38/12/109.abstract

Lee, J. Y., & Deininger, R. A. (2004). Detection of E. coli in beach water within 1 hour using immunomagnetic separation and ATP bioluminescence. *Luminescence*, *19*(1), 31–36. https://doi.org/10.1002/bio.753

Linklater, N., & Örmeci, B. (2014). Evaluation of the adenosine triphosphate (ATP) bioluminescence assay for monitoring effluent quality and disinfection performance. *Water Quality Research Journal of Canada*, *49*(2), 114–123. https://doi.org/10.2166/wqrjc.2013.110

Middleton, B. (2017). *Analysis of ultra-violet disinfection on microbial activity and validation of rapid testing methods*. Dalhousie University.

van Slooten, C., Wijers, T., Buma, A. G. J., & Peperzak, L. (2015). Development and testing of a rapid, sensitive ATP assay to detect living organisms in ballast water. *Journal of Applied Phycology*, *27*(6), 2299–2312. https://doi.org/10.1007/s10811-014-0518-9

Villaverde, A., Guerrero, R., & Barbe, J. (1986). Microbiology ATP Production after Ultraviolet Irradiation in Escherichia coli. *Current Microbiology*, *14*, 31–34.

Xie, X. (2014). *Development of a rapid ATP analysis method: biomass growth ATP method for UV disinfection monitoring in wastewater treatment*. Dalhousie University.

Zhang, S., Ye, C., Lin, H., Lv, L., & Yu, X. (2015). UV disinfection induces a vbnc state in escherichia coli and pseudomonas aeruginosa. *Environmental Science and Technology*, *49*(3), 1721–1728. https://doi.org/10.1021/es505211e

CHAPTER 4: IMPACT OF UV-LED CHARACTERIZATION ON INACTIVATION RATE CONSTANTS

4.1 ABSTRACT

UV-LEDs are an emerging technology and are inherently different then traditional mercury-based technologies. This portion of the study examined how peak wavelength, the spectral nature and intensity characterization instruments impacted inactivation rates. It was found that the peak wavelength of the UV-LED greatly impacted the inactivation rates reported. Furthermore, the spectral outputs of the UV-LEDs were found to have no impact on the inactivation rates for the water matrix used. When examining measurement by means of different instruments, it was discovered that intensity determination by means of a radiometer over estimated the dose when compared to a spectrometer and a ferrioxalate actinometer. Consequently, the inactivation rates were underestimated when a radiometer was used. The inactivation rates in this study were compared to those in the literature, and it was found that the values often fell within the range. However, the range of values reported was large, which may be due to the lack of a standard protocol for UV-LED based systems. A protocol that accounts for the unique features of UV-LEDs that accurately determines the UV dose for UV-LED collimated beam apparatus was suggested.

KEYWORDS: UV Disinfection, UV-LEDs, *E. coli* inactivation, UV dose, standard methods,

4.2 INTRODUCTION

One of the benefits of UV-LEDs is that they increase the wavelengths available to use for treatment. Traditional mercury-based technologies have output spectra that are either monochromatic at 254 nm or spectral if a low pressure or medium pressure lamp is used,

respectively. Greater disinfection efficiencies have been reported when using medium pressure lamps compared to low pressure, and attributed to the wavelengths other than 254 nm in the UV spectrum (Beck, Rodriguez, et al., 2016). As LEDs can be produced at wavelengths ranging from 210 nm into the visible light spectrum (Shur & Gaska, 2010), it is conceivable to isolate the impacts of different wavelengths using UV-LEDs (Beck et al., 2017).

However, some unique challenges surrounding determining UV dose have arisen due to the nature of UV-LEDs. The way the energy is delivered to the system using UV-LEDs is fundamentally different than that of the mercury-based systems (Kheyrandish, Mohseni, & Taghipour, 2017), and many studies have just adopted the standard method by Bolton & Linden (2003) developed for the latter. However, this method uses instruments that were designed to measure intensity at 254 nm and for a monochromatic light output, which may not accurately account for shifts in peak wavelength or the spectral nature of UV-LEDs, all of which could impact important factors used to calculate UV dose. As of yet, there has been no standard protocol accepted by the UV-LED community, and methods of UV dose determination greatly vary from one study to another (Song, Mohseni, & Taghipour, 2016). This adds difficultly when comparing treatments between studies.

4.3 OBJECTIVES

The objectives of this study were to examine the impact that UV-LED peak wavelength, spectral distribution and intensity measurement instrument had on computed inactivation rates of *E. coli*. Furthermore, this study was undertaken with the purpose of determining an optimal method for determining UV dose for disinfection studies completed with UV-LED CBAs.

4.4 MATERIALS AND METHODS

Peak wavelengths and spectral distributions of three UV-LEDs were determined using a spectrometer. Average UV intensities were determined using three measurement tools: a radiometer, a spectrometer, and a chemical actinometer. UV dose-response curves were developed for a pure culture of *E. coli*, and inactivation rate constants were calculated based on the log linear region of the dose-response curves using both radiometer and spectrometer intensity measurements.

4.4.1 Microbial Methods

All growth media and agars were prepared according to instructions provided by the manufacturers and autoclaved at 121 °C for 15 min to ensure sterility (AMSCO Lab 250, Steris Co, United Kingdom). All glassware was triple rinsed with DI water and autoclaved for sterility. Phosphate buffered saline (PBS) solution was prepared in accordance with *Standard Methods for the Examination of Water and Wastewate*r (APHA, AWWA, and WEF 2012) and autoclaved before use. PBS solution was used for cell cleaning and suspension dilution.

4.4.1.1 Glycerol Stock Preparation

New glycerol stocks of *E. coli* K12 (ATCC 47076; Centre for Research in Environmental Microbiology, University of Ottawa) were prepared for this study from previous stocks. To begin, the old stocks were streak plated on Tryptic Soy Agar (TSA; Becton Dickinson and Co., MD, USA) and then incubated at 37 °C overnight. A single colony was then aseptically removed from the plate and placed in 9 mL of sterile Tryptic Soy Broth (TSB; Becton Dickinson and Co., MD, USA). The inoculated TSB was then incubated at 37 °C for 18 – 24 hr After the incubation, 1 mL of the overnight culture was used to inoculate fresh TSB

and incubated at 37 °C for 4 hr. After incubation, equal parts of the 4-hr culture were mixed with sterile 50% glycerol in a 2 mL cryovial and stored at -80 °C.

4.4.1.2 Growth Curve

A growth curve was developed for *E. coli* (Figure 4.1 A). The day before the glycerol stock was diluted 100-fold in sterile TSB and incubated at 37 °C overnight. The next morning, the overnight culture was once again diluted 100-fold in 100 mL of sterile TSB and incubated at 37 °C. Samples were taken periodically over 24 hr. At each time point, the culture was enumerated for colony forming units (CFU) by means of spread plating the sample on TSA plates, and measured for OD600 using a Hach DR 5000 spectrophotometer. CFU concentrations were collect as singlets, and OD600 measurements were collected in duplicate. The resultant plot (Figure 4.1 B) were used in subsequent experiments to verify and quantify the growth phase and concentration of cells using OD600 measurements.

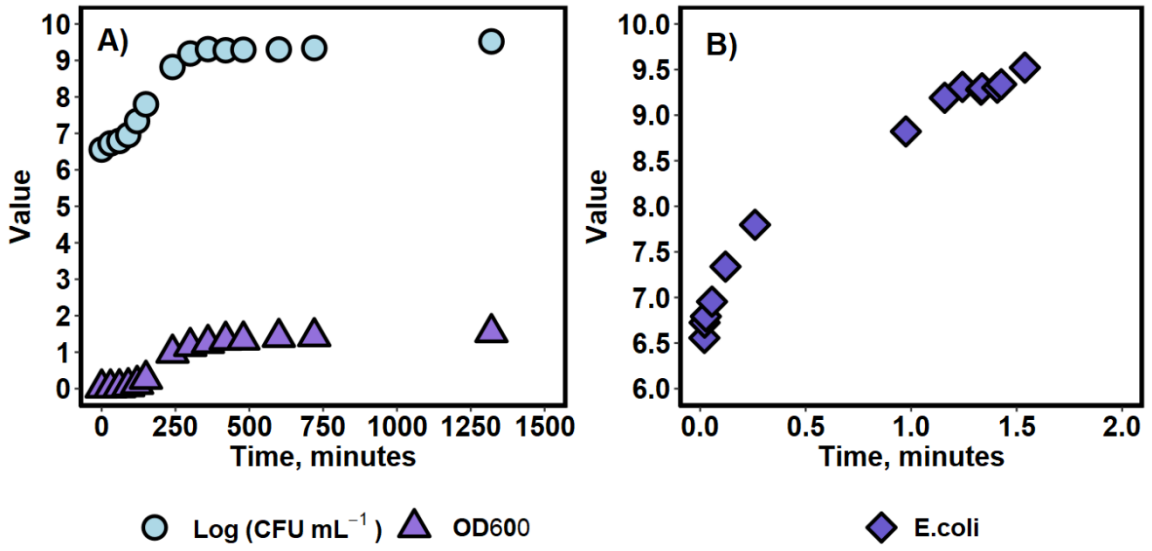

Figure 4.1: A) Growth curves for *E. coli*. Value is either Log of CFU mL^{-1} or OD600 and B) Log of CFU mL^{-1} vs. OD600

4.4.1.3 E. coli Working Solution

On the day prior to running an experiment, 0.5 mL of an *E. coli* glycerol stock was used to inoculate 9 mL of TSB, which was then incubated at 37 °C overnight. The following morning, 1 mL of the overnight culture was suspended in 9 mL of TSB and incubated at 37 °C for approximately 4 hr to ensure the culture was in the late exponential growth phase. The growth phase was verified by previously developed OD600 - CFU growth curves. After incubation, cells were pelleted in sterile 15 mL polypropylene tubes at 3500 RPM for 10 min. The supernatant was removed, and the cells were washed three times by vortexing in approximately 10 mL of PBS at 3000 RPM for 2 min. After the final wash, the cells were resuspended in sterile PBS to achieve a working solution concentration of approximately 10^6 CFU $mL^{-1.}$

4.4.1.4 Enumeration Techniques

A standard plate count (SPC) was used to enumerate pure suspensions of *E. coli*. 10-fold serial dilutions in PBS were used to achieve proper dilution levels prior to plating on sterile TSA plates. Samples were plated using an ethanol flame sterilized glass rod to spread 0.1 mL of sample evenly across the surface of the agar. The plates were incubated at 37 °C for 18 to 24 hr. After the desired incubation time was achieved, plates with colony counts between 0-300 colony forming units (CFU) were counted with the aid of a Quebec colony counter (American Optical Company, NY, USA).

4.4.2 UV-LED Collimated Beam Characterization

4.4.2.1 Radiometer

A modified Bolton method (Bolton & Linden, 2003) was used to determine the UV dose for the UV-LED collimator. The measure irradiance was collected using the radiometer

with 60 s integrations. Irradiance measurements were collected without the fibre optic attachment and corrected with the factors described by Bolton & Linden (2003).

The divergence factor corrects for the divergence of the light and is calculated using Equation 4.1

$$\boldsymbol{D.F.} = \boldsymbol{L}/(\boldsymbol{L}+\boldsymbol{l}) \quad \textbf{(4.1)}$$

Where L is the length from the LEDs to the surface of the water in cm, and l is the pathlength of the water being treated in cm.

The reflection factor is applied to correct for light lost due to reflectance, and is defined as 1-R, where R is the fraction of light reflected. The R value is based on Fresnel Law and is determined by the reflective indices of the two media at the interface. In this case, the two media at the interface are air and water with respective refractive indices of 1.000 and 1.372. These indices give an R value of 0.025, and ultimately a RF of 0.975.

The sensitivity factor, *S.F.*, which accounts for the relative sensitivity of the radiometer at different wavelengths, is calculated using Equation 4.2.

$$\boldsymbol{S.F.} = \boldsymbol{I_{\lambda}}/\boldsymbol{I_{254nm}} \quad \textbf{(4.2)}$$

where I_{λ} is the relative intensity at the wavelength of interest in arbitrary units, and I_{254} is the relative intensity at 254 nm in arbitrary units. Intensity spectrums for the radiometer were provided by Calgon and resulted in S.F.s of 0.75, 0.85 and 0.43 for the 255, 265 and 285 nm UV-LEDs, respectively.

The Petri factor is the ratio of the average intensity over the surface area of the sample being treated and the intensity at the center of the collimator. This factor allows for the user to determine the average intensity based on a single intensity measurement taken at the centre of the collimator. The Petri factors used in this part of the study were developed by previous students. These students collected intensity measurements over a 6 cm square area with a 1 cm spatial resolution using the radiometer and were calculated using Equation 4.3. Petri factors of 0.638, 0.667 and 0.655 were used for the 255, 265 and 285 nm UV-LEDs, respectively.

$$\boldsymbol{P.F. = I_{avg}/I_0} \tag{4.3}$$

Finally, the average intensity was corrected with the water factor, as described by Equation 4.4.

$$\boldsymbol{W.F. = \left(1 - 10^{-A_{1cm} \times l}\right)/\left(2.303 \times A_{1cm} \times l\right)} \tag{4.4}$$

where A_{1cm} is the measured absorbance though a 1 cm pathlength at 254 nm, and l is the total pathlength of the water being treated. Exposure time for required UV dose was determined by dividing the required dose by the actual intensity.

Explicitly the average intensity for the UV-LEDs was determined as the product of the measured intensity and all four of the previous mentioned factors using Equation 4.5.

$$\boldsymbol{I_{avg} = I_0 \times D.F. \times S.F. \times P.F. \times W.F.} \tag{4.5}$$

4.4.2.2 Spectrometer

Intensity profiles and spectral outputs were collected for the UV-LED CBA using a USB4000 spectrometer and the SpectraSquite software (Ocean Optics Inc., Fl, USA). The spectrometer used a fibre optic with an active diameter of 3900 μm, a grating of 600 lines blazed at 300 nm, a slit size of 25, and used a DET4- 200-850 detector. Profiles were collected 10 cm from the edge of the 22 cm collimator over a 6 × 6 cm square grid with a spatial resolution of 0.5 cm (Figure 4.2). Intensity profiles were developed for each the 255, 265, and 285 nm wavelengths.

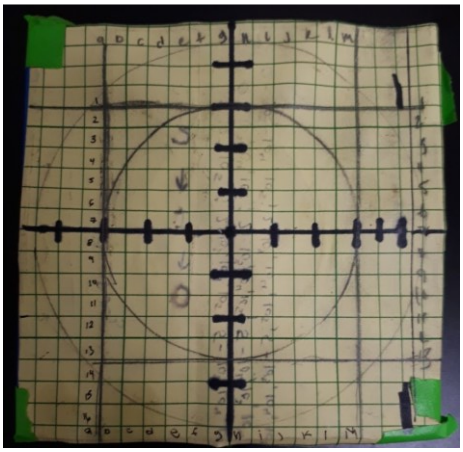

Figure 4.2: Grid arrangement for intensity profiles collected with the spectrometer

Integration times of 10, 7 and 5 s were used for the 255, 265, and 285 nm LEDs, respectively. Furthermore, 3 scans were collected to average and smooth the curve. To convert the collected data from relative absolute intensity to total measured intensity under the entire curve, a rectangular integration technique was used from 250-400 nm in the Spectra Suite software.

Intensity profile areas were reduced to a near circular area with the same dimensions of the base of the 250 mL treatment beaker. The average intensity over this area was then used as

the measured intensity in further dose calculations. The actual intensity was calculated using Equation 4.6.

$$\mathbf{I}_{act} = I_{avg} \times \mathbf{D.F.} \times \mathbf{R.F.} \times \mathbf{W.F.} \quad \textbf{(4.6)}$$

where I_{avg} is defined as the average intensity over the treatment area in mW cm^{-2}; and *D.F.*, *R.F.* and *W.F.* are the same divergence factor, reflectance factor and water factor as described in section 4.4.2.1.

4.4.2.3 Ferrioxalate Actinometry

The Bolton ferrioxalate actinometry method (Bolton, Stefan, Shaw, & Lykke, 2011) was used to determine intensity of the 255, 265 and 285 nm UV-LEDs. The ambient temperature in the room fluctuated between 20 and 22 °C over the course of the experiments. Due to the extreme photosensitivity of the actinometer, all experimental work was completed under subdued red light, with all precautions taken to ensure no ambient light from outside rooms leaked in.

4.4.2.3.1 Chemical Reagents

Six solutions were prepared to conduct the actinometry. A 0.2 M ferric sulfate in 2 N H_2SO_4 was prepared by slowly adding 14 mL of concentrated sulfuric acid to 100 mL of DI water in a 250 mL volumetric flask, and then adding 25 g of $Fe_2(SO_4)_3$. The neck of the bottle was washed with a small amount of DI and then the volume was brought up to the 250 mL mark. After topping up, a small stir bar was added, and the flask was placed on a magnetic stir plate and mixed until the ferric sulfate was completely dissolved. The solution was then stored in an amber bottle. A 1.2 M potassium oxalate solution was prepared by adding 55.26 g of $K_2C_2O_4 \cdot H_2O$ to a 250 mL volumetric flask, and slowing adding DI up to the 250

mL mark. A pH 4.5 sodium acetate solution was prepared by adding 20.5 g of $CH_3COONa \cdot 3H_20$ to a 250 mL volumetric flask containing approximately 100 mL of DI. The solution was mixed until the sodium acetate was completely dissolved, and then 2.5 mL of concentrated sulfuric acid was carefully added. DI water was then used to bring the solution up to the 250 mL mark. A 0.2% 1, 10-Phenanthroline solution was prepare by adding 0.5 g of the compound to a 250 mL flask and adding DI water up to the mark. The flask was then mixed using a magnetic stir bar and plate until the solution was completely mixed. The solution was stored in an amber bottle due to its photosensitivity. A 1 M hydroxylamine hydrochloride solution was prepared by adding 6.95 g of $NH_2OH \cdot HCl$ in to 100 mL volumetric flask and bringing the solution up to the mark with DI water. A 2 M sulfuric acid solution was prepared by slowly adding 14 mL of concentrated H_2SO_4 to 125 mL of DI water in a 250 mL volumetric flask. The solution was then brought up to the mark with DI water.

4.4.2.3.2 Ferric sulfate solution concentration

Prior to experimentation, the concentration of the ferric sulfate solution was confirmed in duplicate by the following method. In a new 100 mL volumetric flask, 0.300 mL of the ferric sulfate solution was added, and the solution was brought to the mark with DI water. 0.8 mL of this solution was added to a 10 mL volumetric flask, along with 2 mL of DI water and 1 mL of the 1 M hydroxylamine hydrochloride solution. This solution was mixed for 2 min, and then 2 mL of each sodium acetate buffer and the 0.2% 1, 10-Phenanthroline solutions were added, and the flask was left to react for 40 min. After the reaction time, the solution was brought up to the mark with DI water. The procedure for the 10 mL solution was repeated but replaced the 1 mL of the 1M hydroxylamine hydrochloride with 1 mL of

DI water. The second sample was used as the blank. The concentration of Fe^{3+} ions was then determined using Equation 4.7.

$$[\boldsymbol{Fe^{3+}}] = (\boldsymbol{A - A_b}) * \boldsymbol{375} \quad \textbf{(4.7)}$$

where A is the absorbance at 510 nm of the sample with the hydroxylamine hydrochloride, and A_b is the absorbance at 510 nm of the sample without the hydroxylamine hydrochloride. Using this method, the molar concentration of Fe^{3+} ions was found to be 0.3993 M.

4.4.2.3.3 Experimental

A fresh 0.0060 M potassium ferrioxalate in 0.1 N H_2SO_4 solution (FeOx) was prepared at the beginning of each experimental day by first adding 15.2 mL of the potassium oxalate solution and 35 mL of the 2 M sulfuric acid solution to approximately 800 mL of DI water in a 1 L volumetric flask and mixed gently. Next, 15 mL of the ferric sulfate solution was added, and then the solution was brought up to the fill mark with DI water. The solution was thoroughly mixed and placed in an amber bottle.

For each UV-LED, 4 different exposure times were used to determine the intensity of the system. The UV-LED collimator was set with a 250 mL beaker placed directly in the center with the surface of the FeOx solution 10 cm from the edge of the collimator. The diameters of the 250 mL beakers used for treatment were measured with a digital caliper, and the average surface area for treatment was calculated to be 32.5 ± 0.2 cm^2 (n=5). Given this surface area, 32.5 mL of the FeOx solution was used in each treatment to give a pathlength of 1 cm. Exposure times used for each UV-LED can be found in Table 4.1. An additional fifth beaker was portioned but left unexposed to light and used as a control.

Table 4.1: Exposure times for three wavelengths used in actinometry experiment

Wavelength, nm	*Exposure Time 1, s*	*Exposure Time 2, s*	*Exposure Time 3, s*	*Exposure Time 4, s*
255	480	600	720	840
265	180	240	300	360
285	60	120	180	240

After exposure, 2 mL of the sodium acetate buffer, 2 mL of the 1,10-Phenanthroline solution and 1 mL of the FeOx solution were added to a 10 mL volumetric flask. The solution was brought up to the mark with DI water, and was placed in the dark for 40 min. After the 40 min, each sample was measured in duplicate for absorbance at 510 nm. Linearity over the range of exposure times was examined to ensure the quality of the results. Intensities were calculated from the absorbances using Equations 4.8 – 4.10.

$$\left[\boldsymbol{Fe^{2+}}\right] = ((\boldsymbol{A_t - A_b}) * \boldsymbol{10} * \boldsymbol{V})/(\boldsymbol{11,100},* \boldsymbol{V_1}) \quad \textbf{(4.8)}$$

where $[Fe^{2+}]$ is the moles of Fe^{2+} formed, A_t is the absorbance at 510 nm of the sample after exposure time t, and A_b is the absorbance at 510 nm of the sample blank. V is the total volume of FeOx irradiated, $11,100$ is the molar absorption coefficient of the formed complex in M^{-1} cm^{-1}, and V_1 is the volume withdrawn from the treated solution in mL.

$$\boldsymbol{U_\lambda = h * c * N_A / \lambda} \quad \textbf{(4.9)}$$

where U_λ is the energy per Einstein at a given wavelength λ, h is the Planck constant defined as $6.62606896 \times 10^{-34}$ J s, c is the speed of light defined as 2.9972458×10^{8} m s^{-1}, N_A is the Avogadro number defined as $6.02214179 \times 10^{23}$ mol^{-1}, and λ is the wavelength in m.

$$I_t = (\left[Fe^{2+}\right] * U_\lambda)/(\phi Fe(II) * R * t * A) \quad \textbf{(4.10)}$$

where I_t is the intensity of the light source after exposure time t, $\phi Fe(II)$ is the wavelength dependant quantum yield of the actinometer solution, R is defined as the reflection coefficient defined as 0.975, t is the exposure time in s, and A is the total treated surface area in cm^2. Quantum yields used in this study were 1.26, 1.25 and 1.25 for the 255, 265, and 285 nm LEDs, respectively (Goldstein & Rabani, 2008). Final intensities reported were the average from all the exposures for each UV-LED used.

4.4.3 UV-LED Disinfection Treatment

UV disinfection was performed using a Pearl Beam UV-LED CBA (AquiSense Technologies, Erlanger, KY, USA). The UV-LED system had a 22 cm collimator (Figure 4.3 A) and used 5 LEDs at 3 wavelengths. Specifically, these are 2 - 265 nm, 2 - 285 nm and 1 - 255 nm UV-LEDs (Figure 4.3 B). Furthermore, the system allowed for any single wavelength to be toggled on via a control box (Figure 4.3 C).

Figure 4.3: A) UV-LED collimated beam apparatus, B) UV-LED light sources and C) UV-LED collimator shutter control box

4.4.3.1 Dose-Response Curves

UV dose-response curves were collected for pure suspensions of *E. coli* for each UV-LED. Doses of 2, 5, 7, 10 and 20 mJ cm^{-2}. Doses were calculated using a radiometric method. All treatments were performed in triplicate, and work was completed under subdued red light when possible to reduce the effects of photoreactivation. All treatments and controls were enumerated using SPC methods described in section 4.4.1.4.

4.4.4 Statistical Methods

Chick-Watson models (Eq. 4.11) were used to determine inactivation kinetics. The disinfection rate constant, k, is the calculated slope of the dose-response curve in the region where the log response is linear with respect to the UV dose. The log linear sections of the Chick-Watson curves were determined visually using the LOESS regression method in the geom_smooth plotting function in the ggplot library in R when the dose-response curve was not linear throughout the dose range. Chick-Watson models were developed using SPC as the response to the dose.

$$\boldsymbol{Log\ (\frac{N_D}{N_0}) = kD} \tag{4.11}$$

where N_D is defined as the concentration of microorganism after exposure to the dose, N_0 is defined as the initial concentration of microorganisms, k is defined as the disinfection rate constant in $cm^2\ mJ^{-1}$, and D is defined as the UV dose in mJ cm^{-2}.

4.5 RESULTS AND DISCUSSION

4.5.1 Impact of Peak Wavelength on Dose Calculation

In this study it was found that some of the peak wavelengths measured differed from the values reported by the manufacturer. For instance, the 255 nm UV-LED actually had a peak

value of 260 nm, the 265 nm UV-LED had a peak wavelength at 268 nm, and the 285 nm wavelength was found to have an actual peak wavelength at 285 nm (Figure 4.4). A previous study by Kheyrandish, Mohseni, & Taghipour (2017), reported findings similar to this. All UV-LED spectra followed Gaussian distributions as expected (Chen, Loeb, & Kim, 2017). In this case, it appears that the manufacturer may have reported nominal wavelength peaks, rather than the actual. This may have been done to show a greater difference between the UV-LEDs in the system.

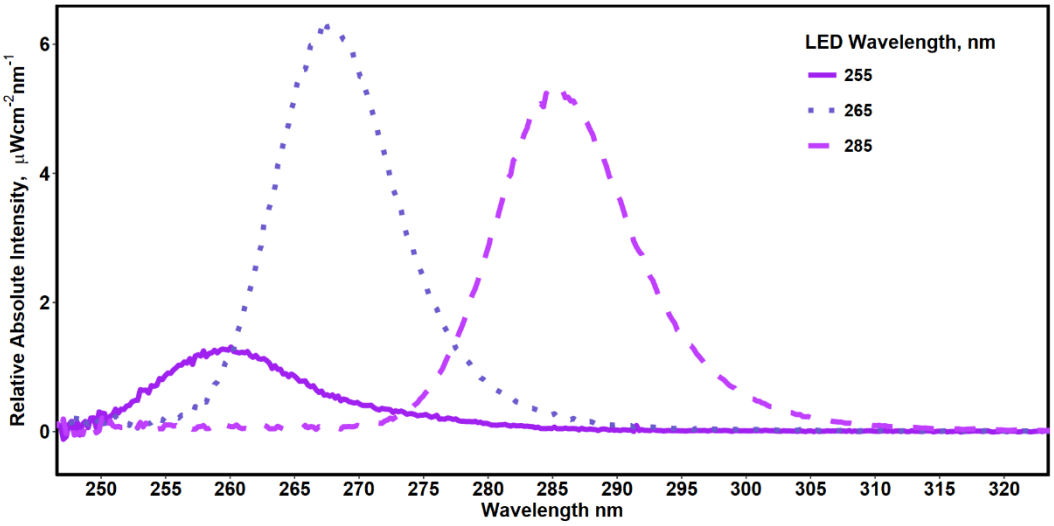

Figure 4.4: Spectral distributions and relative intensities for three UV-LEDs

The water factor is used to determine the attenuation of UV light through the depth of a sample and is calculated based on the absorbance of the sample at the peak wavelength; consequently, a shift in peak wavelength could potentially impact dose calculations. However, when examining the water factors for the nominal and actual peak wavelengths of the 255 nm and 265 nm UV-LEDs, it was found that the water factor remained the same. This is likely due to the shifts of the peaks being relatively small, the largest being 5 nm, and that the absorbance spectrum of the *E. coli* suspension was fairly constant throughout

the 255-270 nm region (Figure 4.5). While the shifts in peak wavelengths did not impact the dose calculations for the pure *E. coli* suspensions, this may not be the case for all water matrix. Organic loadings can impact the absorbance spectra in the UV range, and if the absorbance spectrum of a sample is not constant across the range of wavelength peak shift it may affect the dose calculations. Therefore, it is important to determine peak wavelengths accurately prior to starting experimentation to ensure the water factor, and ultimately the UV dose, are calculated properly.

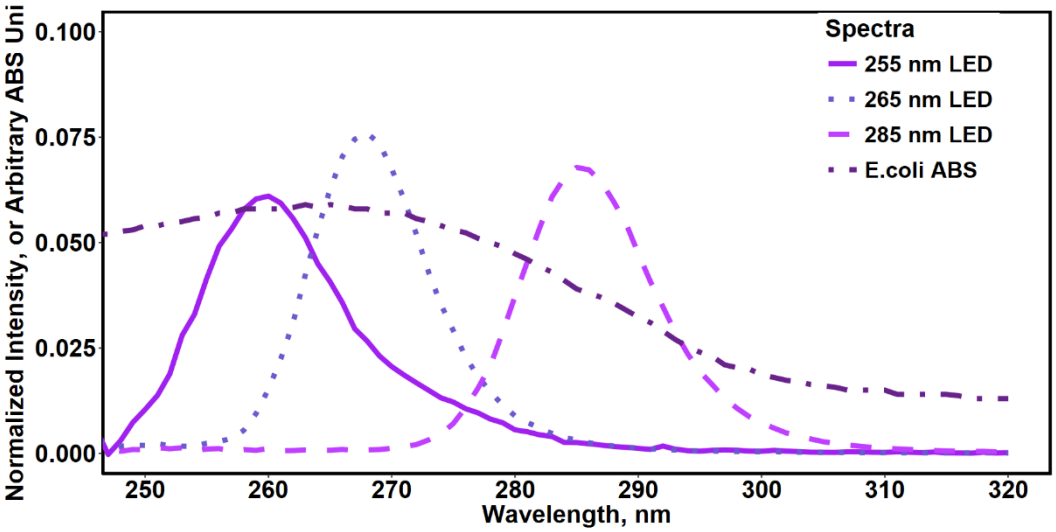

Figure 4.5: Spectral outputs of three UV-LEDs normalized to the average intensity under the curve, and the spectral absorbance of a pure *E. coli* suspension

When examining the action spectra of *E. coli,* it becomes clearer why the peak wavelengths of UV-LEDs should be measured and reported accurately. Wang et al. (2005) show that a shift in wavelength from 255 to 260 nm changes the relative germicidal response of *E. coli* from 79% to 91%. This is less exaggerated for a shift from 265 to 268 nm which shows a

change in germicidal response from 96% to 99%. Ultimately, if peak wavelengths are improperly reported it could misrepresent the inactivation capabilities of the UV-LEDs.

4.5.2 Impact of Spectral Output on Dose Calculations

Unlike mercury-based systems which have approximately 95% of the total energy emitted at 254 nm (Chen et al., 2017), UV-LEDs often have a wider spectrum. The spread of the energy is usually reported as a full width half maximum, which describes the width of the spectrum of the UV-LED at half of the maximum power output. The full width half maxima for the UV-LEDs used in this study were calculated to be 12, 11, and 11 nm for the 255, 265, and 285 nm, respectively. These values compare well to those presented in the literature (Beck et al., 2017; Chatterley & Linden, 2010; Crawford et al., 2005; Oguma, Kita, Sakai, Murakami, & Takizawa, 2013; Würtele et al., 2011), and show that spectral outputs of the UV-LEDs are not monochromatic.

Current methods often consider UV-LEDs as monochromatic light sources and use only the peak wavelength when calculating the water factor. However, some research suggests that spectral output of UV-LEDs should be considered when calculating the water factor using a weighted absorbance value based on the intensities across the entire spectrum of the UV-LEDs (Beck et al., 2017). However, when a weighted absorbance based on the spectrum of an *E. coli* suspension and the spectral outputs UV-LEDs were used to determine water factors, the values were found to be similar to those determined using the absorbance at the peak wavelengths. For example, the 260, 268 and 285 nm UV-LEDs were found to have a peak wavelength absorbance of 0.058, 0.058 and 0.039, respectively. A small difference was found when examining the weighted absorbance of the three

wavelengths (0.056, 0.056, 0.038); however, these had no significant impact on the final calculation of the water factor.

It is likely that there was no impact on the water factor when considering the spectral outputs of the UV-LEDs as the outputs are symmetrical about the peak wavelength. While the absorption spectrum of the *E. coli* suspension was not linear across the UV spectrum, it is relatively linear across the spectrum of the individual LEDs (Figure 4.5). Being relatively linear across the symmetrical spectrum implies that the value obtained for weighted absorbance occurs at the peak wavelength; therefore, it is acceptable to use the absorbance value at the peak wavelength when calculating the water factor. While this was the case when using a pure *E. coli* suspension, if the absorbance spectrum was found to deviate from linearity within the spectrum of the UV-LED, then a weighted absorbance would have to be used to determine the water factor.

4.5.3 Impact of Measurement Technique on Intensity Determination

Intensity profiles were collected for the three UV-LEDs using a spectrometer (Figure 4.6) and were compared to the average intensities determined by previous students by means of a radiometer. All the profiles collected with the spectrometer were found to have a similar distribution of concentric circles with the highest intensities in the centre and gradually decreasing towards the edge. The average intensities for the 265 and 285 nm wavelengths were found to be comparable (0.0235 mW cm^{-2} versus 0.0240 mW cm^{-2}, respectively); whereas, the 255 nm wavelength was found to have a considerably lower average intensity (0.0071 mW cm^{-2}). The average intensities previously determined using the radiometer were considerably higher (255 nm = 0.0233 mW cm^{-2}, 265 nm = 0.0417 mW cm^{-2}, 285 nm

= 0.0311 mW cm^{-2}). These higher intensities could over estimate intensity, and ultimately overestimate the dose.

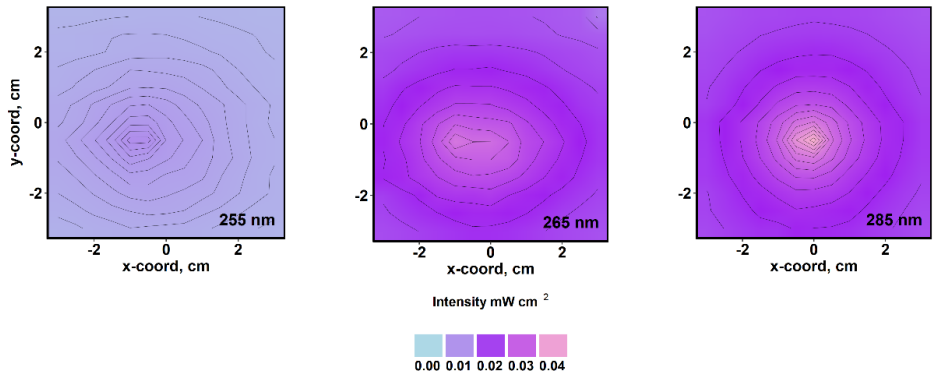

Figure 4.6: Intensity distribution profiles for three UV-LEDs determined by spectrometry

Petri factors were also calculated for the intensity profiles collected with the spectrometer and compared to the Petri factors collected by previous students by means of the radiometer. The Petri factors determined by means of the spectrometer were found to be 0.83, 0.82 and 0.70 for the 255, 265 and 285 nm UV-LEDs, respectively. These values were larger when compared to those found with the radiometer, which were 0.64, 0.67 and 0.67 for the 255, 265 and 285 nm UV-LEDs, respectively. The higher Petri factors seen for the spectrometer measurements indicate that the intensity distribution is more uniform than the those collected using the radiometer. This could be a result of the more refined grid spacing used when collecting the intensity profile with the spectrometer, or due to the inherent differences in the two instruments.

As the intensity averages and distributions varied between the two measurement methods, a detailed look at dosing based on these two intensity profiles was examined and verified

by means of ferrioxalate actinometry. Figure 4.7 shows the average intensities used to calculate the dose using the spectrometer, radiometer and actinometer as measurement tools. The spectrometer and radiometer values reported in this figure have all the necessary correction factors from the Bolton method applied, and represent the corrected actual intensity used to determine the exposure times for a given UV dose. The actinometer results reported have been corrected with only the water factor to represent the corrected actual intensity. Based on these results, the corrected actual intensity using the radiometer significantly overestimates the intensity when compared to spectrometer and actinometer.

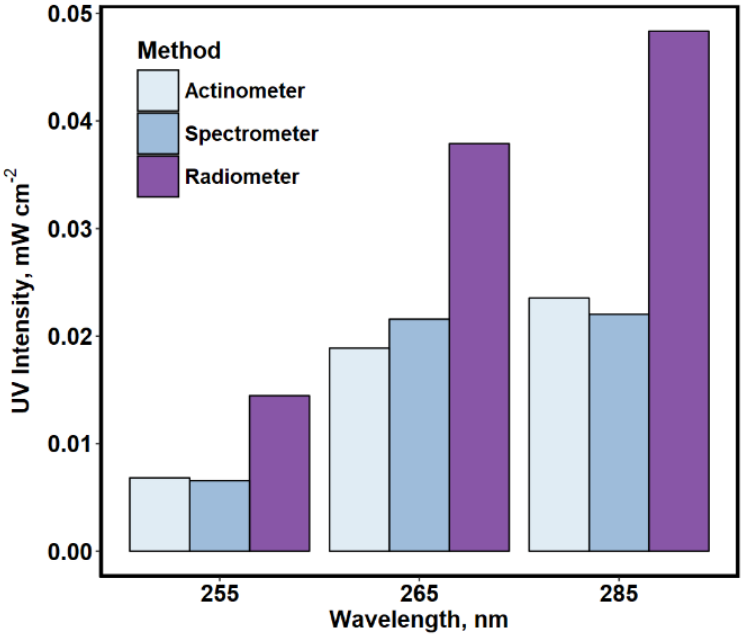

Figure 4.7: Average UV intensities across treatment area calculated using three different methods for three UV-LEDs. Reported intensities have all correction factors applied

The difference in the measured intensity between the spectrometer and radiometer likely stems from the design of the radiometer. The radiometer was designed to determine

intensities for LPUV systems emitting monochromatically at 254 nm. When comparing the measured intensities found using the radiometer versus the spectrometer, it appears that the radiometer overestimated the measured intensity of the 255 and 265 nm UV-LEDs. For the 255 nm UV-LED this value was about double (0.013 versus 0.0069 mW cm^{-2}), and for the 265 nm UV-LED this value was approximately 50% greater (0.030 versus 0.024 mW cm^{-2}). The measured intensity of the 285 UV-LED was found to be similar for both instruments (0.022 and 0.024 mW cm^{-2}). These differences in measured intensity likely result from the radiometer not being calibrated for measurements outside of 254 nm or spectral outputs. Correction factors based on the spectral sensitivity of the radiometer were provided by the manufacturer and applied in an attempt to account for the calibration; however, the application of these factors only exaggerated the effect. Ultimately, the calibration of the radiometer paired with the application of the radiometer sensitivity correction factors were likely the cause of the increased intensities found compared to the values determined using the spectrometer and actinometer.

4.5.4 Impact of Measurement Technique on Disinfection Kinetics

All the dose calculations for the *E. coli* disinfection experiments were originally calculated using intensities determined by means of the radiometer. Using the average intensities determined in (Figure 4.7), correction factors were calculated to adjust the doses as if they were calculated using the average intensities determined by the spectrometric method. The correction factors used for all of the UV treatments are presented in Table 4.2, and indicates that the radiometric method was likely overestimating the UV intensity. Consequently, the dose-response curves, and the inactivation rate constants were impacted.

Table 4.2: Correction factors used to adjust UV dose for spectrometer dose-response curves

Wavelength, nm	*Correction Factor*
UV-LED 255	2.21
UV-LED 265	1.76
UV-LED 285	2.20

The dose-response curves developed for *E. coli* were found to follow a sigmoidal curve with a tailing, a log linear and a shoulder phase for all treatments (Figure 4.8). The tailing phase observed in dose-response curves have also been attributed to reactivation mechanisms (Bolton & Cotton, 2008). While care was taken to perform the disinfection in the absence of light, enumeration of the treated samples was conducted in a brightly lit room for approximately 1 hr. Previous study has shown that a reactivation mechanisms can cause an approximately 1.5 log recovery in that time (Oguma, Katayama, & Ohgaki, 2004). Thus, the tailing phase in the dose-response curves may be due to photoreactivation mechanisms. However, it has also been shown that tailing phases exist in the dose-response curves even if precaution has been taken to limit the exposure to reactivation wavelengths (Rattanakul & Oguma, 2018). The presence of the tailing phase in these cases has been attributed to the rate of repair of damage of DNA being greater than the rate of damage (Mossel, Corry, Struijk, & Baird, 1995). The shoulder phase may also be due to the culture having a subculture with UV resistant genes (Cerf, 1977; Rattanakul & Oguma, 2018). At the higher doses where shouldering was observed, between a 4 and 6 log inactivation was

achieved. When compared to a starting concentration of cells around 10^5 to 10^6 CFU mL^{-1}., this may indicate that these remaining colonies may have some UV resistance.

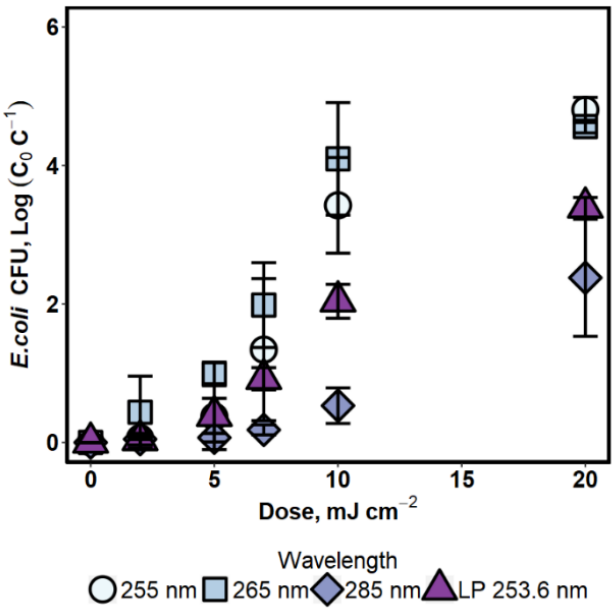

Figure 4.8: Dose-response curves for *E. coli* based on intensities calculated using a radiometric method for UV-LED and LP UV treatments. Error bars represent 1 SD (n = 3-5)

Disinfection rates and tailing phase ranges were found to be impacted by wavelength selection. The 255 and 265 nm UV-LEDs produced very similar results; whereas, the 285 nm UV-LED produced a substantially lower inactivation rate at most of the doses. Additionally, the LPUV system was found to produce lower levels of inactivation when compared to the 255 and 265 nm UV-LED, but higher levels when compared to the 285 nm in the dose range of 5-20 mJ cm^{-2}.

These differences in the disinfection rates between the wavelengths used can be explained if the action spectrum of the organism is considered. Wang et al. (2005) show that the peak

germicidal efficiency for *E. coli* is at 270 nm and tapers off in a gaussian shape about the peak. Interpolating values from these data shows that at 260 nm *E. coli* has a normalized germicidal efficiency, with respect to the peak, around 91%, 254 nm around 77%, 268 nm around 99% and 285 nm around 65%. These interpolated relative germicidal efficiencies also follow similar trends to the relative inactivation rates found in this study (Table 4.3).

Table 4.3: Relative germicidal efficiency from this study and literature.

Wavelength, nm	*Relative Germicidal Efficiency, This Study*	*Relative Germicidal Efficiency, Wang, MacGregor, Anderson, & Woolsey (2005)*
254	53%	77%
260	98%	91%
268	100%	99%
285	28%	65%

After correcting the dose to be based on spectrometer intensities, the relative inactivation rates between all the treatments were found to remain the same, but the shapes of the dose-response curves were compressed with respect to the dose (Figure 4.9).

where A_{1cm} is the measured absorbance though a 1 cm pathlength at 254 nm, and l is the total pathlength of the water being treated. Exposure time for required UV dose was determined by dividing the required dose by the actual intensity.

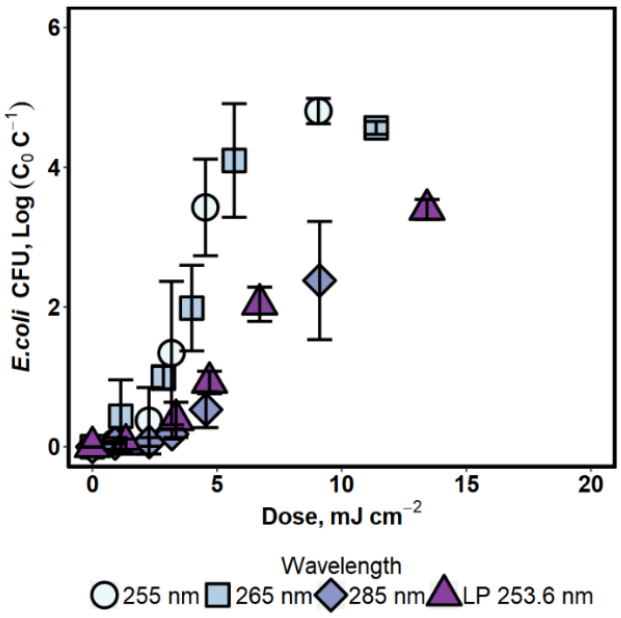

Figure 4.9: Dose-response curves for *E. coli* with applied correction factors for UV-LED and LP UV treatments. Error bars represent 1 SD (n = 3-5)

This compression impacted the tailing phase range and inactivation rate constants. The tailing ranges and inactivation rate constants found for the spectrometer were approximately half of those for the radiometer, which was expected based on the correction factors being approximately 2. Furthermore, the tailing ranges found in this study were all larger than those reported by Rattanakul & Oguma (2018), but were found to follow a similar trend; wherein, the tailing range were larger for wavelength treatments with lower inactivation rates (Table 4.4). The relative rates of inactivation of the monochromatic UV-LED treatments remained the same as those found using the radiometer intensities, which is likely due to all the correction factors being approximately the same value.

Table 4.4: A comparison of tailing phase ranges for *E. coli* using UV-LED treatments

Nominal Wavelength, nm	*Radiometer*	*Spectrometer*	*Rattanakul & Oguma, (2018)*
255	5	2.27	N/A
265	5	2.85	1.25
285	7	3.18	1.95 (280 nm)
300	N/A	N/A	23.4

While the relative rates of inactivation were found to remain the same after the correction factor was applied, the nominal values were found to be greatly impacted. The inactivation rate constants were found to be about twice those for the spectrometer when compared to those found for the radiometer. Furthermore, when the inactivation rates based on both the radiometer and spectrometer intensities were compared to results in literature a range of results was found (Table 4.5). Inactivation rates reported in literature were found to have a wide range of values, and in some cases the rate constant values found in this study fell within that range. The 254 nm, 265 nm radiometer, and 285 nm treatments fell within range, while all other treatments were over the reported ranges. Ultimately, the measurement technique was found to greatly impact the inactivation rate constant.

Table 4.5: A comparison of *E. coli* inactivation rate constants using UV-LED treatments

Wavelength, nm	*k-value Radiometer, $cm^2\ mJ^{-1}$ (± 95% CI)*	*k-value Spectrometer, $cm^2\ mJ^{-1}$ (± 95% CI)*	*k-value Literature, $cm^2\ mJ^{-1}$*
255	0.617 (0.217)	1.36 (0.480)	0.300 (Bowker et al., 2011) 0.290* (Beck et al., 2017)
265	0.628 (0.171)	1.10 (0.301)	0.170 (Chatterley & Linden, 2010) 0.290* (Beck et al., 2017) 0.43 (Oguma et al., 2013) 0.41 (Li, Wang, Huo, Lu, & Hu, 2017) 0.805 (Rattanakul & Oguma, 2018)

Wavelength, nm	*k-value Radiometer, cm^2 mJ^{-1} (± 95% CI)*	*k-value Spectrometer, cm^2 mJ^{-1} (± 95% CI)*	*k-value Literature, cm^2 mJ^{-1}*
285	0.173 (0.054)	0.380 (0.118)	0.157 (Oguma, Rattanakul, & Bolton, 2016) 0.290** (Oguma et al., 2013) 0.30** (Li et al., 2017) 0.310** (Beck et al., 2017) 0.561** (Rattanakul & Oguma, 2018)

*λ = 260 nm

**λ = 280 nm

The range of inactivation rate constants reported in this study and in literature may be caused by a variety of factors. Firstly, Song et al. (2016) discuss difficulties in comparing values across the literature due to a lack of any standard method for UV-LED disinfection. The studies summarized in Table 4.5 have used many different system configurations, characterized the systems differently, and used different techniques to measure and

determine dose. Secondly, *E. coli* has been shown not to follow the law of time-dose reciprocity (Sommer, Cabaj, & Haider, 1996; Sommer, Haider, Cabaj, Pribil, & Lhotsky, 1998), and any differences in the magnitude of the intensity may have produced different inactivation rates for the same dose range. This point is unfortunately only speculative as most of the UV-LED studies have not reported the average intensities used. Finally, the overlap in the spectral distributions of some UV-LEDs may have caused the effects of the different UV-LEDs to mask one another due to the action spectra of *E. coli*. For example, the difference in relative germicidal efficiencies for the 260, 265 and 268 nm UV-LEDs were 91%, 96% and 99%, respectively (Wang et al., 2005). Consequently, the effect of UV-LEDs in this range may be indistinguishable from one another. Moreover, if the effects of UV-LEDs in this range are indistinguishable from one another, then the inactivation rates reported for the 260 nm UV-LED in this study would be in better agreement with those reported in literature as 265 nm UV-LEDs. Given these points, the lack of a standard protocol for characterizing UV-LED collimators and reporting the results have likely led to a wide range of inactivation rate constants being presented in literature.

4.5.5 Proposed Procedure for Determining UV Dose and Reporting UV-LED Disinfection Results

The measurement techniques used in this study showed to significantly impact the average intensities used to determine exposures times in the dose calculations; furthermore, a lack of standardized testing procedure likely increased the variability of the inactivation rate constants reported in the literature. The results discussed in the previous sections indicate that a radiometer may not be the ideal instrument to determine intensities of UV-LED systems as they are not calibrated for wavelengths aside from 254 nm or spectral outputs.

Spectrometers and actinometers are better instruments for intensity determination as spectrometers can be calibrated to measure intensities across the UV spectrum and actinometry directly measures the energy applied to the system. Pairing these instruments with a standard protocol based on the Bolton method would likely lead to more consistent results being reported between studies. The following is a suggested protocol.

To begin, the spectral output of the UV-LEDs used in the collimator should be characterized for the peak wavelength and spectral output using a spectrometer calibrated for the UV region. This should be completed even if the manufacturer has provided specifications for the UV-LEDs. Furthermore, the absorbance spectrum of the sample should be examined to ensure that it is linear across the width of the UV-LED spectrum. If linearity exists, then the peak wavelength measured for the UV-LED can be used to determine the water factor; otherwise, the water factor will need to be determined using an absorbance based on a weighted average of the intensity spectrum of the UV-LED.

Additionally, the average intensity should be determined by means of the spectrometer, or a chemical actinometer. For the spectrometer, intensity measurements should be taken across the entirety of the collimator with a spectral resolution of 0.5 cm (Bolton & Linden, 2003). Moreover, the intensity measurements taken should be the integrated energy for the full spectrum of the UV-LED, not just the intensity at the peak wavelength. Once this has been completed the average intensity should be calculated for the surface area of the treatment vessel. For the chemical actinometer, a ferrioxalate actinometer should be used because the quantum yield of the solution is stable above 260 nm (Goldstein & Rabani, 2008). The results of this testing will provide the average intensity at the surface of the surface of the sample.

Once the average intensity has been calculated, additional correction factors should be applied before determining the exposure times. If the spectrometer was used to determine the average intensity, the actual intensity should be calculated by applying a divergence factor, reflectance factor and water factor (Bolton & Linden, 2003). If the actinometer was used, the actual intensity should be calculated by multiplying the average intensity by the water factor because actinometry gives the actual photon flux into the water, but does not account for attenuation through the water column (Oguma et al., 2016). Once the actual intensity has been calculated, the required exposure times to achieve a given dose can be determined by dividing the dose by the actual intensity.

Additionally, the operation of the UV-LED collimator should maintain some aspects from the Bolton method. These include mixing the sample gently so no vortex is present, allowing the sample to mix for at least 5 seconds prior to beginning treatment, carrying out the treatments and replicates in a random order and conducting the experiments under subdued red light (Bolton & Linden, 2003). These steps ensure that the dose is evenly applied, the sample is properly mixed, that sample bias is reduced and impacts from reactivation mechanisms are reduced. Furthermore, the peak wavelength, spectral outputs and the average intensities should be reported along with any inactivation curves.

4.6 CONCLUSION

The results of this study found that care needs to be taken when characterizing the peak wavelength, spectral output and average intensity of UV-LED collimated systems as it can dramatically impact the inactivation rate constants being reported. The peak wavelengths for the UV-LED collimator were found to be different than those reported by the manufacturer but the shifts in the wavelength had no impact on the dose determination.

However, shifts in peak wavelengths can greatly impact the germicidal efficiency of treatment; therefore, peak wavelengths need to be reported accurately in order to ensure that results across studies are comparable. Furthermore, it was determined that if the absorbance spectrum of the sample being treated is linear across the spectrum of the UV-LED, then the peak wavelength can be used to determine the water factor; otherwise, a weighted absorbance based on the spectral output of the UV-LED should be used. Average intensities determined by means of a radiometer were found to be overestimated when compared to those found by means of the spectrometer. It is likely that the spectrometer was the more accurate of the two as the instrument was properly calibrated across the UV region and able to integrate the intensity across the full spectrum of the UV-LEDs. Ultimately, the overestimation of the intensity led to an overestimation of the UV dose and an underestimation of the inactivation rate constants reported. When comparing the inactivation rate constants found in this study to those presented in the literature, it was found that a wide range of values were reported for similar wavelengths, and the values found in this study were often within this range. This wide range in rate constants being reported may stem from the lack of a standard procedure for testing with UV-LED collimators. As such, a modified version of the Bolton method for UV dose determination was suggested.

4.7 REFERENCES

Beck, S. E., Rodriguez, R. A., Hawkins, M. A., Hargy, T. M., Larason, T. C., & Linden, K. G. (2016). Comparison of UV-induced inactivation and RNA damage in MS2 phage across the germicidal UV spectrum. *Applied and Environmental Microbiology*, *82*(5), 1468–1474. https://doi.org/10.1128/AEM.02773-15

Beck, S. E., Ryu, H., Boczek, L. A., Cashdollar, J. L., Jeanis, K. M., Rosenblum, J. S., … Linden, K. G. (2017). Evaluating UV-C LED disinfection performance and investigating potential dual-wavelength synergy. *Water Research*, *109*, 207–216. https://doi.org/10.1016/j.watres.2016.11.024

Bolton, J. R., & Cotton, C. A. (2008). The Ultraviolet Disinfection Handbook, 168. Retrieved from https://app.knovel.com/web/toc.v/cid:kpUDHE0001/viewerType:toc/root_slug:ultraviolet-disinfection/url_slug:kt008BHMT1

Bolton, J. R., & Linden, K. G. (2003). Standardization of Methods for Fluence (UV Dose) Determination in Bench-Scale UV Experiments. *Journal of Environmental Engineering*, *129*(March), 209–215. https://doi.org/10.1061/(ASCE)0733-9372(2003)129:3(209)

Bolton, J. R., Stefan, M. I., Shaw, P. S., & Lykke, K. R. (2011). Determination of the quantum yields of the potassium ferrioxalate and potassium iodide-iodate actinometers and a method for the calibration of radiometer detectors. *Journal of Photochemistry and Photobiology A: Chemistry*, *222*(1), 166–169. https://doi.org/10.1016/j.jphotochem.2011.05.017

Bowker, C., Sain, A., Shatalov, M., & Ducoste, J. (2011). Microbial UV fluence-response assessment using a novel UV-LED collimated beam system. *Water Research*, *45*(5), 2011–2019. https://doi.org/10.1016/j.watres.2010.12.005

Cerf, 0. (1977). Tailing of Survival Curves of Bacterial Spores. *Journal OfApplied Bacteriology*, *42*, 1–19. https://doi.org/10.1111/j.1365-2672.1977.tb00665.x

Chatterley, C., & Linden, K. (2010). Demonstration and evaluation of germicidal UV-LEDs for point-of-use water disinfection. *Journal of Water and Health*, *8*(3), 479–486. https://doi.org/10.2166/wh.2010.124

Chen, J., Loeb, S., & Kim, J.-H. (2017). LED revolution: fundamentals and prospects for UV disinfection applications. *Environ. Sci.: Water Res. Technol.* https://doi.org/10.1039/C6EW00241B

Crawford, M. H., Banas, M. A., Ross, M. P., Ruby, D. S., Nelson, J. S., Boucher, R., & Allerman, A. A. (2005). Final LDRD Report : Ultraviolet Water Purification Systems for Rural Environments and Mobile Applications, (November).

Goldstein, S., & Rabani, J. (2008). The ferrioxalate and iodide-iodate actinometers in the UV region. *Journal of Photochemistry and Photobiology A: Chemistry*, *193*(1), 50–55. https://doi.org/10.1016/j.jphotochem.2007.06.006

Kheyrandish, A., Mohseni, M., & Taghipour, F. (2017). Development of a method for the characterization and operation of UV-LED for water treatment. *Water Research*, *122*, 570–579. https://doi.org/10.1016/j.watres.2017.06.015

Li, G. Q., Wang, W. L., Huo, Z. Y., Lu, Y., & Hu, H. Y. (2017). Comparison of UV-LED and low pressure UV for water disinfection: Photoreactivation and dark repair of Escherichia coli. *Water Research*, *126*, 134–143. https://doi.org/10.1016/j.watres.2017.09.030

Mossel, D. A. A., Corry, J. E., Struijk, C. B., & Baird, R. M. (1995). *Essentials of microbiology: A textbook for advanced studies.* John Wiley & Sons.

Oguma, K., Katayama, H., & Ohgaki, S. (2004). Photoreactivation of Legionella pneumophila after inactivation by low- or medium-pressure ultraviolet lamp. *Water Research*, *38*(11), 2757–2763. https://doi.org/10.1016/j.watres.2004.03.024

Oguma, K., Kita, R., Sakai, H., Murakami, M., & Takizawa, S. (2013). Application of UV light emitting diodes to batch and flow-through water disinfection systems. *Desalination*, *328*, 24–30. https://doi.org/10.1016/j.desal.2013.08.014

Oguma, K., Rattanakul, S., & Bolton, J. R. (2016). Application of UV Light–Emitting Diodes to Adenovirus in Water. *Journal of Environmental Engineering*, *142*(3), 04015082. https://doi.org/10.1061/(ASCE)EE.1943-7870.0001061

Rattanakul, S., & Oguma, K. (2018). Inactivation kinetics and efficiencies of UV-LEDs against Pseudomonas aeruginosa, Legionella pneumophila, and surrogate microorganisms. *Water Research*, *130*, 31–37. https://doi.org/10.1016/j.watres.2017.11.047

Shur, M. S., & Gaska, R. (2010). Deep-ultraviolet light-emitting diodes. *IEEE Transactions on Electron Devices*, *57*(1), 12–25. https://doi.org/10.1109/TED.2009.2033768

Sommer, R., Cabaj, A., & Haider, T. (1996). Microbicidal effect of reflected UV radiation in devices for water disinfection. In *Water Science and Technology* (Vol. 34, pp. 173–177). https://doi.org/10.1016/S0273-1223(96)00742-1

Sommer, R., Haider, T., Cabaj, A., Pribil, W., & Lhotsky, M. (1998). Time dose reciprocity in UV disinfection of water. *Water Science and Technology*, *38*(12), 145–150. https://doi.org/10.1016/S0273-1223(98)00816-6

Song, K., Mohseni, M., & Taghipour, F. (2016). Application of ultraviolet light-emitting diodes (UV-LEDs) for water disinfection : A review. *Water Research*, *94*, 341–349. https://doi.org/10.1016/j.watres.2016.03.003

Wang, T., MacGregor, S. J., Anderson, J. G., & Woolsey, G. A. (2005). Pulsed ultra-violet inactivation spectrum of Escherichia coli. *Water Research*, *39*(13), 2921–2925. https://doi.org/10.1016/j.watres.2005.04.067

Würtele, M. A., Kolbe, T., Lipsz, M., Külberg, A., Weyers, M., Kneissl, M., & Jekel, M. (2011). Application of GaN-based ultraviolet-C light emitting diodes - UV LEDs - for water disinfection. *Water Research*, *45*(3), 1481–1489. https://doi.org/10.1016/j.watres.2010.11.015

CHAPTER 5: CONCLUSION

Measurement techniques used are crucial to ensure that UV disinfection systems are operating optimally and that the appropriate dose is being determined. This project examined the applicability of a modified ATP assay to be used for rapid determination of UV disinfection efficiency and the impact that characterization of emerging UV-LED based collimated beam systems had on determining the UV dose. It was determined that a biomass recovery method could be used to discern between pre- and post-UV treated samples in 4 hr; however, the results of the test were highly dependant on effluent water quality at each of the plants. Furthermore, it was found that the change in the biomass recovery method was related to UV dose, but had some limitations at higher doses. It was also determined that proper characterization of UV-LED peak wavelength and spectral distributions are required to ensure that the inactivation rates being reported are comparable across studies. Furthermore, it was found that the use of radiometers may not be ideal for intensity determination of UV-LEDs and may underestimate inactivation rates. A new protocol was presented to more accurately determine UV dose when using UV-LED technologies. Overall, the two new methods developed in this work will aid in the monitoring and implementing of traditional and emerging UV technologies.

5.1 RECCOMENDATIONS FOR FUTURE WORK

For the biomass recovery method, the following future work is recommended:

- Develop a better understanding of how the microbial ecology of WWTFs impacts the outcome of the biomass recovery method using DNA analysis, and determine if WWTFs that saw no or a low response with the biomass recovery method would benefit from an extended 6 hr incubation time.

- Examine the impact that water quality parameters have on the growth of the microorganisms, and ultimately the biomass recovery method.

For UV-LED characterization, the following future work is recommended:

- Conduct a thorough investigation of how the spectral absorbances of real water matrices impact the water factor calculations used to determine average UV intensities.

REFERENCES

Allerman, A. A., Crawford, M. H., Fischer, A. J., Bogart, K. H. A., Lee, S. R., Follstaedt, D. M., … Koleske, D. D. (2004). Growth and design of deep-UV (240-290 nm) light emitting diodes using AlGaN alloys. *Journal of Crystal Growth*, *272*(1–4 SPEC. ISS.), 227–241. https://doi.org/10.1016/j.jcrysgro.2004.08.035

Amann, R. I., Ludwig, W., & Schleifer, K. H. (1995). Phylogenetic identification and in situ detection of individual microbial cells without cultivation . Phylogenetic Identification and In Situ Detection of Individual Microbial Cells without Cultivation. *Microbiological Reviews*, *59*(1), 143–169. https://doi.org/10.1016/j.jip.2007.09.009

Aoyagi, Y., Takeuchi, M., Yoshida, K., Kurouchi, M., Yasui, N., Kamiko, N., … Nanishi, Y. (2011). Inactivation of Bacterial Viruses in Water Using Deep Ultraviolet Semiconductor Light-Emitting Diode. *Journal of Environmental Engineering-Asce*, *137*(12), 1215–1218. https://doi.org/Doi 10.1061/(Asce)Ee.1943-7870.0000442

APHA, AWWA, & WEF. (2012). *Standard Methods for the Examination of Water and Wastewater*. District of Columbia: American Public Health Association.

Baron, J., & Bourbigot, M. M. (1996). Repair of Escherichia coli and enterococci in sea water after ultraviolet disinfection quantification using diffusion chambers. *Water Research*, *30*(11), 2817–2821. https://doi.org/10.1016/S0043-1354(96)00159-5

Beck, S. E., Rodriguez, R. A., Hawkins, M. A., Hargy, T. M., Larason, T. C., & Linden, K. G. (2016). Comparison of UV-induced inactivation and RNA damage in MS2 phage across the germicidal UV spectrum. *Applied and Environmental Microbiology*, *82*(5), 1468–1474. https://doi.org/10.1128/AEM.02773-15

Beck, S. E., Ryu, H., Boczek, L. A., Cashdollar, J. L., Jeanis, K. M., Rosenblum, J. S., … Linden, K. G. (2016). Evaluating UV-C LED disinfection performance and investigating potential dual-wavelength synergy. *Water Research*. https://doi.org/10.1016/j.watres.2016.11.024

Beck, S. E., Ryu, H., Boczek, L. A., Cashdollar, J. L., Jeanis, K. M., Rosenblum, J. S., … Linden, K. G. (2017). Evaluating UV-C LED disinfection performance and investigating potential dual-wavelength synergy. *Water Research*, *109*, 207–216. https://doi.org/10.1016/j.watres.2016.11.024

Ben Said, M., Masahiro, O., & Hassen, A. (2010). Detection of viable but non cultivable Escherichia coli after UV irradiation using a lytic Qβ phage. *Annals of Microbiology*, *60*(1), 121–127. https://doi.org/10.1007/s13213-010-0017-4

Berney, M., Vital, M., Hülshoff, I., Weilenmann, H.-U., Egli, T., & Hammes, F. (2008). Rapid, cultivation-independent assessment of microbial viability in drinking water. *Water Research*, *42*(14), 4010–4018. https://doi.org/10.1016/J.WATRES.2008.07.017

Bolton, J. R., & Cotton, C. A. (2008). The Ultraviolet Disinfection Handbook, 168. Retrieved from https://app.knovel.com/web/toc.v/cid:kpUDHE0001/viewerType:toc/root_slug:ultraviolet-disinfection/url_slug:kt008BHMT1

Bolton, J. R., Dussert, B., Bukhari, Z., Hargy, T., & Clancy, J. L. (1998). Inactivation of Cryptosporidium parvum by medium-pressure ultraviolet light in finished drinking water. *Proceedings American Water Works Association Annual Conference*, *A*(June), 389–403.

Bolton, J. R., & Linden, K. G. (2003). Standardization of Methods for Fluence (UV Dose) Determination in Bench-Scale UV Experiments. *Journal of Environmental Engineering*, *129*(March), 209–215. https://doi.org/10.1061/(ASCE)0733-9372(2003)129:3(209)

Bolton, J. R., Stefan, M. I., Shaw, P. S., & Lykke, K. R. (2011). Determination of the quantum yields of the potassium ferrioxalate and potassium iodide-iodate actinometers and a method for the calibration of radiometer detectors. *Journal of Photochemistry and Photobiology A: Chemistry*, *222*(1), 166–169. https://doi.org/10.1016/j.jphotochem.2011.05.017

Bowker, C., Sain, A., Shatalov, M., & Ducoste, J. (2011). Microbial UV fluence-response assessment using a novel UV-LED collimated beam system. *Water Research*, *45*(5), 2011–2019. https://doi.org/10.1016/j.watres.2010.12.005

Calderon, R. L., Mood, E. W., & Dufour, A. P. (1991). Health effects of swimmers and nonpoint sources of contaminated water. *International Journal of Environmental Health Research*, *1*(1), 21–31. https://doi.org/10.1080/09603129109356701

Canadian Council of Ministers of the Environment. (2014). Canada-wide Strategey for the Management of Municipal Wastewater Effluent: 2014 Progress Report, 18. Retrieved from http://www.ccme.ca/files/Resources/municipal_wastewater_efflent/PN_1522_MWWE_Five_Year_Rvw_2014.pdf

Cerf, 0. (1977). Tailing of Survival Curves of Bacterial Spores. *Journal OfApplied Bacteriology*, *42*, 1–19. https://doi.org/10.1111/j.1365-2672.1977.tb00665.x

Chang, J. C., Ossoff, S. F., Lobe, D. C., Dorfman, M. H., Dumais, C. M., Qualls, R. G., & Johnson, J. D. (1985). UV inactivation of pathogenic and indicator microorganisms. *Applied and Environmental Microbiology*, *49*(6), 1361–1365. Retrieved from http://www.ncbi.nlm.nih.gov/pubmed/2990336

Chatterley, C., & Linden, K. (2010). Demonstration and evaluation of germicidal UV-LEDs for point-of-use water disinfection. *Journal of Water and Health*, *8*(3), 479–486. https://doi.org/10.2166/wh.2010.124

Chen, J., Loeb, S., & Kim, J.-H. (2017). LED revolution: fundamentals and prospects for UV disinfection applications. *Environ. Sci.: Water Res. Technol.* https://doi.org/10.1039/C6EW00241B

Chu, C. P., Lee, D. J., Chang, B. V., & Liao, C. S. (2001). Using ATP bioluminescence technique for monitoring microbial activity in sludge. *Biotechnology and Bioengineering*, *75*(4), 469–474. https://doi.org/10.1002/bit.10076

Craun, G. F., Calderon, R. L., & Craun, M. F. (2005). Outbreaks associated with recreational water in the United States. *International Journal of Environmental Health Research*, *15*(4), 243–262. https://doi.org/10.1080/09603120500155716

Crawford, M. H., Banas, M. A., Ross, M. P., Ruby, D. S., Nelson, J. S., Boucher, R., & Allerman, A. A. (2005). Final LDRD Report : Ultraviolet Water Purification Systems for Rural Environments and Mobile Applications, (November).

Dabkowski, B., Lunn, M., De Kock, G., & Ingelright, J. (2011). Reducing Energy Consumption of UV Disinfection Systems by Measuring %UVT. *Proceedings of the Water Environment Federation*, *2011*(6), 765–771. https://doi.org/10.2175/193864711802836148

Davidson, C. a, Griffith, C. J., Peters, a C., & Fielding, L. M. (1999). Evaluation of two methods for monitoring surface cleanliness-ATP bioluminescence and traditional hygiene swabbing. *Luminescence : The Journal of Biological and Chemical Luminescence*, *14*(5), 33–38. https://doi.org/10.1002/(SICI)1522-7243(199901/02)14:1<33::AID-BIO514>3.0.CO;2-I

Deininger, R. A., & Lee, J. Y. (2001). Rapid Determination of Bacteria in Drinking Water Using an ATP Assay. *Field Analytical Chemistry and Technology*, *5*(4), 185–189. https://doi.org/10.1002/fact.1020

Delahaye, E., Welté, B., Levi, Y., Leblon, G., & Montiel, A. (2003). An ATP-based method for monitoring the microbiological drinking water quality in a distribution network. *Water Research*, *37*(15), 3689–3696. https://doi.org/10.1016/S0043-1354(03)00288-4

DOWA Holdings CO., L. (2017). DOWA to be ready for Mass Production of Highest Output Power Deep Ultraviolet LEDs for disinfection. Retrieved from http://www.dowa.co.jp/en/ir/news/2017/20170622.html

First, M. R., & Drake, L. A. (2014). Life after treatment: Detecting living microorganisms following exposure to UV light and chlorine dioxide. *Journal of Applied Phycology*, *26*(1), 227–235. https://doi.org/10.1007/s10811-013-0049-9

Goldstein, S., & Rabani, J. (2008). The ferrioxalate and iodide-iodate actinometers in the UV region. *Journal of Photochemistry and Photobiology A: Chemistry*, *193*(1), 50–55. https://doi.org/10.1016/j.jphotochem.2007.06.006

Government of Canada. (2013). Owners and operators: continuously discharging wastewater systems. Retrieved from https://www.canada.ca/en/environment-climate-change/services/wastewater/system-effluent-regulations-reporting/owners-operators-continuously-discharging.html

Griffin, P. M., & Tauxe, R. V. (1991). The Epidemiology of Infections Caused by Escherichia coli O157: H7, Other Enterohemorrhagic E. coli, and the Associated Hemolytic Uremic Syndrome. *Epidemiologic Reviews*, *13*(1), 60–98. https://doi.org/10.1093/oxfordjournals.epirev.a036079

Health Canada. (2012a). *Guidelines for Canadian Drinking Water Quality*. *Health Canada*. Retrieved from https://www.canada.ca/content/dam/canada/health-canada/migration/healthy-canadians/publications/healthy-living-vie-saine/water-coliforms-coliformes-eau/alt/water-coliforms-coliformes-eau-eng.pdf

Health Canada. (2012b). *Guidelines for Canadian recreational water quality*. https://doi.org/No H129-15/2012E

Hijnen, W. A. M., Beerendonk, E. F., & Medema, G. J. (2006). Inactivation credit of UV radiation for viruses, bacteria and protozoan (oo)cysts in water: A review. *Water Research*, *40*(1), 3–22. https://doi.org/10.1016/j.watres.2005.10.030

Hugenholtz, P., Goebel, B. M., & Pace, N. R. (1998). Impact of culture independent studies on the emerging phylogenetic view of bacterial diversity. *Journal of Bacteriology*, *v*(18), 180p4765-4774. https://doi.org/0021-9193/98/$04.00+0

Ibrahim, M. A. S., MacAdam, J., Autin, O., & Jefferson, B. (2014). Evaluating the impact of LED bulb development on the economic viability of ultraviolet technology for disinfection. *Environmental Technology*, *35*(1–4), 400–406. https://doi.org/10.1080/09593330.2013.829858

Ishii, S., & Sadowsky, M. J. (2008). Escherichia coli in the Environment: Implications for Water Quality and Human Health. *Microbes and Environments*, *23*(2), 101–108. https://doi.org/10.1264/jsme2.23.101

Jenny, R. M., Simmons, O. D., Shatalov, M., & Ducoste, J. J. (2014). Modeling a continuous flow ultraviolet Light Emitting Diode reactor using computational fluid dynamics. *Chemical Engineering Science*, *116*(August), 524–535. https://doi.org/10.1016/j.ces.2014.05.020

Khan, M. A. (2006). AlGaN multiple quantum well based deep UV LEDs and their applications. *Physica Status Solidi (A) Applications and Materials Science*, *203*(7), 1764–1770. https://doi.org/10.1002/pssa.200565427

Kheyrandish, A., Mohseni, M., & Taghipour, F. (2017). Development of a method for the characterization and operation of UV-LED for water treatment. *Water Research*, *122*, 570–579. https://doi.org/10.1016/j.watres.2017.06.015

Knowles, J. R. (1980). Enzyme-catalyzed phosphoryl transfer. *Annu. Rev. Biochem.*, *49*, 877–919. https://doi.org/10.1146/annurev.bi.49.070180.004305

Lappalainen, J., Loikkanen, S., Havana, M., Karp, M., Sjöberg, a M., & Wirtanen, G. (2000). Microbial testing methods for detection of residual cleaning agents and disinfectants-prevention of ATP bioluminescence measurement errors in the food industry. *Journal of Food Protection*, *63*(2), 210–215. Retrieved from http://www.ncbi.nlm.nih.gov/pubmed/10678426

Lasko, D. R., & Wang, D. I. C. (1996). On-line monitoring of intracellular ATP concentration in Escherichia coli fermentations. *Biotechnology and Bioengineering*, *52*(3), 364–372. https://doi.org/10.1002/(SICI)1097-0290(19961105)52:3<364::AID-BIT2>3.0.CO;2-I

Lazarova, V., Janex, M. L., Fiksdal, L., Oberg, C., Barcina, I., & Pommepuy, M. (1998). Advanced wastewater disinfection technologies: short and long term efficiency. *Water Science and Technology*, *38*(12), 109 LP-117. Retrieved from http://wst.iwaponline.com/content/38/12/109.abstract

Lee, J. Y., & Deininger, R. A. (2004). Detection of E. coli in beach water within 1 hour using immunomagnetic separation and ATP bioluminescence. *Luminescence*, *19*(1), 31–36. https://doi.org/10.1002/bio.753

Li, G. Q., Wang, W. L., Huo, Z. Y., Lu, Y., & Hu, H. Y. (2017). Comparison of UV-LED and low pressure UV for water disinfection: Photoreactivation and dark repair of Escherichia coli. *Water Research*, *126*, 134–143. https://doi.org/10.1016/j.watres.2017.09.030

Linden, K. G., Shin, G., & Sobsey, M. D. (2001). Comparative effectiveness of UV wavelengths for the inactivation of Cryptosporidium parvum oocysts in water. *Water Science and Technology*, *43*(12).

Linklater, N., & Örmeci, B. (2014). Evaluation of the adenosine triphosphate (ATP) bioluminescence assay for monitoring effluent quality and disinfection performance. *Water Quality Research Journal of Canada*, *49*(2), 114–123. https://doi.org/10.2166/wqrjc.2013.110

LuminUltra. (2016). *Technical Whitepaper: Comparing 2nd Generation ATP to 1st Generation ATP Technology*. Retrieved from https://www.luminultra.com/

LuminUltra. (2018). Our Technology. Retrieved from https://www.luminultra.com/tech/

Malayeri, A. H., Mohseni, M., Cairns, B., Bolton, J. R., Barbeau, B., & Linden, K. G. (2016). *Fluence (UV Dose) Required to Achieve Incremental Log Inactivation of Bacteria , Protozoa , Viruses and Algae*. Retrieved from http://iuvanews.com/stories/092816/fluence-required-achieve-incremental-log-inactivation-bacteria-protozoa-viruses-algae.shtml

Mamane-Gravetz, H., Linden, K. G., Cabaj, A., & Sommer, R. (2005). Spectral sensitivity of Bacillus subtilis spores and MS2 coliphage for validation testing of ultraviolet reactors for water disinfection. *Environmental Science and Technology*, *39*(20), 7845–7852. https://doi.org/10.1021/es048446t

Mathis, R. R., & Brown, O. R. (1976). ATP concentration in Escherichia coli during oxygen toxicity. *Biochimica et Biophysica Acta (BBA) - Bioenergetics*, *440*(3), 723–732. https://doi.org/10.1016/0005-2728(76)90054-2

Meays, C. L., Broersma, K., Nordin, R., & Mazumder, A. (2004). Source tracking fecal bacteria in water: A critical review of current methods. *Journal of Environmental Management*, *73*(1), 71–79. https://doi.org/10.1016/j.jenvman.2004.06.001

Mempin, R., Tran, H., Chen, C., Gong, H., Kim Ho, K., & Lu, S. (2013). Release of extracellular ATP by bacteria during growth. *BMC Microbiology*, *13*(1), 1–13. https://doi.org/10.1186/1471-2180-13-301

Middleton, B. (2017). *Analysis of Ultraviolet Disinfection on Microbial Activity and Validation of Rapid Testing Methods*. Dalhousie University.

Morita, R., Nakane, S., Shimada, A., Inoue, M., Iino, H., Wakamatsu, T., … Kuramitsu, S. (2010). Molecular mechanisms of the whole DNA repair system: A comparison of bacterial and eukaryotic systems. *Journal of Nucleic Acids*, *2010*(ii). https://doi.org/10.4061/2010/179594

Mossel, D. A. A., Corry, J. E., Struijk, C. B., & Baird, R. M. (1995). *Essentials of microbiology: A textbook for advanced studies.* John Wiley & Sons.

Muramoto, Y., Kimura, M., & Nouda, S. (2014). Development and future of ultraviolet light-emitting diodes: UV-LED will replace the UV lamp. *Semiconductor Science and Technology*, *29*(8), 084004. https://doi.org/10.1088/0268-1242/29/8/084004

Oguma, K., Katayama, H., & Ohgaki, S. (2002). Photoreactivation of Escherichia coli after Low- or Medium-Pressure UV Disinfection Determined by an Endonuclease Sensitive Site Assay, *68*(12), 6029–6035. https://doi.org/10.1128/AEM.68.12.6029

Oguma, K., Katayama, H., & Ohgaki, S. (2004). Photoreactivation of Legionella pneumophila after inactivation by low- or medium-pressure ultraviolet lamp. *Water Research*, *38*(11), 2757–2763. https://doi.org/10.1016/j.watres.2004.03.024

Oguma, K., Kita, R., Sakai, H., Murakami, M., & Takizawa, S. (2013). Application of UV light emitting diodes to batch and flow-through water disinfection systems. *Desalination*, *328*, 24–30. https://doi.org/10.1016/j.desal.2013.08.014

Oguma, K., Rattanakul, S., & Bolton, J. R. (2015). Application of UV Light-Emitting Diodes to Adenovirus in Water. *Journal of Environmental Engineering*, *142*(3), 1–6. https://doi.org/10.1061/(ASCE)EE.1943-7870.0001061

Oguma, K., Rattanakul, S., & Bolton, J. R. (2016). Application of UV Light–Emitting Diodes to Adenovirus in Water. *Journal of Environmental Engineering*, *142*(3), 04015082. https://doi.org/10.1061/(ASCE)EE.1943-7870.0001061

Ohmiya, Y., & Hirano, T. (1996). Shining the light: The mechanism of the bioluminescence reaction of calcium-binding photoproteins. *Chemistry and Biology*, *3*(5), 337–347. https://doi.org/10.1016/S1074-5521(96)90116-7

Rattanakul, S., & Oguma, K. (2018). Inactivation kinetics and efficiencies of UV-LEDs against Pseudomonas aeruginosa, Legionella pneumophila, and surrogate microorganisms. *Water Research*, *130*, 31–37. https://doi.org/10.1016/j.watres.2017.11.047

Rompré, A., Servais, P., Baudart, J., De-Roubin, M. R., & Laurent, P. (2002). Detection and enumeration of coliforms in drinking water: Current methods and emerging approaches. *Journal of Microbiological Methods*, *49*(1), 31–54. https://doi.org/10.1016/S0167-7012(01)00351-7

Salcedo, I., Andrade, J. A., Quiroga, J. M., & Nebot, E. (2007). Photoreactivation and dark repair in UV-treated microorganisms: Effect of temperature. *Applied and Environmental Microbiology*, *73*(5), 1594–1600. https://doi.org/10.1128/AEM.02145-06

Schneider, D. A., & Gourse, R. L. (2004). Relationship between growth rate and ATP concentration in escherichia coli: A bioassay for available cellular ATP. *Journal of Biological Chemistry*, *279*(9), 8262–8268. https://doi.org/10.1074/jbc.M311996200

Sharma, R., Ranjan, R., Kapardar, R. K., & Grover, A. (2005). SPECIAL SECTION: MICROBIAL DIVERSITY "Unculturable" bacterial diversity: An untapped resource. *Current Science*, *89*(1).

Sholtes, K. A., Lowe, K., Walters, G. W., Sobsey, M. D., Linden, K. G., & Casanova, L. M. (2016). Comparison of Ultraviolet Light Emitting Diodes and Low-Pressure Mercury-Arc Lamps for Disinfection of Water. *Environmental Technology*, *3330*(September), 1–23. https://doi.org/10.1080/09593330.2016.1144798

Shur, M. S., & Gaska, R. (2010). Deep-ultraviolet light-emitting diodes. *IEEE Transactions on Electron Devices*, *57*(1), 12–25. https://doi.org/10.1109/TED.2009.2033768

Simons, R., Gabbai, U. E., & Moram, M. A. (2014). Optical fluence modelling for ultraviolet light emitting diode-based water treatment systems. *Water Research*, *66*, 338–349. https://doi.org/10.1016/j.watres.2014.08.031

Soini, J., Falschlehner, C., Mayer, C., Böhm, D., Weinel, S., Panula, J., … Neubauer, P. (2005). Transient increase of ATP as a response to temperature up-shift in Escherichia coli. *Microbial Cell Factories*, *4*, 1–8. https://doi.org/10.1186/1475-2859-4-9

Sommer, R., Cabaj, A., & Haider, T. (1996). Microbicidal effect of reflected UV radiation in devices for water disinfection. In *Water Science and Technology* (Vol. 34, pp. 173–177). https://doi.org/10.1016/S0273-1223(96)00742-1

Sommer, R., Haider, T., Cabaj, A., Pribil, W., & Lhotsky, M. (1998). Time dose reciprocity in UV disinfection of water. *Water Science and Technology*, *38*(12), 145–150. https://doi.org/10.1016/S0273-1223(98)00816-6

Song, K., Mohseni, M., & Taghipour, F. (2016). Application of ultraviolet light-emitting diodes (UV-LEDs) for water disinfection : A review. *Water Research*, *94*, 341–349. https://doi.org/10.1016/j.watres.2016.03.003

Staley, J. T., & Konopka, A. (1985). Microorganisms in Aquatic and Terrestrial Habitats.

Taniyasu, Y., Kasu, M., & Makimoto, T. (2006). An aluminium nitride light-emitting diode with a wavelength of 210 nanometres. *Nature*, *441*(7091), 325–328. https://doi.org/10.1038/nature04760

Trojan UV. (2018). UV Disinfection & Water Treatment Solutions. Retrieved August 20, 2006, from http://www.trojanuv.com/

Turner, D. E., Daugherity, E. K., Altier, C., & Maurer, K. J. (2010). Efficacy and limitations of an ATP-based monitoring system. *Journal of the American Association for Laboratory Animal Science : JAALAS*, *49*(2), 190–195. https://doi.org/20353694

van Slooten, C., Wijers, T., Buma, A. G. J., & Peperzak, L. (2015). Development and testing of a rapid, sensitive ATP assay to detect living organisms in ballast water. *Journal of Applied Phycology*, *27*(6), 2299–2312. https://doi.org/10.1007/s10811-014-0518-9

Vartoukian, S. R., Palmer, R. M., & Wade, W. G. (2010). Strategies for culture of "unculturable" bacteria. *FEMS Microbiology Letters*, *309*(1), 1–7. https://doi.org/10.1111/j.1574-6968.2010.02000.x

Villaverde, A., Guerrero, R., & Barbe, J. (1986). Microbiology ATP Production after Ultraviolet Irradiation in Escherichia coli. *Current Microbiology*, *14*, 31–34.

Wang, T., MacGregor, S. J., Anderson, J. G., & Woolsey, G. A. (2005). Pulsed ultra-violet inactivation spectrum of Escherichia coli. *Water Research*, *39*(13), 2921–2925. https://doi.org/10.1016/j.watres.2005.04.067

Whitmore, S. E., Potten, C. S., Chadwick, C. A., Strickland, P. T., & Morison, W. L. (2001). Effect of photoreactivating light on UV radiation-induced alterations in human skin. *Photodermatology Photoimmunology and Photomedicine*, *17*(5), 213–217. https://doi.org/10.1034/j.1600-0781.2001.170502.x

WHO. (2014). Preventing diarrhoea through better water, sanitation and hygiene. *WHO Library Cataloguing-in-Publication Data*, 1–48. https://doi.org/ISBN 978 92 4 156482 3

Würtele, M. A., Kolbe, T., Lipsz, M., Külberg, A., Weyers, M., Kneissl, M., & Jekel, M. (2011). Application of GaN-based ultraviolet-C light emitting diodes - UV LEDs - for water disinfection. *Water Research*, *45*(3), 1481–1489. https://doi.org/10.1016/j.watres.2010.11.015

Xie, X. (2014). *Development of a rapid ATP analysis method: biomass growth ATP method for UV disinfection monitoring in wastewater treatment*. Dalhousie University.

Yokoyama, H., & Mizutani, R. (2014). Structural biology of DNA (6-4) photoproducts formed by ultraviolet radiation and interactions with their binding proteins. *International Journal of Molecular Sciences*, *15*(11), 20321–20338. https://doi.org/10.3390/ijms151120321

Zhang, S., Ye, C., Lin, H., Lv, L., & Yu, X. (2015). UV disinfection induces a vbnc state in escherichia coli and pseudomonas aeruginosa. *Environmental Science and Technology*, *49*(3), 1721–1728. https://doi.org/10.1021/es505211e

Zmirou, D., Pena, L., Ledrans, M., & Letertre, A. (2003). Risks Associated with the Microbiological Quality of Bodies of Fresh and Marine Water Used for Recreational Purposes: Summary Estimates Based on Published Epidemiological Studies. *Archives of Environmental Health: An International Journal*, *58*(11), 703–711. https://doi.org/10.3200/AEOH.58.11.703-711

APPENDIX A – REQUIRED FLUENCES TO ACHIEVE LOG REDUCTIONS IN DIFFERENT MICROORGANISMS

Required fluences for log reduction of various spores

		UV Fluence to achieve a given log reduction (mJ cm^{-2})						
Spore	**λ**	**1**	**2**	**3**	**4**	**5**	**Protocol**	**Reference**
Bacillus atrophaeus								
ATCC 9372	260 nm	6	10	14	19	31	Yes	(Sholtes et al., 2016)
Bacillus subtillis								
ATCC 6633	269 nm	2	10	17	25	-	Yes	(Würtele et al., 2011)
ATCC 6633	282 nm	3	11	18	26	-	Yes	(Würtele et al., 2011)

Required fluences for log reductions of *Escherichia coli*

		UV Fluence to achieve a given log reduction (mJ cm^{-2})						
	λ	**1**	**2**	**3**	**4**	**5**	**6**	**Reference**
Escherichia coli								
ATCC 11229	255 nm	5.9	7.9	-	-	-		(Bowker et al., 2011)
ATCC 11229	275 nm	4.3	6.2	7.7	-	-		(Bowker et al., 2011)
ATCC 29425	265 nm	3.6	5.9	17	20	-		(Chatterley & Linden, 2010)
B ATCC 13033	260 nm	1.2	3.0	4.7	6.5	8.2	10	(Sholtes et al., 2016)
K 12 IFO 3301	265 nm	2.6	4.7	6.6	9.0	12	-	(Oguma et al., 2013)
K 12 IFO 3301	280 nm	3.4	6.9	10	14	-	-	(Oguma et al., 2013)

K 12 IFO 3301	285 nm	7.8	3	16	23	34	-	(Oguma et al., 2015)

Required fluences for log reductions of various viruses

			UV Fluence to achieve a given log reduction (mJ cm^{-2})				
Virus	**Host**	**λ**	**1**	**2**	**3**	**4**	**Reference**
Adenovirus							
Type 5 ATCC VR5	A549 cell line (CCL-185)	285 nm	50	82	126	-	(Oguma et al., 2015)
MS2 coliphage							
	n/a	255 nm	14	26	38	-	(Aoyagi et al., 2011)
	E. *coli* Famp ATCC 700891	260 nm	13	36	40	53	(Sholtes et al., 2016)
ATCC15977-B1	E. coli ATCC 15597	255 nm	25	50	-	-	(Bowker et al., 2011)
ATCC15977-B1	E. coli ATCC 15597	275 nm	25	55	-	-	(Bowker et al., 2011)
ATCC15977-B1	E. coli ATCC 15597 C3000	260 nm	15	32	48	-	(Jenny, Simmons, Shatalov, & Ducoste, 2014)
ATCC15977-B1	E.coli ER2738	255 nm	19	42	72	-	(Simons, Gabbai, & Moram, 2014)
ATCC15977-B1	E. coli K12 A/λ(F+)	285 nm	32	70	106	-	(Oguma et al., 2015)
ϕ X 174							

	N/A	255 nm	1.6	3.3	5.1	-	(Aoyagi et al., 2011)
	N/A	280 nm	2.3	5.1	8.5	-	(Aoyagi et al., 2011)
Qβ							
	N/A	255 nm	11	23	-	-	(Aoyagi et al., 2011)
	N/A	280 nm	27	-	-	-	(Aoyagi et al., 2011)
	E. coli ATCC 15597 C3000	260 nm	9	19	29	41	(Jenny et al., 2014)
ATCC 23631 B1	E. coli K12 A/λ(F+)	285 nm	27	54	81	-	(Oguma et al., 2015)
T7							
coliphage	E. coli ATCC 11303	255 nm	2.9	6.9	14	-	(Bowker et al., 2011)
coliphage	E. coli ATCC 11303	275 nm	2.7	6.0	12	17	(Bowker et al., 2011)

APPENDIX B – COPYRIGHT TRANSFERS

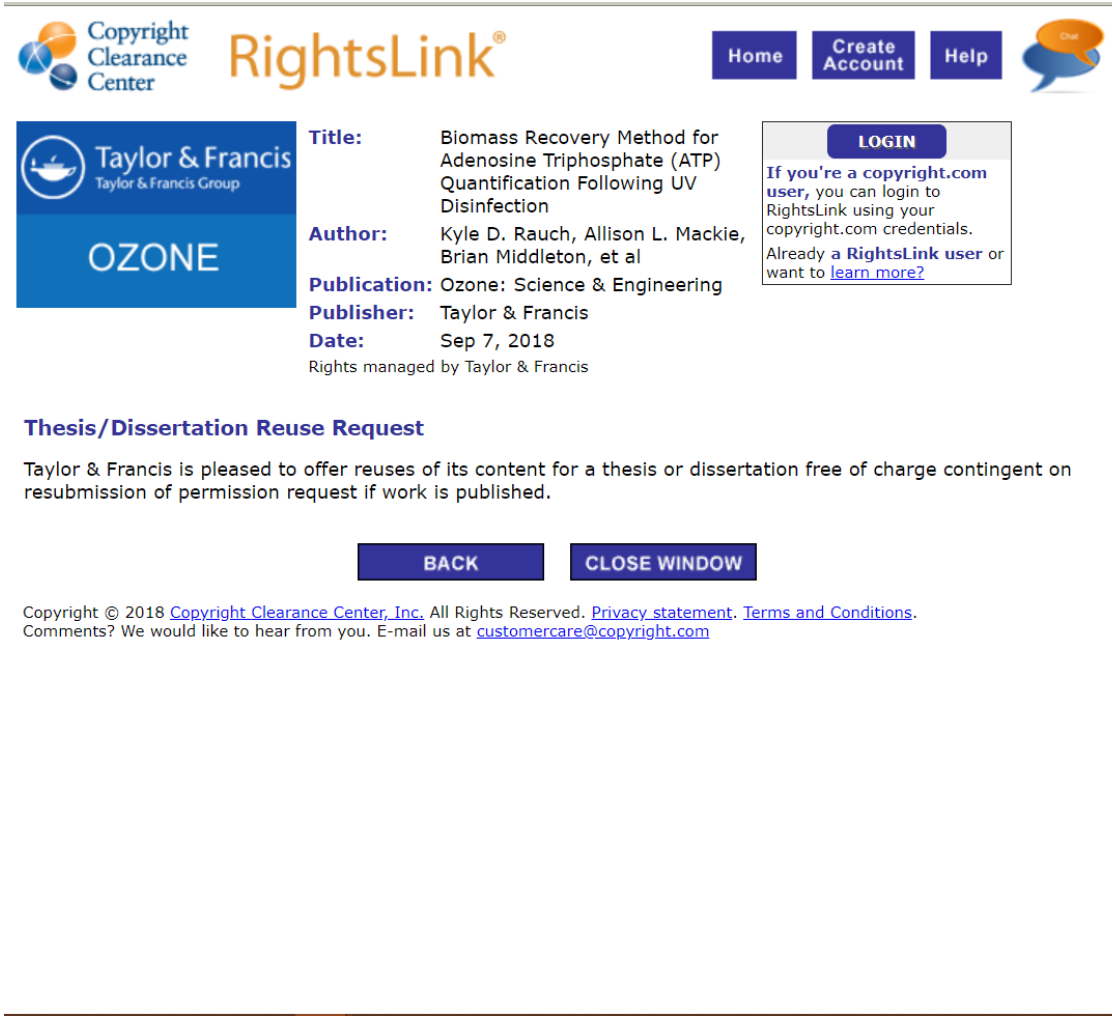

Copyright Clearance Center RightsLink®

Home | Create Account | Help

Taylor & Francis
Taylor & Francis Group
OZONE

Title: Biomass Recovery Method for Adenosine Triphosphate (ATP) Quantification Following UV Disinfection
Author: Kyle D. Rauch, Allison L. Mackie, Brian Middleton, et al
Publication: Ozone: Science & Engineering
Publisher: Taylor & Francis
Date: Sep 7, 2018
Rights managed by Taylor & Francis

LOGIN
If you're a copyright.com user, you can login to RightsLink using your copyright.com credentials.
Already **a RightsLink user** or want to learn more?

Thesis/Dissertation Reuse Request

Taylor & Francis is pleased to offer reuses of its content for a thesis or dissertation free of charge contingent on resubmission of permission request if work is published.

BACK | CLOSE WINDOW

Copyright © 2018 Copyright Clearance Center, Inc. All Rights Reserved. Privacy statement. Terms and Conditions.
Comments? We would like to hear from you. E-mail us at customercare@copyright.com

APPENDIX C – SAMPLE R CODES

FWHM.R

```
This script reads in spectral output data for UV-LEDs and determines the Full-Width Half Maximum

library(tidyverse)

setwd("C:/Users/Kyle/OneDrive - Dalhousie University/CWRS/Masters/Data/Thesis")

#Read in  data and select monochromtic outputs
data <- read.csv("spectralOutputs.csv")
data2 <- subset(data, LED %in% c(255, 265, 285) )

#Determine maximum intensity for each LED
maxis <- data %>%
  group_by(LED) %>%
  summarise_each(funs(max))

m255 <- maxis[1,3]
m265 <- maxis[5,3]
m285 <- maxis[7,3]

#Calculate Half Maximum Power
h255 <- round(m255/2,1)
h265 <- round(m265/2,0)
h285 <- round(m285/2,0)

#Calculate FWHM for 255 nm UV-LED
L255 <- subset(data, LED == "255")
L255$Relative.Absolute.Intensity <- round(L255$Relative.Absolute.Intensity,1)
lambda255 <- L255[L255$Relative.Absolute.Intensity %in% h255,]
lambda255R <- lambda255[1:3,2]
lambda255L <- lambda255[4:6,2]
FWHM255 <- mean(lambda255L)-mean(lambda255R)
FWHM255

## [1] 12.13333

#Calculate FWHM for 265 nm UV-LED
L265 <- subset(data, LED == "265")
L265$Relative.Absolute.Intensity <- round(L265$Relative.Absolute.Intensity,0)
lambda265 <- L265[L265$Relative.Absolute.Intensity %in% h265,]
lambda265R <- lambda265[1:6,2]
lambda265L <- lambda265[7:14,2]
FWHM265 <- mean(lambda265L)-mean(lambda265R)
FWHM265

## [1] 11.48167

#Calculate FWHM for 285 nm UV-LED
L285 <- subset(data, LED == "285")
L285$Relative.Absolute.Intensity <- round(L285$Relative.Absolute.Intensity,0)
lambda285 <- L285[L285$Relative.Absolute.Intensity %in% h285,]

lambda285R <- lambda285[1:7,2]
lambda285L <- lambda285[8:16,2]
FWHM285 <- mean(lambda285L)-mean(lambda285R)
FWHM285

## [1] 11.0227
```

regressionSpectro.R

```r
#This script subsections the monochromatic  dose response curves using spectrometer doses and perf
orms a linear regression on that subsection

library(tidyverse)

setwd("C:/Users/Kyle/OneDrive - Dalhousie University/CWRS/Masters/Data/Thesis")

data<-read_csv("synergy.csv")

#255 nm UVLED
ss255 <- subset(data, Wavelength == "255")
ss255 <- ss255[c(3:5,9:11,15:17),]
rss255 <- lm(Value~Dose, data = ss255)
summary(rss255)

##
## Call:
## lm(formula = Value ~ Dose, data = ss255)
##
## Residuals:
##     Min      1Q  Median      3Q     Max
## -0.9739 -0.3358 -0.2047  0.6478  0.9878
##
## Coefficients:
##             Estimate Std. Error t value Pr(>|t|)
## (Intercept)  -2.8120     0.8906  -3.157  0.01599 *
## Dose          1.3610     0.2580   5.276  0.00115 **
## ---
## Signif. codes:  0 '***' 0.001 '**' 0.01 '*' 0.05 '.' 0.1 ' ' 1
##
## Residual standard error: 0.7209 on 7 degrees of freedom
## Multiple R-squared:  0.7991, Adjusted R-squared:  0.7704
## F-statistic: 27.84 on 1 and 7 DF,  p-value: 0.001153

#265 nm UVLED

ss265 <- subset(data, Wavelength == "265")
ss265 <- ss265[c(3:5,9:11,15:17),]
rss265 <- lm(Value~Dose, data = ss265)
summary(rss265)

##
## Call:
## lm(formula = Value ~ Dose, data = ss265)
##
## Residuals:
##      Min       1Q   Median       3Q      Max
## -0.80276 -0.10586 -0.00656  0.22934  0.91108
##
## Coefficients:
##             Estimate Std. Error t value Pr(>|t|)
## (Intercept)  -2.2480     0.7005  -3.209 0.014875 *
## Dose          1.1031     0.1616   6.827 0.000247 ***
## ---
## Signif. codes:  0 '***' 0.001 '**' 0.01 '*' 0.05 '.' 0.1 ' ' 1
##
## Residual standard error: 0.567 on 7 degrees of freedom
## Multiple R-squared:  0.8694, Adjusted R-squared:  0.8508
## F-statistic:  46.6 on 1 and 7 DF,  p-value: 0.0002472

#285 nm UVLED

ss285 <- subset(data, Wavelength == "285")
ss285 <- ss285[c(4:6,10:12,16:18),]
rss285 <- lm(Value~Dose, data = ss285)
summary(rss285)
```

```
##
## Call:
## lm(formula = Value ~ Dose, data = ss285)
##
## Residuals:
##     Min      1Q  Median      3Q     Max
## -0.9536 -0.0390  0.1035  0.1281  0.5341
##
## Coefficients:
##             Estimate Std. Error t value Pr(>|t|)
## (Intercept) -1.10265    0.39002  -2.827 0.025511 *
## Dose         0.37960    0.06327   5.999 0.000543 ***
## ---
## Signif. codes:  0 '***' 0.001 '**' 0.01 '*' 0.05 '.' 0.1 ' ' 1
##
## Residual standard error: 0.4807 on 7 degrees of freedom
## Multiple R-squared:  0.8372, Adjusted R-squared:  0.8139
## F-statistic: 35.99 on 1 and 7 DF,  p-value: 0.0005426
```

orthogonalRegression.R

```
library(tidyverse)
setwd("C:/Users/Kyle/OneDrive - Dalhousie University/CWRS/Masters/Data/Disinfection")

data <- read.csv("RegData2.csv")
#DT Plant RBGO and Ecoli
xID <- "DT_RBGO.1"
yID <- "DT_Ecoli"
x <- data[,c(xID)]
y <- data[,c(yID)]

xy <- as.data.frame(cbind(y,x)) %>% na.omit

xmin <- min(xy[,2])
xmax <- max(xy[,2])
means <- colMeans(xy)

reg <- lm(y~x, xy)
#variance explained:
rsl <- reg$coefficients[2]
rb <- reg$coefficients[1]

e <- var(xy,use = "complete") %>% eigen #spectral decomposition

exp <- e$values[1] / sum(e$values) #variance explained by first principal component (orthogonal re
gression line)
esl <- e$vectors[1]/e$vectors[2]
b <- means[1]-esl*means[2]


#DT Lab RBGO and Ecoli
xID2 <- "DT_RBGO2"
yID2 <- "DT_Ecoli2"
x2 <- data[,c(xID2)]
y2 <- data[,c(yID2)]

xy2 <- as.data.frame(cbind(y2,x2)) %>% na.omit

xmin2 <- min(xy2[,2])
xmax2 <- max(xy2[,2])
means2 <- colMeans(xy2)
```

```
reg2 <- lm(xy2)
#variance explained:
rsl2 <- reg2$coefficients[2]
rb2 <- reg2$coefficients[1]

e2 <- var(xy2,use = "complete") %>% eigen #spectral decomposition

exp2 <- e2$values[1] / sum(e2$values) #variance explained by first principal component (orthogonal
regression line)
esl2 <- e2$vectors[1]/e2$vectors[2]
b2 <- means2[1]-esl2*means2[2]


#MC Plant RBGO and Ecoli
xID3 <- "MC_RBGO"
yID3 <- "MC_Ecoli"
x3 <- data[,c(xID3)]
y3 <- data[,c(yID3)]

xy3 <- as.data.frame(cbind(y3,x3)) %>% na.omit
xmin3 <- min(xy3[,2])
xmax3 <- max(xy3[,2])
means3 <- colMeans(xy3)

reg3 <- lm(xy3)
#variance explained:
rsl3 <- reg3$coefficients[2]
rb3 <- reg3$coefficients[1]

e3 <- var(xy3,use = "complete") %>% eigen #spectral decomposition

exp3 <- e3$values[1] / sum(e3$values) #variance explained by first principal component (orthogonal
regression line)
esl3 <- e3$vectors[1]/e3$vectors[2]
b3 <- means3[1]-esl3*means3[2]


#MC Lab RBGO and Ecoli
xID4 <- "MC_RBGO2"
yID4 <- "MC_Ecoli2"
x4 <- data[,c(xID4)]
y4 <- data[,c(yID4)]

xy4 <- as.data.frame(cbind(y4,x4)) %>% na.omit

xmin4 <- min(xy4[,2])
xmax4 <- max(xy4[,2])
means4 <- colMeans(xy4)

reg4 <- lm(xy4)
#variance explained:
rsl4 <- reg4$coefficients[2]
rb4 <- reg4$coefficients[1]

e4 <- var(xy4,use = "complete") %>% eigen #spectral decomposition

exp4 <- e4$values[1] / sum(e4$values) #variance explained by first principal component (orthogonal
regression line)
esl4 <- e4$vectors[1]/e4$vectors[2]
b4 <- means4[1]-esl4*means4[2]
```

weightedAbsorb.R

```
library(tidyverse)

setwd("C:/Users/Kyle/OneDrive - Dalhousie University/CWRS/Masters/Data/Thesis")

data <- read.csv("spectralOutputs.csv")
absorb <- read.csv("ScanData_6.csv")


#Clean and filter absorbance data
absorb$nm <- round(absorb$nm, 0)
absorbClean <- absorb %>%
  filter(nm >=230) %>%
  filter(nm <= 320) %>%
  group_by(nm) %>%
  summarize(ABS = mean(Abs))

#Subset and determine weighted absorbance value for 255 UV-LED
L255 <- subset(data, LED == "255")
L255$Wavelength <- round(L255$Wavelength,0)
L255 <- subset(L255, L255$Wavelength >= 230)
L255 <- subset(L255, L255$Wavelength <= 320)
L255

AVG255 <- L255 %>%
  group_by(Wavelength) %>%
  summarize(mean = mean(Relative.Absolute.Intensity))
AVG255

t255 <- sum(AVG255$mean)

AVG255W <- AVG255$mean/t255
sum(AVG255W*absorbClean$ABS)

## [1] 0.05559862 #Weighted absorbance value

absorbClean[absorbClean$nm==260,]

## # A tibble: 1 x 2
##      nm    ABS
##   <dbl>  <dbl>
## 1  260. 0.0580 #Peak absorbance value

#Subset and determine weighted absorbance value for 265 UV-LED

L265 <- subset(data, LED == "265")
L265$Wavelength <- round(L265$Wavelength,0)
L265 <- subset(L265, L265$Wavelength >= 230)
L265 <- subset(L265, L265$Wavelength <= 320)

AVG265 <- L265 %>%
  group_by(Wavelength) %>%
  summarize(mean = mean(Relative.Absolute.Intensity))
AVG265

t265 <- sum(AVG265$mean)

AVG265W <- AVG265$mean/t265
sum(AVG265W*absorbClean$ABS)

## [1] 0.05610454 #Weighted absorbance value

absorbClean[absorbClean$nm==268,]

## # A tibble: 1 x 2
##      nm    ABS
```

```
##   <dbl>  <dbl>
## 1  268. 0.0580 #Peak absorbance value



#Subset and determine weighted absorbance value for 285 UV-LED

L285 <- subset(data, LED == "285")
L285$Wavelength <- round(L285$Wavelength,0)
L285 <- subset(L285, L285$Wavelength >= 230)
L285 <- subset(L285, L285$Wavelength <= 320)

AVG285 <- L285 %>%
  group_by(Wavelength) %>%
  summarize(mean = mean(Relative.Absolute.Intensity))
AVG285

t285 <- sum(AVG285$mean)

AVG285W <- AVG285$mean/t285
sum(AVG285W*absorbClean$ABS)

## [1] 0.03771425 #Weighted absorbance value

absorbClean[absorbClean$nm==285,]

## # A tibble: 1 x 2
##      nm    ABS
##   <dbl>  <dbl>
## 1  285. 0.0390 #Peak absorbance value
```

APPENDIX D – RAW DATA

WWTF B

	Plant Data					Lab Water Quality Data				
Date	Sampling Time	UVT (%)	Flow Rate (m3/hr)	TSS (mg/L)		UVT (%)	ABS	pH	Turbidity (NTU)	TSS (mg/L)
22-Mar-16	8:55	58.90	1516	18		58.2	0.235		14.3	12
24-Mar-16	10:15	52.00	1364	11.4		57.3	0.254	6.82	9.08	2
29-Mar-16	ND	50.20	2246	19.7		61.4	0.254	6.48	12.7	12
01-Apr-16	ND	44.60	ND	12.3		50.1	0.304	6.4	10.6	10
04-Apr-16	ND	41.90	1520	25		49.1	0.309		18	8
06-Apr-16	ND	52.80	ND	14.9		54.3	0.266		12.3	24
08-Apr-16	ND	48.40	ND	14.5		50.4	0.297	7.4	13.6	14
11-Apr-16	ND	54.40	ND	13.4		59.3	0.227	7.04	11.3	15
14-Apr-16	ND	49.8	ND	ND		59.2	0.228		10.2	
15-Apr-16	9:00	45.2	ND	ND		61.5	0.211		12.8	18
18-Apr-16	9:22	41.6	ND	14		54.6	0.263	7.1	11.1	11
20-Apr-16	9:35	38.60	1352	14.6		52.4	0.281	7.33	11.3	10
22-Apr-16	ND	45	ND	ND		51.9	0.285	6.65	8.94	9
25-Apr-16	9:00	52.8	ND	ND		56.6	0.248	6.7	8.41	18
27-Apr-16	9:43	ND	ND	ND		52.7	0.278	7.25	9.88	15
29-Apr-16	8:45	64.40	ND	ND		52.9	0.277	7.46	7.61	
09-May-16	8:30	63.70	ND	ND		53.9	0.268	6.71	9.44	12
11-May-16	8:30	54.00	ND	ND		45.1	0.346	7.62	9.46	26
13-May-16	ND	62.70	ND	9.52		52.4	0.281	7.88	8.33	13
16-May-16	9:30	59.60	1148	9.33		50.3	0.298	6.65	8.41	4
18-May-16	8:30	44.80	ND	ND		37.2	0.430	6.68	12.5	15
19-May-16	8:30	44.80	ND	ND		41.0	0.387	7.43	13.2	3
26-May-16	8:30	49.20	ND	ND		40.5	0.393			
31-May-16	9:00	57.00	ND	10.4		46.6	0.332	6.72	8.47	

E.coli (MPN/100mL)					
Untreated	Plant	10 mJ/cm2	20 mJ/cm2	40 mJ/cm2	60 mJ/cm2
6440	1203.3	1211	328	816.4	770.1
3930	1299.791	900	1	1	1
1299.7	727	520	197	127.4	41
90800	1523	3110	327	63	20
178200	1731	4040	249	86	10
68300	256	2820	134	85	75
14670	132	4800	256	97	10
20100	30	3310	323	63	10
11530	52	980	395	41	1
8400	132	410	90.9	35.5	18.9
43520	121	2966.5	213	98	31
13170	213	2041.5	738	148	41
7715	214.3	1623	565.15	271.3	73.65
11430	117.9	1905	399	191.65	110.75
9265	219.8	1681	549.7	176.15	99
32860	194.75	2571.5	320.95	127.4	103
140155	86	7595.5	1223	246	41
36020	292	5091	784	355	213
27360	171	3422.5	487	189	281.2
26160	51	2880	309	201	20
14270	379	1850	613	233	86
35520	355	2880	292	145	63
23800	288	3550	298	201	75

Total Coliforms (MPN/100mL)					
Untreated	Plant	10 mJ/cm2	20 mJ/cm2	40 mJ/cm2	60 mJ/cm2
92080	1210	17329	4352	959	272
77000	2419.6	8164	#N/A	#N/A	#N/A
866400	9208	5480	4352	#N/A	195.6
920800	1523	26130	2014	187	20
1986300	4611	14210	23590	295	31
648800	3654	14010	1576	269	122
148300	771	29870	3654	565	135
248100	262	32550	5794	474	233
53800	384	10190	684	171	120
261300	836	7540	2723	148	148
365400	327	18500	3448	389	134
261300	1396	30760	8664	644	134
81800	2057.45	24810	12033	1200.1	426.2
118295	1627.4	18339.5	4352	435.15	196.3
122645	2320.95	21043.5	4352	579.05	188.45
245030	2231.05	16658	4611	711.1	406.6
770100	355	32550	6488	1236	187
266430	1500	30760	6867	1789	677
186000	474.2	19711.5	3654	431.25	403.25
88030	145	11620	2187	576	75
131685	3448	30760	6488	855	231
344800	1789	19560	3255	650	292
228200	2035	23590	4352	1198	309

c-ATP (pg-cATP/mL)					
Untreated	Plant	10 mJ/cm2	20 mJ/cm	40 mJ/cm2	60 mJ/cm2
11419.4	4681.5	7546.6	7775.8	4298.4	4635.6
12004.6	3783.6	7575.2	9507.1	8504.7	8709.2
8532.1	1981.1	2561.4	1091.7	1096.7	567.4
27256.6	2452.4	3258.1	1277.6	1303.9	2141.3
14792.7	3009.1	1256.1	962.9	918	1278.5
6942.9	1168.4	1310.8	911.6	951.9	897.2
12504.1	3223.4	7220.4	5782.8	3799.4	3164
9345.5	2114	4716.4	3422.4	2619.9	2549.7
#N/A	#N/A	#N/A	#N/A	#N/A	#N/A
21283.8	1493.7	4795.9	253.9	1503.6	2537
9030	1802.3	4976.2	3933.6	2384.3	2304
13514.8	2667.5	4502.8	4175.6	3530.6	2343.6
13098.4	3195.3	4219.4	3301.6	2880.8	2343.9
11904.4	3213.1	8069.5	4963.1	5744.7	4511.7
21993.7	1607.8	5443.4	4045.7	3681.7	3192.2
15085.2	1816.8	4171.1	3238.1	3238.1	1872.7
25980.4	1220.5	3009.3	3475.5	2466.9	1854
15500.8	2950.7	7484.6	3672.9	3940.9	3722.9
6903.2	2500.6	3233.5	3477.6	2729.1	2975.9
10797.3	3133.8	4621.4	3311.8	3602	3844.2
10715.7	4037.2	5931.2	6636.7	4458.6	4708.5
#N/A	#N/A	#N/A	#N/A	#N/A	#N/A
10798.5	2568.4	5219.3	3047.1	3174.3	1988.8
6234.4	1176.3	2191.2	1719.9	1071.9	1440

WWTF D

	Plant Data					Lab Water Quality Data				
Date	Sampling Time	UVT (%)	pH	Flow Rate (m3/hr)	TSS (mg/L)	UVT (%)	ABS@254nm	pH	Turbidity (NTU)	TSS (mg/L)
17-Aug-16	8:00	74.50		5169		69.3	0.159	6.48	5.87	5
19-Aug-16	8:31	61.10	6.80	1280	25	54.7	0.262	6.82	3.78	7
22-Aug-16	8:30	61.40	6.80	1423		58.9	0.230		4.41	10
24-Aug-16	8:49	46.70	6.78	1400		38.5	0.415	6.96	11.63	11
26-Aug-16	8:30	46.80	6.70	1532		40.3	0.395	7.14	10.90	13
03-Sep-16	8:17	48.00	6.78	1310		44.1	0.356	6.98	9.60	15
07-Sep-16	8:42	49.40	6.55	1330		40.9	0.388	7.04	9.58	4
09-Sep-16	9:20	37.5	6.78	1336		30.3	0.519	6.6	30.80	23
12-Sep-16	11:13	45.4	6.92	1317		40.3	0.395	7.18	13.53	15
14-Sep-16	8:10	37.1		1642		29.5	0.530	6.99	57.77	
15-Sep-16	8:05	53.70	6.56	1230		46.7	0.331	6.96	18.85	
21-Sep-16	8:47	56.7	6.97	1574				7.02		13
23-Sep-16	8:30	42.3	5.98	1318		40.3	0.395	7.07	39.10	13
26-Sep-16	10:20	58.50	6.84	1454	29	51.3	0.290	7.16	14.40	5
28-Sep-16	9:20	60.30	6.80	1196				7.34		12
03-Oct-16	8:05	61.00	6.64	1313		57.4	0.241	7.46	3.39	3
05-Oct-16	9:07	55.00	6.97	1371		50.5	0.297	7.04	8.18	5
07-Oct-16	8:30	47.10	6.88	1320		43.1	0.366	7.07	25.70	

E-coli nj(MPN/100mL)									
Untreated	UV Channel 1	UV Channel 2	10 mJ/cm2	20 mJ/cm2	25 mJ/cm2	30 mJ/cm2	35 mJ/cm2	40 mJ/cm2	60 mJ/cm2
20870	2098	1169	980	195	187	203	161	132	63
283730	292	86	2650	135	657	249	187	275	187
165800	20	86	4530	278	132	119	86	86	41
1526550	1553	1670	6290	422	305	331	216	158	299
989600	187	733	2690	504	317	487	275	1473	201
1071900	644	110	6200	613	529	379	275	259	98
1728950	1019	4884	7800	644	323	122	350	767	109
3076000	> 24196.0	> 24196.0	8130	1126	960	733	538	538	238
1066950	2359	8164	34480	11199	4352	3873	2187	7701	323
2086650	> 2419.6	> 2419.6	3930	613	399	309	437	226	86
1081650	12033	591	20640	650	323	2282	538	305	84
509250	327	30	1480	723		146		201	41
109560	9208	2851	2380	441		121		148	20
51270	2950	960	5380	789		323		189	134
31840	300	< 100.0	4670	1483		1500		906	110
45060	10	31	4170	272		122		228	41
50910	1046	62	2590	393		197		74	41
97610	231	933	10390	2755		1354		1067	146

Total Coliforms (MPN/100mL)									
Untreated	**UV Channel 1**	**UV Channel 2**	**10 mJ/cm2**	**20 mJ/cm2**	**25 mJ/cm2**	**30 mJ/cm2**	**35 mJ/cm2**	**40 mJ/cm2**	**60 mJ/cm2**
155305	19863	6131	6020	1860	884	1274	457	435	546
> 241960.0	3654	609	20980	2224	3654	1597	771	4611	2909
> 241960.0	213	602	15000	3448	1515	3873	1597	733	315
24196000	14136	24196	15530	11199	7701	6488	1850	805	4611
10462000	556	19863	43520	6867	6867	2247	2613	17113.33333	3076
8542050	5172	657	32550	5475	2382	1658	1439	1616	384
1046200	10462	> 24196.0	81640	9804	8664	3076	3448	6867	563
>24196000	> 24196.0	> 24196.0	41060	6488	5475	5172	3255	6488	3255
15531000	24196	> 24196.0	> 241960.0	> 24196.0	> 24196.0	24196	24196	> 24196.0	4106
>24196000	> 24196.0	> 24196.0	46110	9208	4884	2247	5172	2909	1793
17329000	> 24196.0	14136	241960	9208	5475	14136	2247	3654	1956
15531000	9804	663	12910	4884		1935		2187	448
2419600	> 24196.0	> 24196.0	64880	5794		3448		3654	259
613100	2098	537	34480	5794		5475		1658	1259
1203300	1580	100	32550	9208		17329		2909	9208
517200	41	121	22240	3448		1396		3076	512
7270000	3654	759	36540	3255		2014		933	309
1299700	2613	9208	81640	15531		15531		12997	905

ATP (pg-cATP/mL)									
Untreated	**UV Channel 1**	**UV Channel 2**	**10 mJ/cm2**	**20 mJ/cm2**	**25 mJ/cm2**	**30 mJ/cm2**	**35 mJ/cm2**	**40 mJ/cm2**	**60 mJ/cm2**
1376.8	516.3	452.0	238.8	117.8	141.2	161.1	125.8	87.7	95.9
206818.8	437.3	144.0	2279.5	730.1	415.6	510.5	349.3	408.6	378.5
#N/A	#N/A	#N/A	#N/A	#N/A	#N/A	#N/A	#N/A	#N/A	#N/A
#N/A	#N/A	#N/A	#N/A	#N/A	#N/A	#N/A	#N/A	#N/A	#N/A
#N/A	#N/A	#N/A	#N/A	#N/A	#N/A	#N/A	#N/A	#N/A	#N/A
#N/A	#N/A	#N/A	#N/A	#N/A	#N/A	#N/A	#N/A	#N/A	#N/A
175383.5	530.1	687.1	2685.7	1735.3	1479.8	1442.9	1274.3	1485.2	1219.1
256140.5	5263.7	2594.7	3631.0	2432.0	1594.4	1660.7	1559.5	1537.9	1451.7
114471.8	627.2	775.5	4549.7	3670.0	2987.4	1973.6	1791.7	1522.8	1580.6
120811.4	5623.7	4277.7	1247.6	774.5	974.4	930.0	741.2	634.6	6333.8
#N/A	#N/A	#N/A	#N/A	#N/A	#N/A	#N/A	#N/A	#N/A	#N/A
102555.9783	1535.434783	698.0434783	3427.391304	1500.108696	#N/A	1501.956522	#N/A	1632.717391	1544.673913
114020.4189	759.6667253	519.0400751	2733.790999	1341.723875	#N/A	1188.405797	#N/A	904.6529367	915.0384322
198705.927	1887.274106	959.9393403	4602.931884	2288.133451	#N/A	2302.034627	#N/A	2726.778719	2021.736383
113749.5188	335.3009111	298.3446683	1167.586295	583.023226	#N/A	558.5140511	#N/A	477.6081098	447.1320416
143266.5274	399.2547846	553.43533	2746.683227	1349.517304	#N/A	949.8108734	#N/A	1018.009372	927.6802349
#N/A	#N/A	#N/A	#N/A	#N/A	#N/A	#N/A	#N/A	#N/A	#N/A
401322.9178	956.1649994	1695.065753	6735.641227	2360.233787	#N/A	2558.390469	#N/A	2901.539845	1786.220074

UV-LED Ecoli Data

LP	CFU1	CFU2	CFU3	Average	STD	log(c/co)
0	4200000	7000000	5500000	5566667	1401190	0
2	4700000	5700000	4700000	5033333	577350.3	-0.0437395
5	3370000	2140000	1560000	2356667	924247.4	-0.3732971
7	750000	800000	470000	673333	177857.6	-0.9173651
10	51000	92000	26200	56400	33230.71	-1.9943161
20	1420	2290	3250	2320	915.3688	-3.3801072

255	CFU1	CFU2	CFU3	Average	STD	log(c/co)
0	4000000	4300000	5000000	4433333	513160.1	0
2	2480000	4600000	4200000	3760000	1126410	-0.07154
5	230000	520000	600000	450000	194679.2	-0.99352
7			16000	16000		-2.44261
10			300	300		-4.16961
20	10	20	100	43	49.32883	-5.00991

265	CFU1	CFU2	CFU3	Average	STD	log(c/co)
0	4200000	7000000	5500000	5566667	1401190	0
2	390000	4300000	4700000	3130000	2381323.2	-0.2500509
5	670000	530000	490000	563333	94516.313	-0.9948298
7	190000	19000	50000	86333	91106.165	-1.8094167
10	2000	80	520	867	1005.8496	-3.8077431
20	130	150	170	150	20	-4.569504

285	CFU1	CFU2	CFU3	Average	STD	log(c/co)
0	4200000	7000000	5500000	5566667	1401190	0
2	4700000	5500000	4500000	4900000	529150.3	-0.0554
5	4200000	5300000	4500000	4666667	568624.1	-0.07659
7	3345000	4300000	3200000	3615000	597641.2	-0.18749
10	2360000	1230000	1420000	1670000	605062	-0.52288
20	166000	9000	7900	60967	90963.2	-1.9605

UV-LED ATP Data

LP	ATP1	ATP2	ATP3	Average	STD	Log C/C0
0	1467	5959	3987	3804	2251.784	0
10	2225	3215	2199	2546	579.3426	-0.1743966
0+	2176406	804818	1274049	1418424	697098.7	0
2+	591025	362603	369929	441186	129816.5	-0.5071845
5+	70423	55060	57213	60899	8318.505	-1.3671973
7+	31604	32712	34062	32793	1231.016	-1.6360275
10+	29119	29927	35612	31553	3538.621	-1.6527692
20+	8546	12442	8933	9974	2146.268	-2.1529493

255	ATP1	ATP2	ATP3	Average	STD	Log C/C0
0	3941	2373	2565			
10	3108	3851	2933			
0+	2528346	1944070	1851986	2108134	366815.1	0
2+	180034	152473	189191	173899	19112.38	-1.0836
5+	34435	37566	39237	37079	2438.123	-1.75476
7+	30748	31326	36603	32892	3226.599	-1.8068
10+	14557	16416	19670	16881	2588.3	-2.0965
20+	15783	17084	20977	17948	2702.839	-2.06988

265	ATP1	ATP2	ATP3	Average	STD	Log C/C0
0	1467	5959	3987			
10	3063	7510	4459			
0+	2176406	804818	1274049	1418424	697098.68	0
2+	537885	148926	212111	299641	208730.33	-0.6752054
5+	35159	27916	30763	31279	3649.3916	-1.6565467
7+	18478	30454	29881	26271	6754.9707	-1.732329
10+	13647	12206	16180	14011	2012.0906	-2.0053391
20+	12862	15264	14053	14060	1201.2512	-2.0038358

285	ATP1	ATP2	ATP3	Average	STD	Log C/C0
0	1467	5959	3987			
10	1865	4835	2906			
0+	2176406	804818	1274049	1418424	697098.7	0
2+	1654972	355344	870654	960323	654437.9	-0.16939
5+	486034	73851	117734	225873	226371.9	-0.79794
7+	129178	44179	58934	77430	45417.71	-1.26289
10+	90322	38821	30238	53127	32496.6	-1.42649
20+	34520	39398	21149	31689	9448.045	-1.6509

E.coli Growth Curve

time		OD600	CFU	CFU
0	0	0.02	3600000	6.556303
0.5	30	0.021	5300000	6.724276
1	60	0.027	6200000	6.792392
1.5	90	0.056	9000000	6.954243
2	120	0.12	21800000	7.338456
2.5	150	0.26	62700000	7.797268
3	180	0.483	#N/A	#N/A
4	240	0.975	662000000	8.820858
5	300	1.159	1550000000	9.190332
6	360	1.243	2040000000	9.30963
7	420	1.331	1900000000	9.278754
8	480	1.336	1970000000	9.294466
10	600	1.408	2000000000	9.30103
12	720	1.427	2180000000	9.338456
22	1320	1.539	3320000000	9.521138

Spectrometer Data (Measurements are in µW cm^{-2})

255 - 100mm	-3	-2.5	-2	-1.5	-1	-0.5	0	0.5	1	1.5	2	2.5	3
-3	5.7142	5.8932	6.1742	6.2654	6.4843	6.4054	6.3372	6.3005	6.1241	5.8828	5.6604	5.5176	5.3209
-2.5	6.1682	6.3761	6.6131	6.8421	7.0217	7.1865	7.137	6.9949	6.631	6.408	6.1062	5.8073	5.701
-2	6.5021	6.7187	7.0418	7.3686	7.6869	7.7662	7.5834	7.4012	7.2081	6.8778	6.5229	6.2194	5.9017
-1.5	6.728	7.0541	7.4557	7.8342	8.3493	8.2594	7.9399	7.8661	7.593	7.0347	6.6543	6.2227	5.9208
-1	7.07	7.4382	7.9157	8.5456	9.411	9.0536	8.6116	8.194	7.7289	7.32	6.8558	6.3598	6.0569
-0.5	7.2661	7.8298	8.448	9.2511	10.746	10.745	8.9683	8.4672	8.0064	7.2247	6.7687	6.3043	6.0161
0	6.9095	7.2612	7.8496	8.4971	9.2677	9.3025	8.6614	8.1873	7.7044	7.1424	6.706	6.2338	5.8682
0.5	6.8131	7.0701	7.58E+00	8.0341	8.4557	8.5176	8.2332	7.808	7.3948	7.0858	6.6763	6.2761	5.9158
1	6.2158	6.5534	6.80E+00	7.06	7.4396	7.4787	7.4346	7.2246	6.9682	6.6264	6.2704	5.9579	5.6233
1.5	6.0518	6.3113	6.49E+00	6.703	6.9891	6.952	6.8748	6.8202	6.6545	6.3715	5.9997	5.8183	5.6091
2	5.7231	5.7624	5.90E+00	6.0602	6.2166	6.2706	6.3118	6.2022	6.0847	5.926	5.7143	5.5823	5.4192
2.5	5.6513	5.7406	5.86E+00	5.9819	6.0139	6.0202	5.9926	5.9091	5.7723	5.6706	5.5758	5.4801	5.3253
3	5.2452	5.258	5.38E+00	5.4579	5.5031	5.5469	5.5514	5.571	5.4835	5.4174	5.3404	5.1716	5.1123

265 - 100mm	-3	-2.5	-2	-1.5	-1	-0.5	0	0.5	1	1.5	2	2.5	3
-3	18.963	19.453	20.045	20.613	21.134	21.584	21.529	21.274	20.742	20.04	19.419	19.023	18.437
-2.5	19.732	20.488	21.362	21.932	22.643	23.244	23.155	22.714	22.043	21.277	20.281	19.664	19.074
-2	20.287	21.322	22.245	24.211	24.744	24.604	25.213	24.018	23.187	22.313	21.387	20.488	19.796
-1.5	22.162	23.343	24.891	25.909	27.132	27.749	27.492	26.683	25.491	24.011	22.915	21.517	20.389
-1	21.828	23.546	25.393	27.613	29.342	30.035	30.0129	29.249	26.816	25.094	23.606	22.076	21.044
-0.5	22.21	24.279	25.874	28.836	33.721	32.049	32.002	30.058	27.148	25.964	24.218	22.498	21.155
0	21.959	23.573	25.568	27.802	29.881	29.108	28.76	28.389	26.304	24.89	23.292	22.04	21.036
0.5	21.424	22.583	2.39E+01	25.066	26.29	26.299	26.2	25.355	24.591	23.394	22.279	21.135	20.375
1	20.711	21.802	2.27E+01	23.642	24.338	24.259	24.239	23.771	23.123	22.244	21.341	20.454	19.842
1.5	19.504	20.339	2.10E+01	21.597	22.121	22.111	22.276	21.852	21.475	20.768	20.086	19.568	18.953
2	19.076	19.464	2.00E+01	20.547	20.821	20.751	20.823	20.602	20.267	19.819	19.349	18.967	18.312
2.5	17.792	18.223	1.85E+01	18.733	18.864	18.758	18.847	18.848	18.614	18.374	17.878	17.501	16.997
3	17.295	17.582	1.80E+01	18.153	18.312	18.439	18.504	18.293	18.108	17.808	17.506	17.105	13.737

285 - 100mm	-3	-2.5	-2	-1.5	-1	-0.5	0	0.5	1	1.5	2	2.5	3
-3	19.345	20.041	20.769	21.444	21.439	22.208	21.974	21.863	21.556	20.892	20.231	19.663	18.99
-2.5	19.783	20.701	21.511	22.37	23.131	23.851	23.608	23.2	22.622	21.686	20.767	20.034	19.259
-2	19.912	20.984	22.128	23.403	24.406	25.501	25.351	24.967	23.923	22.588	21.562	20.579	19.775
-1.5	20.595	21.627	23.148	24.713	26.553	28.326	28.462	27.208	25.218	23.802	22.433	21.258	20.202
-1	20.721	22.117	23.939	26.047	28.663	32.676	33.672	30.392	27.081	24.96	23.194	21.722	20.525
-0.5	20.857	22.433	24.238	26.647	30.379	37.964	43.233	32.411	28.28	25.485	23.581	22.012	20.712
0	21.025	22.437	24.235	26.269	29.069	32.684	34.265	30.941	27.587	25.253	23.497	22.04	20.675
0.5	20.06	21.169	2.26E+01	24.248	26.38	27.833	28.071	27.503	25.555	23.901	22.402	21.236	20.207
1	19.883	20.657	2.18E+01	23.231	24.278	25.217	25.348	24.969	24.082	22.886	21.644	20.681	19.826
1.5	19.445	20.08	2.10E+01	21.909	22.527	23.167	23.187	23.228	22.632	21.832	20.928	20.217	19.62
2	19.065	19.622	2.01E+01	20.837	21.353	21.567	21.787	21.713	21.25	20.711	20.225	19.727	19.043
2.5	18.497	19.067	1.95E+01	19.932	20.186	20.348	20.481	20.434	20.28	20.012	19.59	19.121	18.607
3	18.224	18.566	1.90E+01	19.421	19.46	19.684	19.801	19.693	19.578	19.35	18.982	18.582	18.123